Functional role of the neuron-satellite glial cell unit in the autonomic nervous system

Sohyun Kim

The Graduate School

Yonsei University

Department of Medicine

Functional role of the neuron-satellite glial cell unit in the autonomic nervous system

Directed by Professor Seong-Woo Jeong

A Dissertation

Submitted to the Department of Medicine and

the Graduate School of Yonsei University

In partial fulfillment of the requirements for the degree of

Doctor of Philosophy

Sohyun Kim

February, 2024

This certifies that the Doctoral Dissertation of

Sohyun Kim is approved.

Thesis Supervisor: Seong-Woo Jeong, Ph.D.

Kum Whang, M.D, Ph.D.: Thesis Committee Member

Ji-Yong Lee, M.D., Ph.D.: Thesis Committee Member

Kyu-Sang Park M.D., Ph.D.: Thesis Committee Member

Ki Woo Kim, Ph.D.: Thesis Committee Member

The Graduate School

Yonsei University

February, 2024

ACKNOWLEDGEMENTS

This thesis would not have been possible without God's love and a universal amount of luck. I was never capable to finish this PhD marathon on my own. This is still not perfect on its own but it is finally completed with the generous help of multiple people around me.

Firstly, I would like to deeply thank Professor Seong-Woo Jeong who has been an endlessly patient and kind supervisor to guide and teach a student who had very little experiences in the laboratory life and in many other ways. I was too brave to start a basic research for my PhD course and I started everything from the scratch. Professor Jeong helped me out so that I did not give up. My graduate school training was not easy due to the lack of my ability to go through the scientific rigor but I have learned many lessons through a hard way. I must also thank Professor Kum Whang, Professor In Deok Kong, and Professor Joong-Woo Lee for their strong encouragement and prayers so that I could endure during the graduate school life. Including Professor Kum Whang, my sincere thanks also go to my committee members - Professor Ji-Yong Lee, Professor Kyu-Sang Park, and Professor Ki Woo Kim - for their prayers, professional guidance, and critical comments to enrich my research contents. Equally, I would like to thank Professor Seung-Kuy Cha and Yang-Sik Jeong for praying for me and generously letting me use their experimental facilities available to do my experiments.

I am heavily indebted to many good friends at the Department of Physiology. As a person who had very scarce basic research experiences, I was very ignorant in many aspects, but all the members and colleagues in the Physiology department were very kind and helped

me willingly whenever I asked questions related to research or requested for help in general issues: Thank you, Seong-Jun Kang, Huu Son Nguyen, Hyun Kyung Choi, Chung-Ku Lee, Jae Seung Chang, Kyu-Hee Hwang, Ji Hee Kim, Soo-Jin Kim, Nhung Thi Nguyen, Luong Dai Ly, Da Dat Ly, Bao Ngo Thi Dang, Anh Phan Nguyen, Sae Bom Kwon, Hee Kyoung Lee, Do Phuong Anh, and Vo Thi Anh Vu. The time spent with you was and is still very happy and precious which I will remember, and thankfully treasure for the rest of my life.

Furthermore, I must show my sincere thanks to the members of Wonju College of Medicine for teaching me scientific techniques and sharing their experiences: Drs. Mee-Sook Song, Jin-Suk Lee, Yeo-Wool Kang, Yun Jae Lee, Myoung Ha Kim, Min Kyu Kim, Dong Ju Yang, Professor Kyoung Hye Yoon, Professor Joon Hyung Sohn, Professor Jun NamKung, and Drs. Dong-Jin Seo and Keun-Soo Park from the Animal Lab. Lastly, and not the least, I am obliged to give huge thanks and love to my parents and my family. They have prayed and waited for me with unconditional love so that I can finish what I started.

February 2024

Sohyun Kim

CONTENTS

LIST OF FIGURES

LIST OF TABLES

LIST OF ABBREVIATIONS

2-MeS-ADP	2-Methylthio-adenosine diphosphate
AC	Adenylyl cyclase
ACh	Acetylecholine
ADP	Adenosine diphosphate
ANS	Autonomic nervous system
ATP	Adenosine triphosphate
AUC	Area under the curve
BzATP	2'(3')-O-(4-Benzoylbenzoyl)-adenosine-5'-triphosphate
CAD	CRAC activation domain
cAMP	Cyclic adenosine monophosphate
CCh	Carbachol
cDNA	Complementary DNA
CGRP	Calcitonin gene-related peptides
CON	Control
CNS	Central nervous system
CPA	Cyclopiazonic acid
CRAC	Calcium release activated calcium channel
Ct	Cycle time
DAG	Diacylglycerol

DAPI	4’,6’-diamidino-2-phenylindole
DMSO	Dimethylsufoxide
DMEM	Dulbecco's modified eagle medium
DNA	Deoxyribonucleic acid
DRG	Dorsal root ganglion
EBSS	Earle’s balanced salt solution
EC_{50}	Effective concentration (half maximal)
EGTA	Ethylene-bis(oxyethylenenitrilo) tetraacetic acid
ER	Endoplasmic reticulum
FBS	Fetal bovine albumin
GABA	Gamma-aminobutyric acid
GAPDH	Glyceraldehyde-3-phophate dehydrogenase
gDNA	Genomic DNA
GFAP	Glial fibrillary acidic protein
GPCR	G-protein coupled receptor
GS	Glutamine synthase
HPSS	Hanks' Balanced Salt Solution
HRP	Horseradish peroxidase
IACUC	Institutional animal care and use committee
IHC	Immunohistochemistry
IF	Immunofluorescence

IgG	Immunoglobulin G
IP_3	Inositol 1,4,5- triphosphate
IVM	Ivermectin
Kir	Delayed inwardly rectifying potassium channel
LPS	Lipopolysaccharides
mRNA	Messenger ribonucleic acid
NC	Nitrocellulose
NCX	Sodium/calcium exchanger
NE	Norepinephrine
NF-κB	Nuclear factor kappa B
NPY	Neuropeptide Y
OCT	Optimal cutting temperature
PBS	Phosphate buffer saline
PCR	Polymerase chain reaction
$PI(4,5)P_2$, PIP_2	Phosphatidylinositol-4,5-bisphosphatase
PLC	Phospholipase C
PMCA	Plasma membrane Ca^{2+} ATPase
PNS	Peripheral nervous system
PPADS	Pyridoxalphosphate-6-azophenyl-2',4'-disulfonic acid
QPCR	Quantitative polymerase chain reaction
RIPA	Radioimmunoprecipitation assay buffer

RNA	Ribonucleic acid
ROCE	Receptor-operated calcium entry
RT-PCR	Reverse transcription polymerase chain reaction
RyR	Ryanodine receptor
SAM	Sterile alpha motif
SCG	Superior cervical ganglia
SDS	Sodium dodecyl sulfate
SERCA	Sarcoplasmic/endoplasmic reticulum Ca2+ ATPase
SGC	Satellite glial cell
SOCE	Store-operated calcium entry
STIM	Stromal interaction molecule
TLR4	Toll-like receptor 4
TRPC	Transient receptor potential channel (Canonical)
UDP	Uridine-5’-diphosphate
UTP	Uridine-5’-triphosphate
VEH	Vehicle
VIP	Vasoactive intestinal peptide
VGCC	Voltage-gated calcium channel

ABSTRACT

Functional role of the neuron-satellite glial cell unit in the autonomic nervous system

Sohyun Kim

Department of Medicine

The Graduate School, Yonsei University

Directed by Professor Seong-Woo Jeong

The sympathetic and parasympathetic nervous system, constituting the autonomic nervous system, play a central role in maintaining homeostasis in our body by coordinating the functions of internal organs. While autonomic ganglia have traditionally been viewed as relays for neural signals from the brain stem and spinal cord to the effector tissues, emerging evidences suggests that ganglia internally process and integrate a variety of signals to modulate the functions of terminal effector organs. This highlights the importance of an interplay between individual cells within the ganglia for balanced autonomic function.

Autonomic ganglia are composed of neurons and satellite glial cells (SGCs) that surround

them. The anatomically close proximity between these neurons and SGCs is believed to contribute to the regulation of homeostasis in autonomic ganglia through mutual neuro-glial communication. While most of the research on autonomic ganglia has mainly focused on the structure and function of neurons, recently, many scientists have sought to elucidate the roles of SGCs. SGC is a major type of glial cell in the autonomic ganglia, found to wrap around the neuronal cell body. This unique organization of neuron-glial unit is well-noted. However, little is known about the functional roles of the autonomic neuron-SGC units.

In this study, I established a culture system for partially dissociated neuron-SGC units from the superior cervical ganglia (SCG). The first part of the project involves identifying calcium (Ca^{2+}) signaling machinery of store-operated Ca^{2+} entry (SOCE) and receptor-operated Ca^{2+} entry (ROCE) in sympathetic neurons and SGCs in responding to the various extracellular stimuli. The second part of the project aims to investigate purinergic communications between sympathetic neurons and SGCs, where a somatic ATP release may have a potential role.

The rat SCG was isolated, and sympathetic neurons attached to SGCs were dissociated using a partial enzymatic digestion method. Immunohistochemical and immunofluorescent experiments confirmed the presence of sympathetic SGCs attached to the neurons. Subsequently, I investigated the components of SOCE and ROCE, critical for cellular Ca^{2+} homeostasis in rat sympathetic ganglia under normal and pathological states. Quantitative RT-PCR was employed to detect the expressions of Orai 1/2/3 channels, stromal interaction molecules 1/2 (STIM1/2), and the transient receptor potential cation channels 1/3/6

(TRPCs) in sympathetic ganglia. Functional studies were performed using Ca^{2+} imaging technique with Fura-2/AM. Both neurons and SGCs exhibited SOCE when the internal storage of Ca^{2+} was depleted by cyclopiazonic acid (CPA) along with the removal of extracellular Ca^{2+}. The subsequent recovery from the ER depletion upon the restoration of extracellular Ca^{2+} via SOCE was rapid. Intracellular Ca^{2+} imaging revealed that the magnitude of SOCE was significantly larger in the SGCs than in the neurons. Unlike neurons, the SOCE in the SGCs were accompanied with substantial Ca^{2+} oscillation. Orai1 and STIM1 were identified as the major components of SOCE machinery in sympathetic ganglia. SOCE was significantly suppressed by GSK7975A (1 μM), a selective Orai1 blocker, and Pyr6 (3 μM), a SOCE blocker. Acute inflammation was induced with lipopolysaccharide (LPS) to assess changes in the function of neuron-SGC unit. Glial fibrillary acidic protein (GFAP) and Toll-like receptor 4 (TLR4) were upregulated to indicate neuro-glial inflammation in sympathetic ganglia. Importantly, LPS attenuated SOCE by downregulating Orai1 and STIM1 expressions. This suggests that SOCE is highly susceptible to inflammation, potentially influencing sympathetic neuronal activity and thereby autonomic output.

In an effort to characterize the ROCE components in sympathetic ganglia, TRPC3 and TRPC6 were further investigated. In this regard, carbachol and selective TRPC inhibitors, Pyr3 (TRPC 3 inhibitor, 10 μM), and SAR7334 (TRPC 6 inhibitor, 10 μM), were employed to identify the presence of TRPCs in SCG neurons and SGCs. Additionally, TRPCs, especially TRPC3, may also be a partial component of SOCE machinery as CPA-induced

SOCE activity was reduced by lanthanum chloride (non-selective TRPC inhibitor, 50 μM) and Pyr3. In contrast to sympathetic SOCE profiles, Ca^{2+} signaling through TRPCs was significantly larger in sympathetic neurons compared to the SGCs. Collectively, these findings suggested that Ca^{2+} is mediated by Orai, STIM, and TRPC channels in sympathetic ganglia, potentially contributing to functions of sympathetic neuron-SGC units.

Neuronal and glial Ca^{2+} signaling is critical for controlling sympathetic neural excitability and communications in neuron-SGC units. Adenosine triphosphate (ATP) is co-released with norepinephrine from postganglionic sympathetic nerve terminals, mediating fast excitatory synaptic transmission to various visceral tissues. In addition, ATP is also extrasynaptically released from autonomic neurons. To date, however, the functional significance of somatic ATP release in the sympathetic ganglia remains elusive. Upon depolarization of the SCG neurons by application of high potassium (K^+), intracellular Ca^{2+} is significantly increased in the SGCs attached to the SCG neurons, but not in singly isolated glial cells. This strongly suggests that neuronal excitation causes a local release of mediator that selectively affects the attached SGCs. Furthermore, the extracellular application of high K^+ significantly diminished the FM1-43-stained and quinacrine-stained vesicular puncta in the soma of SCG neuron, suggesting somatic ATP release. ATP luminescence assay was conducted to quantify ATP released from cultured sympathetic neurons. Upon high K^+ stimulation, the extracellular ATP concentration was significantly increased to confirm the somatic ATP released from sympathetic neurons. The pretreatment of neurons with the voltage-gated calcium channel (VGCC) inhibitor,

cadmium chloride (Cd^{2+}, 100 μM), and Ca^{2+} ion chelator, BAPTA (30 μM), hindered the Ca^{2+} influx from the external buffer upon neuronal depolarization, and no significant ATP release was observed. Next, the purinergic agonist, ATP (100 μM), and pan-purinergic antagonists such as suramin (P2 inhibitor, 30 μM) and PPADS (P2X blocker, 30 μM) were applied to characterize the purinergic Ca^{2+} signaling in sympathetic neurons and SGCs. Both inhibitors almost abolished the ATP-induced Ca^{2+} responses in sympathetic neuron-SGC units. The screening of transcripts encoding purinergic receptors confirmed the presence of P2X4, P2X7, and P2Y1 receptors in rat SCG. Intracellular Ca^{2+} was increased in both neurons and SGCs after ATP (50 μM) stimulation. BzATP (selective P2X7 agonist, partial agonist for P2X4/P2Y1, 50 μM) induced activation of purinergic Ca^{2+} signaling which was differentially inhibited by A438079 (potent P2X7 inhibitor, 30 μM) in SGCs, and by MRS2179 (selective P2Y1 inhibitor, 30 μM) in sympathetic neurons. Based on the provided context, the allosteric modulators of P2X4 and P2X7 receptors, zinc chloride (Zn^{2+}, 5 μM) and cadmium chloride (Cd^{2+}, 20 μM), exhibited variable Ca^{2+} responses to ATP and BzATP in sympathetic SGCs. This suggests the potential presence of both heteromeric or homomeric P2X4/7 receptors in sympathetic SGCs. Consequently, this diversity in receptor composition contributes to the provision of a wide range of Ca^{2+} responses in SGCs when exposed to external stimuli. Taken together, these data suggested that the vesicular ATP released from the sympathetic neurons may trigger the activation of multiple candidate purinergic receptors in the SGCs through Ca^{2+} signaling.

In conclusion, the unique anatomical arrangement suggests signal exchanges between

sympathetic neurons and SGCs. The sympathetic neurons and SGCs functionally express multiple Ca^{2+} signaling machineries, which are essential for mediating sympathetic neuro-glial communication.

Key words: Autonomic, ATP, calcium signaling, ROCE, satellite glial cell, SOCE, somatic ATP release, sympathetic ganglia, TRPC, vesicular release

I. INTRODUCTION

1.1. Autonomic nervous system

The autonomic nervous system (ANS) plays a crucial role in maintaining homeostasis in our body by regulating multiple internal organ functions in a coordinated manner. The ANS is largely composed of two types of neurons: preganglionic and postganglionic neurons. Preganglionic neurons of the ANS are located in the central nervous system (e.g. brainstem and spinal cord), while the postganglionic neurons are found in the peripheral autonomic ganglia. The axon fibers that emerge from the postganglionic neurons within the autonomic ganglia are eventually connected to the terminal effectors of the visceral organs. The long connections of neuronal signaling pathway in the ANS can be variable with different types of neuronal communications producing diverse autonomic output [1, 2].

The ANS is composed of largely two sub-systems: parasympathetic and sympathetic nervous system. Parasympathetic and sympathetic systems are often considered to function oppositely, and the individual actions of each system are antagonistic by its nature. However, these two systems are now known to counterbalance each other to maintain the bodily homeostasis, as they are complementary to function most of the time. When this regulated balance is disrupted, autonomic dysfunction may occur. The neurotransmitters released from parasympathetic and sympathetic postganglionic nerve terminals are acetylcholine (Ach) and norepinephrine (NE), respectively. However, the preganglionic nerve terminals commonly release Ach as a primary neurotransmitter. The primary

neurotransmitters are synthesized and stored in the vesicles at nerve terminal axon branches before release. After mentioning the different features between the parasympathetic and sympathetic systems, this thesis will primarily focus on the cervical part of the sympathetic system of the ANS.

1.2. Parasympathetic and sympathetic nervous system

The parasympathetic system functions by promoting the recovery and sustaining the resting state of the internal environment. The pre-ganglionic neurons of parasympathetic system originate from craniosacral regions in the brainstem and spinal cord. Their terminal ganglia are usually closely located to the target effector organs, and the parasympathetic activities are typically limited to certain organs. The parasympathetic system uses ACh as a primary neurotransmitter, and is characterized by long cholinergic preganglionic axons and short cholinergic postganglionic axons. It is noted that the intrinsic neurons of the ANS exist in almost all major parts of the body. Many of them are part of the parasympathetic nervous system, but the neurons can differ in their origins and also their functions in different organs, indicating that a local control system is independently maintained by the balance of parasympathetic and sympathetic systems.

The sympathetic system regulates during the emergent flight-or-fright reactions and exercise. The preganglionic neurons originate from the T1-L2 thoracolumbar locations for the sympathetic system. The terminal ganglion is located in the paravertebral sympathetic chain system. The system has short cholinergic preganglionic axons. Unlike

parasympathetic system, most sympathetic postganglionic fibers are adrenergic as they release norepinephrine in the terminal endings. Sympathetic ganglionic neurons can be coordinated by divergent levels of spinal cord with various signaling from the whole body. The axonal projections of paravertebral ganglia innervate the pupil, heart, respiratory system, blood vessels, and exocrine glands of the head, and limbs, whereas prevertebral neurons innervate abdominal organs and pelvis [3]. Thus, the sympathetic activities are usually acting on the entire bodily system with massive systematic discharge of the neurotransmitters in the multiple target organs.

1.3. Superior cervical ganglia (SCG)

The study model for this research utilized the rodent superior cervical ganglion (SCG) from the sympathetic system. The SCG is commonly chosen to study sympathetic nervous system due its simple structural features to reproduce experiments [4]. It is one of the largest cervical sympathetic ganglia. The SCG is located in the bifurcation of the common carotid artery, close to the distal nodose ganglion of the vagal nerve [5, 6]. SCG axons project either along internal or external carotid arteries to innervate tissues to the cervicocephalic regions of the head and neck [7, 8]. SCG plays an important role in severe neuropathies and systemic disorders, including Horner's syndrome, ischemic cerebrovascular diseases, and seizures [9-12].

The sympathetic ganglia usually serve as a relay system to transmit the neural signals from the brainstem to the target organ. However, these ganglia also receive various signals

from multiple sources within the ganglia to modulate the functions of the effector organs. The sympathetic ganglia are mainly composed of principal neurons and satellite glial cells (SGCs). Unlike other glial cells, SGCs tightly wrap around the neuronal soma. The structural proximity between these neurons and SGCs is believed to contribute to the regulation of homeostasis in autonomic ganglia through their interaction and mutual influence. In addition to ganglionic neurons and SGCs, sympathetic ganglia also contain several other cell types, including small intensely fluorescent (SIF) cells, and fibroblasts [4, 13].

1.3.1. Sympathetic neurons

In general, the gross anatomy of SCG neurons is very visibly distinctive, characterized by a large cellular size and volume, along with noticeable nucleus and nucleolus. Ganglion neurons are typically surrounded by intra-ganglionic capillary vessels and multiple SGCs whose processes form glial capsule around the neuron [14-16]. The SCG contains various types of neurons. Based on the electrophysiology profiles of the firing rates of action potential and the expressions of neuropeptide Y (NPY), the low-threshold NPY-negative neurons are usually secretomotor neurons, innervating salivary glands, whereas the high-threshold, NPY-negative neurons are vasomotor neurons, innervating blood vessels. NPY-positive neurons are vasoconstrictor neurons, which affect the iris and pineal gland [17-19].

The sympathetic nervous system can also be organized into the categories of neurons according to the target tissues. For instance, most postganglionic vasoconstrictor neurons

innervating to skin and skeletal muscles contain NE and NPY. Vasoconstrictor neurons innervating to small arteries contain dynorphin and NE while those to the precapillary sphincters contain only dynorphin. Pilomotor neurons are noradrenergic neurons containing calcitonin gene-related peptides (CGRP) without NPY. On the other hand, muscle vasodilator neurons are cholinergic contain NPY, vasoactive intestinal peptide (VIP) and dynorphin. In summary, sympathetic neurons exhibit considerable differences in the phenotypic morphology of neurons and glial cells as well as the expression of neurotransmitters and neuropeptides, and electrophysiological properties [20, 21]. Recent study reported seven neuronal populations in stellate and thoracic sympathetic ganglia defined by expression profiles of growth factors, neurotransmitters, and neuropeptides [22].

1.3.2. Sympathetic satellite glial cells (SGC)

A Greek word “Glia” was first mentioned by Virchow as a part of non-neuronal cells in the brains [23]. Glial cells are initially appreciated functionally less important than neurons as they are part of supportive structures to aid neuronal function. However, a growing number of evidences suggest that the interplay between neurons and glial cells is fundamental in the development and regulation of nervous system [24-26]. Functional roles of glial cells are diverse. They include supports for neural metabolism, release of growth factors and trophic factors for neural signaling, and active response to pathological conditions such as infection and injuries [27-32].

In peripheral nervous system (PNS), SGCs are the major types of glial cells which are

present in both sensory and autonomic ganglia [33]. There are largely two types of glial cells in autonomic ganglia - Schwann cells and SGCs. Schwann cells may also be found in the axonal nerve fibers [34-37].

SGCs usually wrap around neurons and synaptic regions (Fig. 1) [35, 36, 38]. In an intact ganglion, principal neurons are enveloped around with more than one SGCs [38, 39]. The closed extracellular space between the tightly bound SGCs to neurons is as approximately 20 nm where only small bioactive molecules can be passed between neurons and SGCs [33, 40]. SGCs are originated from the neural crest cells but they can be transcriptionally subdivided into different populations depending on their activation [41]. Hanani group also reported that the phenotypic changes are observed in the long-term cultured SGCs which suggest their ability to differentiate and proliferate under various environment [42]. These glial cells participate in multiple modulations of synaptic transmission. This unique structural arrangement implies a functional unit between neurons and SGCs, indicating that mutual communication is necessary for regulating autonomic ganglia function [33, 43].

Recent studies have highlighted that sympathetic SGCs play critical roles in the physiological regulation of neuronal metabolism and survival, cell excitability, synaptic transmission, and overall sympathetic output [44, 45]. The main difference of SGCs between sensory and sympathetic ganglia is the extension of sympathetic SGCs to envelop the dendrites and synapses of neurons as well as neuronal soma [43]. SGCs form a layer over the synapses, enabling them to control synaptic transmission. It is interesting to observe that in the co-culture system of neurons SGCs, SGCs selectively enhanced the

dendrite, subsequently increasing the synaptic activities [44, 46]. Ach is the major neurotransmitter in sympathetic ganglia, and indeed it was found that SGCs in the mouse SCG are sensitive to ACh. This raises the possibility that SGCs influence synaptic transmission in sympathetic ganglia. Other works showed that selective injury to sympathetic nerve terminals activated SGCs in SCG, but not in sensory ones. SGCs have also been proposed to modulate neuronal activity through the regulation of ion channel expression and controlling extracellular K^+ concentrations [47].

Under pathological conditions, an injury to the distal peripheral nerve endings increases the glial fibrillary acidic protein (GFAP) in SGCs [48, 49] and the functions of SGCs are well described in the models of chronic pain [33, 40]. The upregulation of GFAP is accompanied by enhanced SGC-SGC coupling through gap junctions, downregulation of delayed inwardly rectifying potassium channels Kir4.1, and augmented sensitivity of SGCs to soluble mediators such as ATP. Moreover, pathological conditions stimulate the release of pro-inflammatory cytokines such as Il-1β, Il-6 and TNF-α via activation of SGCs (i.e. gliosis), which subsequently interfere with the neuronal excitability [50]. Furthermore, the activities of gap junctions are increased to disrupt the neuronal activities under inflammatory conditions [51, 52]. In the orofacial pain studies [53, 54], pannexin 1 (Panx1) mediated the aggravation of pain via Panx1-mediated ATP release.

Information on the receptors of SGCs, especially in sympathetic ganglia, are still elusive. Using calcium imaging technique, the SGCs in sensory ganglia were found to express functional metabotropic P2Y receptors (e.g. P2Y1/4/6 and P2Y12/13 receptors in

trigeminal ganglia). For example, bradykinin, inflammatory cytokine, increased the SGC P2Y receptor sensitization of SGCs. Release of ATP by sensory neurons can activate purinergic receptors in SGCs, providing one mechanism for neuron-SGC communication [55-58].

The concept of neuron-SGC communication can be extended to its possible role in the sympathetic nervous system under pathological inflammation. Most of the inflammation studies were reported on the sensory ganglia. It is important to note that the ANS also plays a critical role in the regulation of immune system via a synergistic balance between the sympathetic and parasympathetic systems. The dynamic interplay orchestrated among the autonomic neurons, SGCs, and the target organs is the key functional hub of maintaining normal physiological conditions. However, if the immune activation and immune tolerance are not balanced due to autonomic dysfunctions, chronic inflammatory responses accumulate to cause many systemic inflammatory diseases [59]. The visceral branches of the sympathetic nervous system innervate and control immunological organs such as the thymus and spleen. The beta-adrenergic neurotransmitter, NE, is known to act on immune cells such as macrophages and microglia to inhibit the production of anti-inflammatory cytokines while aggravating the elevated levels of proinflammatory cytokine [60-62]. Whether the SGCs of sympathetic ganglia have roles to control inflammation is a task for further investigation. However, it is clear that these immune cells may become dysfunctional when there is a continuous imbalance between the anti-inflammatory and pro-inflammatory immune systems due to autonomic dysfunction. Accumulation of

multiple events of acute inflammation would systemically affect the autonomic homeostasis. This may further lead to chronic inflammation causing a vicious cycle of permanently impairing the autonomic control over the immune system. Consequently, the dysregulation of the sympathetic nervous system at the peripheral level immensely influences the overall immune system by sustaining inflammation and increasing cardiovascular risks [63]. Further study of SGC pharmacology is imperative in order to understanding the function of sympathetic SGCs because chemical signaling is ultimately the major pathway of neuro-glial communication under both physiological and pathological states of individuals. Recent studies reported that lipopolysaccharides (LPS) injection induced the generation and maintenance of pain in systemic inflammation in sensory ganglia [64]. LPS-induced changes in SGCs, which include SGC activation and increased SGC-SGC dye coupling via gap junctions. This concept can be further extended to examine the roles of sympathetic SGCs as the previous studies which showed that certain pathological conditions including chronic heart failure [65], cirrhosis [66], and traumatic brain injury [67] cause autonomic imbalance due to sympathetic overactivity. The functional mechanism of SGCs in many diseases with abnormal sympathetic output is not known much, thus, it requires further research. For example, there is an evidence that the sympathetic nervous system is involved in pain mechanisms. *In vivo* studies have shown that nerve damage enhanced the interactions between sympathetic and sensory ganglia [51].

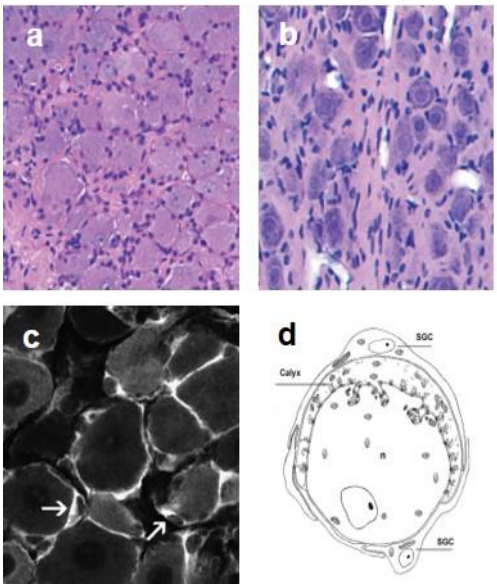

Figure 1. Immunohistochemical images of SGCs in peripheral ganglia. (a) Dorsal root ganglion from a cynomolgus monkey as a representative sensory ganglion. (b) Cervicothoracic ganglion (stellate ganglion) from the same species as (a) as a representative sympathetic ganglion. Adopted from Butt [68]. (c) Murine trigeminal ganglion was stained with glutamine-synthetase-positive SGCs (arrows) that closely surround the neuronal soma. Adopted from Hanani [43]. (d) A schematic diagram of chick ciliary ganglion as a representative parasympathetic ganglion. A similar ensheathing patterns of SGCs around a large neuronal soma can be observed. Adopted from Hanani [69]. Scale bars = 10 μm.

1.4. Calcium signaling and regulation in the nervous system

Calcium (Ca^{2+}) is important in many cellular processes such as a cell proliferation and cell death [70]. It acts as a second messenger to regulate various physiological signaling pathways [71, 72]. Numerous external stimuli such as membrane depolarization or agonist activation can lead to the elevation of intracellular Ca^{2+}, increasing it from the resting concentration of 0.1 μM upto 1 μM. In general, there are two major routes of Ca^{2+} influx: (1) extracellular Ca^{2+} coming in via plasma membrane Ca^{2+} channels or (2) from the release of Ca^{2+} in the endoplasmic reticulum (ER) stores mostly via the inositol 1,4,5-triphosphate (IP_3) receptor and ryanodine receptor (RyR).

The maintenance of higher Ca^{2+} stores of ER and lower intracellular Ca^{2+} is a delicate balance regulated by multiple Ca^{2+} channels and pumps in the plasma membrane and ER. For instance, the activities of pumping out increased intracellular Ca^{2+} via plasma membrane Ca^{2+} ATPase pump (PMCA) and sodium/calcium exchanger (NCX) are strictly counterbalanced by sarcoplasmic/endoplasmic reticulum Ca^{2+} ATPase (SERCA) that refills the ER. Ca^{2+} sensing proteins are present in every cell, and their continuous monitoring of intracellular Ca^{2+} concentration contributes to the balanced regulation of Ca^{2+} homeostasis. Ca^{2+} increase can be transient or oscillating in nature leading to the synchronized feedback that activates the relevant Ca^{2+} channels or pumps to maintain constant intracellular calcium levels. The Ca^{2+} binding affinity of PMCA and SERCA pumps is high, while their kinetic action is slow, allowing them to respond to modest elevations in cytoplasmic Ca^{2+} levels and to reestablish the resting state [73, 74]. On the other hand, NCX has a low

binding affinity to Ca^{2+} with faster kinetics enabling it to respond to a rapid and transient Ca^{2+} influx [75]. Different cell types have unique sets of Ca^{2+} channels to perform their physiological functions.

Ca^{2+} is the key mediator of neuronal activities. One of the key functions of neurons is the release of neurotransmitters. The biochemical mechanism of this process is Ca^{2+}-dependent. Neurotransmitters transmit neural signals through the axon fibers across the synapses between the neurons. These neurotransmitters are initially stored in the synaptic vesicles. Upon docking of the vesicles in the presynaptic terminals, Ca^{2+} acts to release the neurotransmitters to the receptors in the post-synaptic neurons. The depolarization of plasma membrane activates the VGCCs, allowing Ca^{2+} to enter the neurons and control various processes such as transmitter release, cell excitability, and gene expressions [76]. In terms of modulating excitability of neurons, Park *et al*. also demonstrated that stromal interaction molecule (STIM) physically binds to the VGCCs to control the excitability of the neurons [77]. This means that some portions of STIM is pre-occupied with VGCC and not available as functional part of store-operated calcium entry (SOCE) machinery, hence low SOCE activities in neurons are observed under normal physiology.

Glial Ca^{2+} signaling is a key mechanism for neuron-glial communication, regulating the release of various gliotransmitters such as adenosine triphosphate (ATP), which affects neuronal activity [78, 79]. This signaling cascade is activated in response to diverse extracellular stimuli, such as neurotransmitters released from neurons [80]. Due to its non-excitable nature, the primary source of glial Ca^{2+} signaling is Ca^{2+} release from the ER

through the activation of the GPCR-PLC-IP_3R cascade. The restoration of intracellular Ca^{2+} stores following receptor-activated ER Ca^{2+} release requires SOCE [81]. The primary machinery that activates SOCE is the calcium release-activated calcium channel (CRAC), which comprises Orai channels spanning the plasma membrane and STIM, an ER Ca^{2+} sensor. The depletion of ER Ca^{2+} triggers the oligomerization of STIM1 and STIM2 monomers leading to their translocation near the plasma membrane, where they form distinct puncta with Orai1, Orai2, and Orai3, thereby activating the Orai Ca^{2+} channels [82]. This activation results in a transient increase in cytosolic Ca^{2+} via activated Orai Ca^{2+} channels, and subsequent refilling of ER stores occurs through Ca^{2+} pumps on the ER membrane.

While glial SOCE has been extensively studied in various glial cells within the central nervous system, including astrocytes, oligodendrocytes, and microglia [83-88], information on glial Ca^{2+} signaling and its mechanisms in the autonomic ganglia remains little. For example, evidence suggests that dysregulation of SOCE in astrocytes and microglia occurs under conditions like LPS-induced inflammation [87, 89]. However, the role of SOCE in SGCs in the physiological and pathological conditions need further studies.

1.4.1. Store-operated Ca^{2+} entry (SOCE)

The concept of Ca^{2+} refilling of ER "stores" through the Ca^{2+} influx upon ER Ca^{2+} release was first introduced by James Putney in 1976 [90, 91]. In non-excitable cells, the predominant pathway of cytosolic Ca^{2+} influx is SOCE. The major signaling event to

trigger the cellular SOCE process is the activation of GPCR signaling cascades. Upon activation of GPCRs, the cascade of signal transduction passes to phospholipase C (PLC) by G protein. PLC breaks down the transmembrane phosphatidylinositol 4,5-bisphospahte (PIP_2) into diacyglycerol (DAG) and IP_3. IP_3 receptors in the ER senses the increase of cytosolic IP_3, and subsequently, the ER releases Ca^{2+} from its store. The consequent increase in the intracellular Ca^{2+} is sensed STIM. STIM oligomerizes with plasma membrane SOCE channel, Orai, to allow Ca^{2+} influx from extracellular fluid [92-95].

SOCE is activated by the depletion of ER Ca^{2+} or GPCR activation to produce IP3, which can release ER calcium. GPCR agonists such as carbachol and ATP can be used for this purpose. The SERCA pump can be blocked by thapsigargin and cyclopiazonic acid (CPA). The introduction of fluorescent Ca^{2+} indicators such as Fura-2/AM and fluo-4 have facilitated the widespread study of Ca^{2+} signaling in SOCE using the mentioned chemicals [96, 97].

The SOCE components, STIM and Orai, were discovered and their fundamental roles were demonstrated by many groups [98-101]. STIM plays a role as a calcium sensor when ER calcium is depleted [99, 102]. Another crucial component of SOCE is Orai channel, which is located in the plasma membrane where it opens the channel upon the oligomerization with STIM from the ER [98, 101, 103]. The molecular interaction between STIM and Orai functions to increase SOCE activities in many genetic overexpression model culture [104-106]. Both isoforms of STIM 1/2 have similar functions, and the same applies to the three isoforms of Orai 1/2/3 [99, 104].

The molecular mechanisms of STIM lies in its structure. STIM is an ER protein and it has its N terminus with EF hands and sterile alpha motif (SAM) domains in the lumen [107, 108]. This EF hand has a Ca^{2+} binding site, allowing it to sense the changes in the ER Ca^{2+} level. SAM plays a role in STIM oligomerization. STIM also has a CRAC activation domain (CAD) and STIM1-Orai activating region (SOAR) [109, 110]. CAD/SOAR domains of STIM are responsible for interacting with the C and N terminus of Orai1 to activate the channel [111, 112]. This phenomenon can be microscopically observed as the changes in the ER Ca^{2+} induces STIM aggregation and membrane localization to interact with Orai channels [99, 113]. STIM1 clusters form local aggregates with Orai channels forming multiple puncta-like region in the plasma membrane [114, 115]. Orai channels subsequently open and calcium influx occurs to refill the ER store. All these processes are closely regulated to maintain multiple cellular functions.

SOCE proteins are widely expressed in diverse types of cells. STIM and Orai genes are related to many immune disorders, where they were initially discovered, leading to extensive studies in immune cells [116]. Deficiency in STIM1 is related with autoimmune diseases [117]. Immune cells deficient in Oria1, such as T cells, exhibit showed dysfunctional cytokine secretion [118]. These proteins play a profoundly critical role in the regulation of immune functions. SOCE proteins are also actively involved in the cardiovascular system. Overexpression of STIM can induce cardiac hypertrophy in rat disease models [119]. Orai and STIM are reported to critical in breast cancer proliferation and migration [95]. Evidently, SOCE in many types of tissues and cells is also associated

with diverse biological and medical conditions, including metabolism, cancer, pain, and stress. The study of the functions of glial SOCE in PNS physiology and pathophysiology is one of the research areas to be explored extensively.

1.4.2. Receptor-operated Ca^{2+} entry (ROCE)

In the nervous system, the receptor-operated calcium entry (ROCE) is activated by binding of ligands (e.g. hormones, neurotransmitters) to the receptors in the plasma membrane. For instance, a rapid transient depolarization of neurons can be activated by Ca^{2+} from ER stores while a larger and long-acting depolarization of neurons can be activated via transient receptor potential (TRP) channels through ROCE mechanisms. Usually the metabotropic receptors such as metabotropic glutamate receptors or muscarinic receptors are coupled to G proteins and are organized with the canonical seven transmembrane domains in CNS. Ca^{2+} signals are generated through the activation of signaling cascades involving PLC and adenylyl cyclase (AC). They are widely expressed and present in CNS and peripheral neurons. For instance, mGluR1 is the most abundantly expressed metabotropic receptor in the mammalian CNS [120]. In this study, TRP channels are one of the topics studied as a part of ROCE to understand the Ca^{2+} signaling mechanisms in neurons and SGCs of the autonomic ganglia.

The TRP channels are expressed in a wide range of tissues and in both excitable and non-excitable cells. They constitute a unique class of channels that can modulate the intracellular Ca^{2+} concentration either by acting as a direct Ca^{2+} entry or by indirectly

causing membrane depolarization which subsequently activates the voltage-dependent ion channels such as VGCCs. They are tetramers with six transmembrane domains per subunit. Twenty-eight TRP channel subtypes are identified in mammals and are categorized into six different subtypes: TRPC (canonical), TRPV (vanilloid), TRPM (melastatin), TRPA (ankyrin), TRPML (mucolipin), and TRPP (polycistin) [121]. Although well-known as a part of ROCE, TRPC is also related to SOCE since ORAI1 has been proposed to interact with TRPCs. However, in comparison to SOCE, TRPC channels have small conductance with different calcium modulatory mechanisms [122]. The ROCE channels usually refer to TRP channels. Some TRPCs can also be activated by G-protein stimulation either directly (TRPC 4 and TRPC5) or indirectly by the by-product DAG (TRPC3 and TRPC6) [123, 124]. Other TRPCs can be activated by ER calcium store depletion [125].

TRPC1 was the first member of the TRPC family to be discovered demonstrated by electrophysiological measurements as a calcium-permeable channel [126]. TRPC1 can be activated by IP_3 or thapsigargin to deplete ER stores. TRPC1 current was measured with a conductance of 16 pS. TRPC1 current was often described as *I*crac despite the fact that the current was not Ca^{2+}-selective [127]. TRPC3 and TRPC6 form non-selective cation channels that the current-voltage relationships for these TRPCs demonstrated with larger outward current with a reversal potential at 0 mV. TRPC3 could also be activated directly by DAG analogues [123]. TRPC6 is known to be a DAG-activated channel and is very similar to TRPC3 with conductance of 35 pS [123]. Unlike TPRC3, TRPC6 can also be enhanced by TRPC channel blocker flufenamic acid [128]. Including TRPC3 and TRPC6,

all TRPC channels can be blocked by SKF96365 and lanthanides (e.g. La^{3+}) [129].

Of the seven subtypes of TRPCs, TRPC1 is widely known to be part of SOCE channel in many cellular systems such as exocrine glands, epithelial cells [130], and smooth muscle, as TRPC1 has been reported to directly interact with STIM and Orai channels [131-134]. STIM1 is also known to form heteromers with other TRPC1 channels to indirectly regulate TRPC3 and TRP6 [135]. Although it is still controversial, many studies have reported that TRPCs act as a part of SOCE machinery in some cells and further studies are needed to explore the regulatory role of TRPCs in SOCE. Briefly describing the participation of TRPCs in SOCE, the inactivated form of TRPCs are supposedly stabilized by Orai proteins. The metabotropic GPCR stimulation will release the Orai from TRPC, activating TRPCs for Ca^{2+} permeability. Consequently, STIM1 is activated to co-localize with Orai in the ER-plasma membrane and cytosolic Ca^{2+} is restored upon ER Ca^{2+}stores depletion (Fig.2) .

Many TRPCs are reported to be associated with cardiac functions [136-139]. As mentioned earlier, TRPC1 has been reported to be a part of SOCE machinery and plays a wide range of physiological roles in many types of cells such as cardiac cells and neurons [134, 140]. Similar to TRPC1, TRPC3 is most widely studied in hypertensive diseases as it causes hypertrophy in vascular structures such as the heart through the nuclear factor of activated T cell signaling pathway [141-143]. TRPC4 is reported to regulate the vascular tone [144]. TRPC5 and TRPC6 are important for endothelial cell migration while they are detected in other tissues such as brains [145, 146]. TRPC is abundantly present in the dorsal root ganglia (DRG) neurons in the fields of pain studies [147-149]. Of 7 subtypes of TRPCs,

TRPC1/3/6 are present in the sympathetic ganglia.

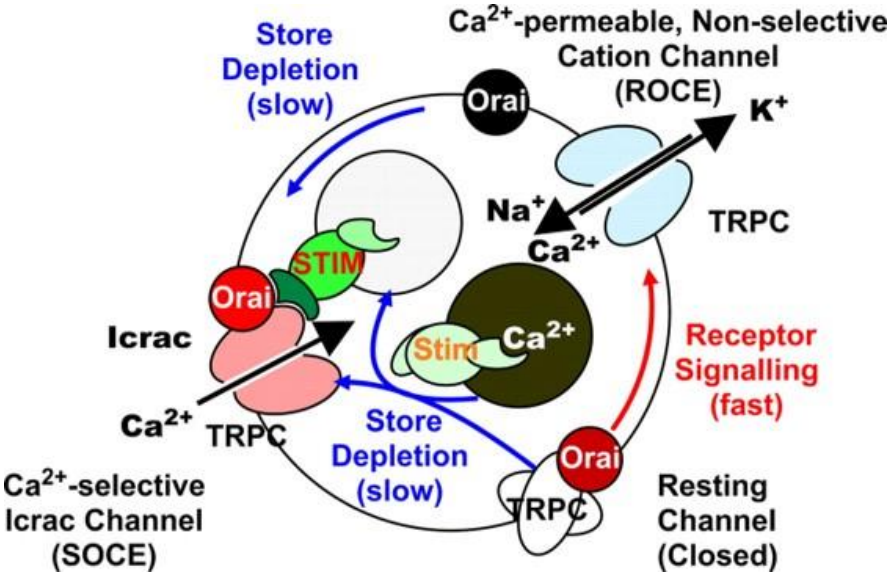

Figure 2. Schematic diagram of subunits of TRPC and Orai complexes regulated by STIM. Inactivated form of TRPCs are supposedly stabilized by Orai proteins. Gq/11 stimulation will free the Orai from TRPC, subsequently activating TRPCs for Ca^{2+} permeability. As the ER Ca^{2+}stores are depleted, STIM1 is activated to co-localize with Orai in the ER-plasma membrane microdomain. Cytosolic Ca^{2+} is restored and the cycle resets until the next stimulation. Diagram is adopted from Liao et al. [150].

1.5. Purinergic signaling in the ANS

The presence of purinergic receptors has been intensively studied in sympathetic ganglia [151-153]. For instance, both ionotropic P2X and metabotropic P2Y receptors are widely present in presynaptic and postsynaptic sympathetic nerves [154, 155]. Upon preganglionic stimulation, co-release of ATP and Ach in rat SCG was well reported [156]. A similar set of P2 receptors and the effects of ATP are observed in parasympathetic ganglia [152]. However, there are differences in the expression levels of P2 subtype receptors, and the effects evoked by ATP can be variable in multiple cellular processes.

Purinergic signaling is crucial in the modulation of the ANS. As mentioned earlier, ATP is the key functional player to be co-released with other neurotransmitters such as NE or NPY to affect the terminal target tissues (Fig. 3) [157, 158]. Under physiological and pathological situations, the multiple co-transmitters with ATP can be variably controlled to regulate the sympathetic tones of the bodily system, and this is possible because there are diverse subtypes of purinergic receptors to control sympathetic functions [152]. Purinergic signaling is pivotal in the autonomic cell-to-cell communication. As demonstrated in hypertensive rat models, the dysregulated sympathetic system is closely related to the systemic diseases. Alterations in the regulation of sympathetic ATP metabolism and ATP signaling pathway in the sympathetic nervous systems may ultimately result in higher cardiovascular risk with autonomic dysfunction [159]. These findings further suggest the possible involvement of the extra-synaptic purinergic communications of sympathetic neuron-SGC units in controlling sympathetic tones at the peripheral ganglionic level.

1.5.1. ATP in neuro-glial communication

Neural communications no longer belong extensively to neurons. Synaptic transmissions in the CNS and PNS can be affected by the microenvironment of neurons. The electrical stimulation to a neuron produced action potentials and caused neuronal depolarization not only to itself but also to the adjacent neurons [160]. This indicated the release of some unknown mediators from the depolarized neuron to the adjacent resting neurons. Neuronal activity triggered Ca^{2+} signaling in glial cells as well. In PNS, evoked Ca^{2+} signaling was observed in Schwann cells when co-cultured with neurons [161]. Possible mechanisms include the activation of metabotropic receptors (e.g. muscarinic and P2Y receptors) with a subsequent IP_3-induced Ca^{2+} release or by the activation of Ca^{2+}-induced Ca^{2+} release after depolarization through VGCCs. Changes in glial Ca^{2+} signals may subsequently alter the functional features of the cell by affecting the expression levels of glial transporters and channels as well as glial phenotypes [162, 163].

Now, accumulating evidences suggest that SGCs of PNS can also contribute to participate in the active cross-talk with soluble molecules between neurons and SGCs via purinergic receptors and by gap junctions [40, 164, 165]. This “cross-talk” effect was greatly enhanced under pathological conditions with nerve injury or inflammation with upregulation of gap junction proteins in SGCs [64, 164]. Ca^{2+} wave propagation among the SGCs further confirms the coupling of cells with active communication via chemical release such as ATP [166]. These observations continuously demonstrated that gap junctions, ion channels, and

receptors in SGCs are important players in the “coupled” activation as a part of neuro-glial communication. The underlying mechanism of this synergistic activation is not fully investigated; thus, more intensive studies are underway to find the roles of SGCs in the neuro-glial communications in the autonomic neural network.

This activity-dependent neuron-glia signaling is mediated by various extra-synaptic sources. The extra-synaptic release of neurotransmitters, growth factors, or even gliotransmitters is vital to regulate the neuronal excitability during the synaptic transmission as well as to control the glial cell proliferation and maturation under physiological and pathological conditions. Ca^{2+} imaging techniques have shown that neuronal depolarization causes the release of ATP from neuronal soma and axons, subsequently affecting the synchronous increase in cytosolic Ca^{2+} in the nearby SGCs of DRG [167]. Many evidences have revealed that neuronal somatic release seem to occur in a Ca^{2+}-dependent manner and appears to require the neuronal depolarization by VGCCs [168-171]. Again, the purinergic communications between sympathetic postganglionic neurons and the surrounding SGCs as well as the interstitial microenvironment expand many fields of research to study the potential roles of neuron-SGC units in autonomic function.

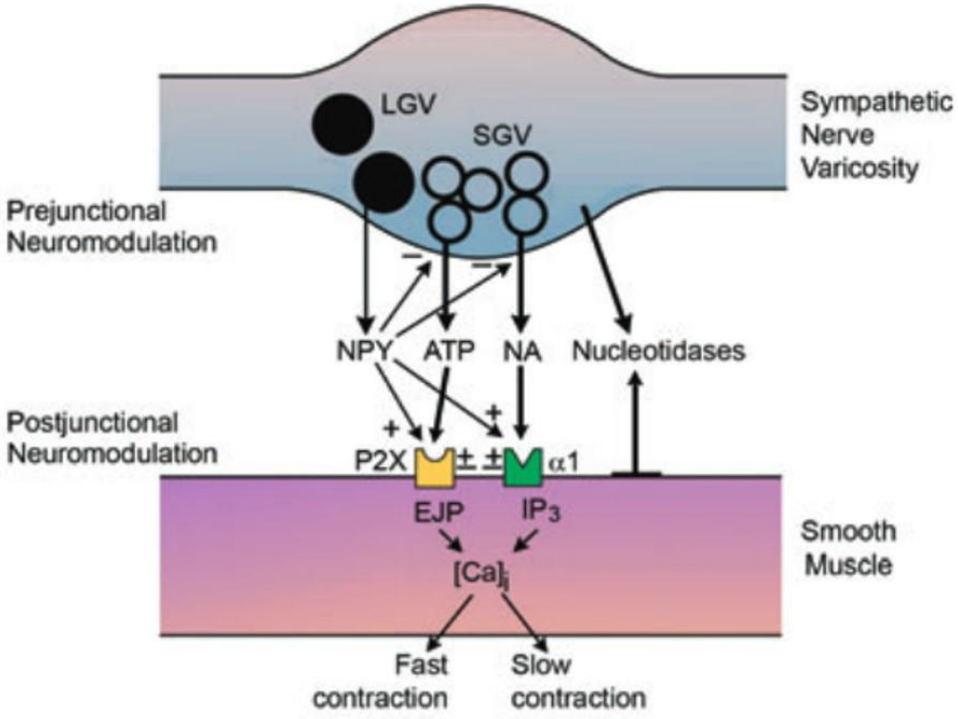

Figure 3. Neurotransmitter release from the sympathetic nerve variosity. This schematic diagram illustrates the sympathetic co-transmission. Neuropeptide Y (NPY) and noradrenaline (NA) as well as ATP are packed in vesicles being ready to be released to act as either activating modulators or inhibitory modulators in the sympathetic nerve terminal endings. Adopted from Burnstock [157].

1.5.2. Purinergic receptors

Purinergic receptors are largely divided into two groups: P1 and P2 receptors. While P2X receptors are ionotropic, P1 and P2Y are known to be metabotropic receptors which require GPCR activation. Both types of purinergic receptors can co-exist in the same cell type. For instance, ATP released during synaptic transmission activates astrocytic calcium signaling via P2X receptors, and also causes the propagation of Ca^{2+} waves in the neighboring astroglia through the activation of metabotropic P2Y receptors [79]. The Ca^{2+} signaling is strictly coordinated together where P2X receptor regions in charge of controlling the rapid astrocytic signaling processes while P2Y receptors mediate long-term calcium signaling effects many cellular processes. The purinergic receptor types are summarized in Fig. 4.

Four different P1 receptor subtypes: A_1, A_{2A}, A_{2B}, and A_3. Polymorphic variations have been reported in A_1 and A_{2A} receptors [172]. P1 receptors are activated by coupling with adenylyl cyclase (AC). A_1 and A_3 receptors are negatively activated by AC while A_2 receptors are positively regulated by AC [173]. The mechanisms of P1 receptor activation is summarized in Fig. 4. P1 receptors mediate various physiological regulations in CNS as well as other organ systems [174, 175].

Ionotropic P2X receptors are composed of seven different subtypes (P2X1-7), all of which are ligand-gated ion channels activated by ATP. In the nervous system, these receptors are widely present in different cell types [176]. P2X receptors have high Ca^{2+} permeability. The permeability of P2X2, P2X4, and P2X7 is higher, with large pores that allow large cations and macromolecules passing through the receptor while cells are exposed to ATP

for a longer term. For instance, P2X7 receptors can undergo conformational change to allow the influx of macromolecules larger than the size of 700 kD after ATP exposure .

P2X receptors are activated by ATP with an inward flux of sodium and calcium ions. An increase in the cytosolic Ca^{2+} upon the activation of P2X receptors switch on various intracellular signaling pathways for neurotransmitter release, cell migration, and cytokine release in many neural cells including Schwann cells [82, 152, 177-179]. The consequent Ca^{2+} entry initiates the release of growth factors and cytokines. A high concentration of cellular ATP can result in the hyper-activation of P2X receptors causing cell death [180]. Many studies on the identification and functions of P2X receptors in central and peripheral glial cells are still on-going. All seven subtypes are expressed in the peripheral glial cells while the functions of P2X7 receptors are mostly studied in pathological conditions (e.g. inflammation, cancer) where receptor expressions are usually upregulated. Using Ca^{2+} imaging techniques and electrophysiological studies with patch clamp techniques, the functional roles of P2X receptors in different types of glial cells can be extensively studied.

P2X1 and P2X3 receptors have the highest apparent affinity for ATP as they can activated at low ATP concentrations (as low as 1 μM) [181, 182]. In contrast, P2X7 receptors have low apparent affinity [183]. The kinetics of the P2X receptors are variable [184]. The activation of P2X1/2/3/4 receptors are rapid compared to P2X7 receptors. The desensitization is faster in P2X1 and P2X3 receptors while it is slower in P2X receptors. The channel activities of P2X receptors have different conductance: approximately 12 pS (P2X1), 26 pS (P2X2), 6 pS (P2X3), 13 pS (P2X4), less than 6 pS (P2X5), and 12 pS

(P2X7). P2X2 and P2X4 receptors can substantially increase the opening of channel pores [185]. ATP is a pan-purinergic agonist for P2X receptors. For functional studies of P2X receptors, many agonist and antagonists have been developed to differentiate the activities of different receptors. However, traditionally trace metals were used as allosteric modulators to segregate the functions of P2X receptors before the introduction of synthetic purinergic agonists or antagonists [186]. For instance, compared to other P2X receptors, P2X4 receptors are desensitizing ion channels and they are activated by ATP and 2'(3')-O-(4-Benzoylbenzoyl)-adenosine-5'-triphosphate (BzATP) [187]. Pharmacologically P2X4 receptors can be potentiated by ivermectin (IVM) [188]. IVM increases the ATP current by shifting the EC_{50} and changes the desensitization state of the receptor [189]. In contrast, P2X7 is a non-desensitizing ion channel activated by both ATP and BzATP [187]. P2X7 receptors need high concentrations of ATP to be activated with large pore. Cadmium, zinc, and copper are known to be negative allosteric modulators of P2X7 receptors [190] (Fig. 5).

The P2Y receptors are metabotropic GPCRs and there are eight subtypes: P2Y1/2/4/6/11/12/13/14. The agonist for P2Y receptors differs depending on the subtypes (i.e. ATP, adenosine diphosphate (ADP), uridine-5'-triphosphate (UTP), and uridine-5'-diphosphate (UDP)) (Fig. 4) [191]. All P2Y receptors were reported to be expressed in rat and mouse peripheral glial cells playing major roles in cell death and cellular signaling [176, 186, 192, 193]. For instance, P2Y4 receptor is expressed in the neurons of sensory ganglia [194] while P2Y12 and P2Y14 receptors are reported to be expressed in rat SGCs

mediating cytokine secretion [195-198]. Of many P2Y receptors, I discovered that P2Y1 receptor appeared to be abundantly expressed in rat sympathetic ganglia. P2Y1 receptors are Gq-protein coupled and activated by ADP as well as by 2-methylthio-ADP (2MeSADP) [199]. Selective P2Y1 receptor antagonists have been developed such as MRS2179.

Purinergic Receptor Type	Main signaling mechanism	Agonist	Antagonist
P1	**A1** (Perussis toxin-sensitive Gαi proteins, low adenylate cyclase activates PKC) **A2A** (Cholera toxin-sensitive Gαs proteins, high adenylate cyclase activates PKA) **A2B** (Gαs proteins and Gq proteins, either PKA or PKC can be activated) **A3** (Gi proteins, low adenylate cyclase activates PLC and PKC) All P1R use **cAMP** as second messengers	**Adenosine** 2-chloriadenosine (non-selective) CV1808 (A1 selective) CGS21680 (A2 selective) MRS5698, MRS5841(A3 selective)	Methylxantines Pyrimidine- and pyridine-based inhibitors
P2X	**P2X1-7**: Ligand-gated ion channels for mono- and di-valent cations such as Ca^{2+}	**ATP** Aβ-meATP (P2X1) Ivernectin (P2X4, positive allosteric activator) BzATP (P2X7, partial agonist for P2X4 and P2Y1)	Suramin, PPADS TNP-ATP 5' BDBD (P2X4) oATP (P2X7) A438079 (P2X7)
P2Y	**P2Y1/2/4/6** (Gq/11 proteins, PLC activates PKC) **P2Y11** (Gs or Gq/11 proteins, PKA or PKC activation) **P2Y12/13/14** (Gi/o, low adenylate cyclase activates PLC and PKC or PLA_2 activates arachidonic acid)	**ATP, ADP, UTP, UDP** P2Y1: ADP, 2-MeS ADP, BzATP (partial agonist) P2Y2: UTP, ATP P2Y4: UTP P2Y6: UDP P2Y11: ATP, UTP P2Y12/13: ADP, ATP P2Y14: UDP-glucose	Suramin MRS2179 (P2Y1) MRS2578 (P2Y6) NF157 (P2Y11) AR-C 66096 (P2Y12) MRS2211 (P2Y13) PPTN (4,7-disubstituted 2-naphthoic acid derivative, potent blocker of P2Y14)

Figure 4. Summary of purinoreceptors. There are three major subtypes of receptors: P1, P2X, and P2Y receptors. Main signaling mechanisms vary in different tissues and cells. P2X receptors are ligand-gated ion channels while P1 and P2Y receptors are G-protein mediated receptors. P1 receptors primarily use cAMP as a second messenger while P2Y receptors use Ca^{2+} and cAMP as a second messenger (This table is produced by the author based on the literature reviews.) [151-153, 158].

A

Effects of allosteric modulators on homomeric P2X receptors

Modulators	P2X1R	P2X2R	P2X3R	P2X4R	P2X5R	P2X7R
Zinc(μM)	1: inhibition	30: potentiation[a, b]	10: potentiation[a]	5: potentiation[a]	10: potentiation[a]	80: inhibition
Copper (μM)		3: potentiation[a]		10: inhibition		2: inhibition
Cadmium (μM)	inhibition	3: potentiation[a]	inhibition	20: potentiation		100: inhibition
Mercury*(μM)		3: potentiation[a]		10: inhibition		10: inhibition
Protons (pH)	6.3: inhibition	7.3: potentiation	6.0: inhibition	7.0: inhibition	inhibition	6.1: inhibition
H_2O_2 (mM)		0.3: potentiation		1: inhibition		
Myxothazol (mM)		0.3: potentiation				
Rotenone (mM)		0.3: potentiation				
Mercury**(μM)		3: potentiation[a]		10: inhibition		
CO		potentiation	no effect	inhibition		
IVM (μM)		no effect	no effect	3: potentiation		no effect

B

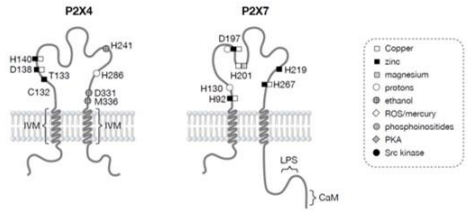

C

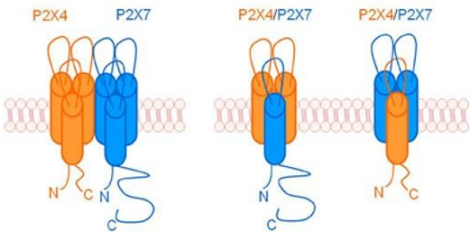

Figure 5. Differential comparison of P2X4 and P2X7. (A) The effects of allosteric modulators are analyzed to pharmacologically differentiate the types of P2X receptors. Table is adopted and modified from Coddou et al. [190]. (B) A Schematic representation of ways in which P2X4 and P2X7 may interact. (C) Individual P2X4 and P2X7 homotrimers physically associating with one another, possibly via C-terminal tail interactions or intermediate scaffolding proteins. P2X4 and P2X7 subunits forming heterotrimeric receptors.

II. PURPOSES

2.1. Hypotheses

There is a functional communication through Ca^{2+}signaling between neurons and satellite glial cells, which plays a role as a functional unit in the peripheral sympathetic ganglia. Ca^{2+} influx can be mediated by many channels on the plasma membranes. Non-excitable cells, such as SGCs may have SOCE and ROCE for Ca^{2+} signaling.

When a neuron is electrically excited, it subsequently influences glial Ca^{2+} signaling. ATP may be released from a sympathetic neuron and mediates Ca^{2+} signaling in the neuron-attached SGC through the activation of purinergic receptors.

2.2. Objectives

The objective of this study is twofold. Firstly, it aims to identify major Ca^{2+} signaling pathways and their molecular components in sympathetic neurons and SGCs. Secondly, it aims to unravel the role of purinergic Ca^{2+} signaling as a part of sympathetic neuron-SGC communications.

(1) To characterize the Ca^{2+} signaling mechanisms underlying SOCE and ROCE in sympathetic neurons and SGCs

(2) To examine somatic ATP release in sympathetic ganglia and the purinergic signaling mechanisms involved in communication between neurons and SGCs

III. MATERIALS AND METHODS

3.1. Chemicals and stocks

A438079 (competitive P2X7 antagonist, 30 mM), Cyclopiazonic acid (CPA, SERCA blocker, 30 mM), GSK7975A (Orai1 inhibitor, 1 mM), Pyr3 (TRPC3 inhibitor, 10 mM), Pyr6 (SOCE blocker, 3 mM), and SAR7334 (selective TRPC6 inhibitor, 10 mM) were purchased from Tocris (Avonmouth, Bristol, UK). Adenosine triphosphate (ATP, 100 mM), BzATP (P2X7 agonist, partial agonist of P2X1/P2X4/P2Y1, 50 mM), cadmium chloride (non-selective VGCC blocker, 100 mM), carbamacholine (carbachol, M3 GPCR agonist, 100 mM), ivermectin (IVM, positive allosteric modulator of P2X4, 10 mM), lanthanum chloride (non-selective TRPC blocker, 100 mM), lipopolysaccharide (LPS, 2 mg/ml), MRS2179 (P2Y1 inhibitor, 30 mM), pyridoxal phosphate-6-azo(benzene-2,4-disulfonic acid) (PPADS, pan-P2X antagonist, 30 mM), quinacrine (10 mM), suramin (pan-P2 antagonist, 30 mM), and zinc chloride (positive allosteric modulator of P2X4, 10 mM) were purchased from Sigma-Aldrich (St. Louis, MO, USA).

3.2. Experimental Animals

All animal care and experimental procedures followed the National Institutes of Health Guidelines for Care and Use of Experimental Animals and were approved by the Institutional Animal Care and Use Committee of Yonsei University, Wonju College of Medicine (Approval No. YWC-181002-1). Six-week-old male Sprague-Dawley rats

obtained from DBL Co. (Eumseong-Gun, Republic of Korea) were kept under pathogen-free conditions with a 12:12 h light-dark cycle, temperature of 23 ± 2°C, and ad libitum access to food and water.

3.3. Preparation of sympathetic neuron-SGC units

SCG was harvested and dissected and enzymatically dissociated using some modifications of the previously described methods to obtain cell culture containing the sympathetic neuron-SGC units [200]. Briefly, the ganglia were isolated and the epineural sheath was removed, cut into small pieces, and transferred to Earle's balanced salt solution (EBSS, pH 7.4) (Sigma-Aldrich, St. Louis, MO, USA) containing 1.5 mg/ml collagenase type D (Roche, Diagnostics, Germany), 0.5 mg/ml trypsin (Worthington Co. Harrison, New Jersey, USA), and 0.1 mg/ml DNase type I (Sigma-Aldrich) in a 25-cm^2 tissue culture flask. The EBSS was modified by adding 3.6 mg/l glucose, 10 mM HEPES (Sigma-Aldrich), and 1% penicillin-streptomycin (PS) (HyClone, Logan, UT, USA). After bubbling with 95% O_2-5% CO_2, the flask was placed in a shaking water bath at 37°C for 45 min. Following incubation, DMEM (Gibco, Grand Island, NY, USA) with 10% fetal bovine serum (FBS) (HyClone) and 1% PS were added to the flask to inactivate the enzymatic acitivites. The ganglia were mechanically dispersed into a pool of partially dissociated cells by gentle trituration using a wide-bore fire-polished pasteur pipette. After centrifugation at 600 rpm for 6 min, dissociated cells were resuspended in the culture media. Then, as described previously [201], the myelin debris and small cell fragments were removed using a cushion

of 10% and 5% bovine serum albumin (Sigma-Aldrich). This step is critical for separating the partially dissociated neurons attached to the SGCs. The cells were subsequently plated on 12-mm cover glasses coated with poly-D-lysine (Sigma-Aldrich) and maintained in a humidified 95% air-5% CO_2 incubator at 37°C until use. The outline of methods to isolate and culture sympathetic neuron-SGC units is depicted in Fig. 6.

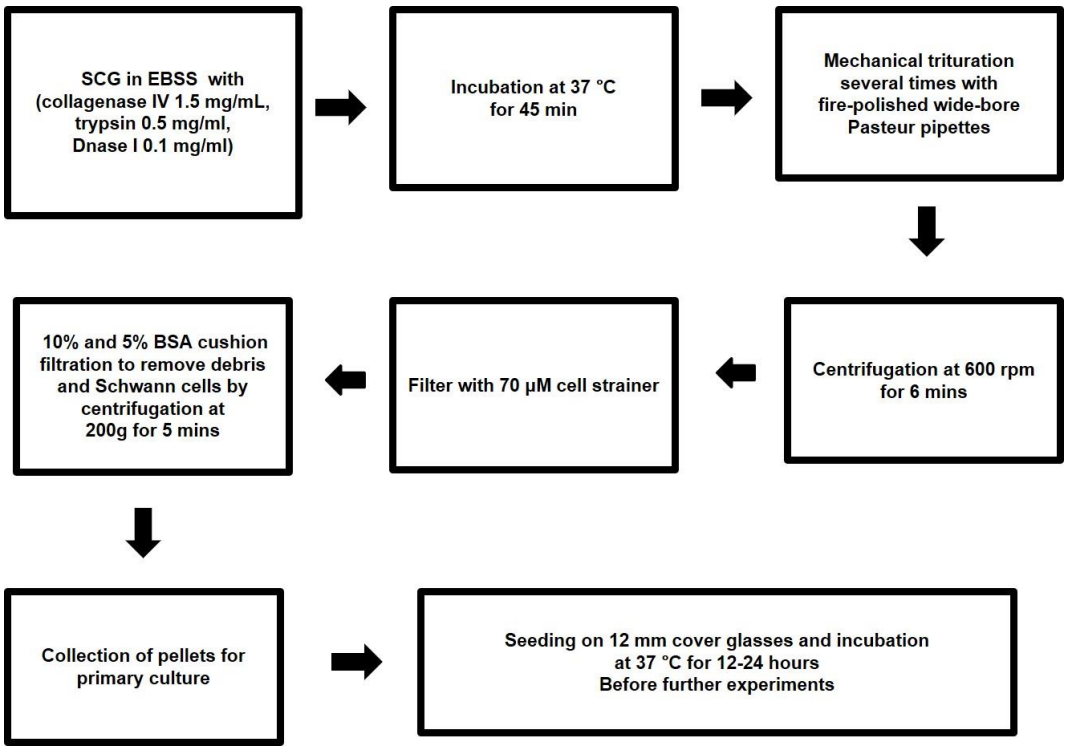

Figure 6. Experimental processes for obtaining the sympathetic neuron-SGC units.

3.4. Immunohistochemistry and immunocytochemistry

The animals were anesthetized with isoflurane (Troika, Gujarat, India) and perfused transcardially with phosphate-buffered saline (PBS) followed by 4% paraformaldehyde (PFA) (GeneAll Biotechnology, Republic of Korea) in PBS. Ganglia tissues were quickly harvested, post-fixed in 4% PFA for 6 hours at 4°C, then cryoprotected with 30% sucrose in PBS (Sigma-Aldrich) overnight at 4°C. SCGs were embedded in the Tissue-Tek OCT compound (Sakura Finetek, USA) in plastic molds and stored at -80°C. Frozen tissues were sectioned at 7 μm thickness on a crytostat (Leica CM1850, Leica Biosystem, Wetzlar, Germany), and attached to microscope slides (Fisher Scientific, PA, USA). For immunocytochemical studies of cultured neurons attached with SGCs, the cells were fixed with 4% PFA for 10 min at 4°C. The tissue or cultured cell samples were washed with PBS, blocked with 5% normal goat serum (Jackson ImmunoResearch, PA, USA) for 1 h at room temperature (RT) to prevent non-specific binding, and incubated overnight with the appropriate primary antibodies. The primary antibodies used are rabbit Kir4.1 (1:500, Alomone Labs, Israel), mouse Orai1 (1:200, Novus International, MO, USA), rabbit STIM1 (1:200, Cell Signaling Technology, MA, USA), mouse toll-like receptor 4 (TLR4) (1:300, Santa Cruz Biotechnology, TX, USA), and mouse glial fibrillary acidic protein (GFAP) (1:300, Santa Cruz Biotechnology, TX, USA). After washing with PBS, the samples were incubated with goat anti-rabbit/mouse AlexaFluor488 (1:400, Invitrogen, MA, USA) or goat anti-rabbit/-mouse AlexaFluor594 (1:400, Invitrogen) for 1 hour at RT. After secondary antibody incubation, the samples were counterstained for 5 min with 4,6-

diamino-2-phenylindole dihydrochloride (DAPI) (1:1000) (Sigma-Aldrich) to stain the nuclei. After washing steps, the samples were mounted onto glass microscope slides with Vectashield antifade mounting medium (Vector Laboratories, CA, USA). For negative controls, all staining procedures were performed in the absence of primary antibodies. The immunofluorescent images were) images were acquired by using a Zeiss LSM800 confocal laser scanning microscope at high magnification (10x objective, NA 0.45; 20x objective, NA 0.8) controlled by ZEN2.3 software (Zeiss, Oberkochen, Germany).

For hematoxylin and eosin (H&E) staining, paraffin-embedded ganglionic tissues were prepared and sectioned at 4μm. The staining was performed at RT using 0.1% hematoxylin (Fisher Scientific) for 5 min and 0.4% eosin (Sigma-Aldrich) for 75 s. Neuronal counterstain of SCG sections were visualized with 0.125% thionin (Sigma-Aldrich) staining for 4 mins at RT. Bright-field micrographs of H&E staining were captured using a 20x objective on an Olympus BX51 microscope (Olympus, Japan).

3.5. Image analysis

Confocal images including differential interference contrast (DIC) images were acquired by using a Zeiss LSM800 confocal laser scanning microscope at high magnification (10x objective, NA 0.45; 20x objective, NA 0.8) controlled by ZEN2.3 software (Zeiss, Oberkochen, Germany). For image processing and quantification of Orai1-positive puncta, the open-source software ImageJ (version 1.54, http:imagej.nih.gov/ij, NIH, USA) was used[202]. The background noises were removed using a Gaussian blur filter (sigma = 1).

The images were made binary using the Otsu threshold method, and the puncta were counted using the “Analyze Particles” function in ImageJ.

3.6. Reverse transcription polymerase chain reaction (RT-PCR)

After a short sonicating homogenization of a whole sympathetic ganglion, total RNA of a tissue sample was extracted by using Hybrid-R Total RNA purification kit (GeneAll, Seoul, Korea) following the manufacturer’s instructions. 500 ng of complementary DNA (cDNA) was synthesized by applying ReverTraAce qPCR RT Master Mix with genomic DNA Remover (Toyobo, Osaka, Japan). The PCR amplification was carried out with AccuPower HotStart PCR Premix (Bioneer, Daejeon, Korea). RT-PCR experimental condition was as follows: denaturation for 3 min at 95℃ and 30 cycles of 95℃ for 30 sec, 60℃ for 30 sec, and 72℃ for 1 min, then, ended with an extension step at 72℃ for 5 min. Final PCR products were confirmed and analyzed with 2% agarose gel electrophoresis. The PCR primers used are listed in Table 1-4.

3.7. Semi-quantitative real-time polymerase chain reaction (qPCR)

Total RNA was extracted from SCG using TRIzol Reagent (GeneAll Biotechnology). RNA quantity and purity were assessed using spectrophotometry. 500 ng of cDNA was synthesized with the same method section 3.5. Parallel reactions without reverse transcription were performed to confirm the absence of genomic DNA amplification. Using QuantStudio Real-Time PCR System (Applied Biosystems, MA, USA), SybrGreen-based

real-time semi-quantitative PCR was initiated with an initial denaturation step of 96°C for 5 min, followed by 40 cycles of 96°C for 30 s, 57°C for 30 s, and 72°C for 2 min. The threshold cycle for each gene was determined and analyzed using the relative quantitation software. The relative expression of the target genes was calculated using the $2^{-\Delta\Delta CT}$ method. The mRNA levels of the genes of interest were normalized to those of housekeeping gene GAPDH or beta-actin. Tables 1-4 present the primer sequences used for qPCR.

Table 1. Primer sequences used for PCR analysis of Orai, STIM, GFAP, and TLR4

Gene	Primer Sequence (F: Forward / R: Reverse)	Size product (bp)
GAPDH	**F:** CATCACTGCCACTCAGAAGACTG	**153**
	R: ATGCCAGTGAGCTTCCCGTTCAG	
Orai1	**F:** ACCGGGCACCCACTATGC	**140**
	R: ACTCTGCCCTGGTGAAGCCAG	
Orai2	**F:** TCCACCATCATCATGGTAC	**162**
	R: CACCTGTAGGCTTCTCTC	
Orai3	**F:** GCCCAGCTTTAGACTGTTGC	**126**
	R: CTGAGCAGGAATTTGGCTTC	
STIM1	**F:** ATGCCAATGGTGAATGTGGAT	**97**
	R: CCATGGAAGGTGCTGTGTTT	
STIM2	**F:** ACGGAAACCAAGAGCATG	**199**
	R: CGTGCGGGATGCTGCCTAC	
GFAP	**F:** CCAGATCCGAGAAACCAGCC	**88**
	R: CCGCATCTCCACCGTCTTTA	
TLR4	**F:** TCATGCTTTCTCACGGCCTC	**142**
	R: AGGAAGTACCTCTATGCAGGGAT	

Table 2. Primer sequences used for PCR analysis of the expression of TRPCs

Gene	Primer Sequence (F: Forward / R: Reverse)	Size product (bp)
Beta-actin	**F:** CTCTGTGTGGATTGGTGGCT	**122**
	R: AGCTCAGTAACAGTCCGCCT	
TRPC1	**F:** TTGGTTCGGACAGATGTCAGG	**431**
	R: TGTGAGCCACCACTTTGAGGG	
TRPC3	**F:** AAAGGCTATGTGCGCATCGTG	**225**
	R: GCCTTTGCTTCTCAGCACAGTC	
TRPC4	**F:** CCTCTCAGCACATCGACAGGT	**280**
	R: GGCAGTGAACAGAAGATCAGG	
TRPC5	**F:** GTGAGGACCCTATCCTCACAG	**184**
	R: CCAGGTCATGGTACTTCTGTGG	
TRPC6	**F:** GTGCATACCCTCCTGAGAAAGG	**276**
	R: CTTGCACTGCATGGACAGCT	
TRPC7	**F:** AGAGGTCACTGAACTGCTGCTG	**287**
	R: CCTTGAGCAGCAGGATGTGTAC	

Table 3. Primer sequences used for PCR analysis of the expression of Kir4.1 and P2X receptors

Gene	Primer Sequence (F: Forward / R: Reverse)	Size product (bp)
Kir4.1	**F:** TCCACCTCTGTGCCAAGATGA	**156**
	R: TGCTCCATTCTCACGTTGCTC	
P2X1	**F:** GCTTTCCACGCTTCAAGGTC	**141**
	R: TGACTCTCGCACCACATAGC	
P2X2	**F:** TGGGACTACGAGACGCCTAA	**138**
	R: CTCGCTGTCCTGGTAGCTTT	
P2X3	**F:** GGCACCTCTGTCTTTGTCATCA	**105**
	R: ACACAGCGGTACTTCTCTTCA	
P2X4	**F:** CTCATCCGCAGCCGTAAAGT	**101**
	R: TTTTCCCACACGAACACCCA	
P2X5	**F:** TCAAGGGGGTGGCCTATACT	**148**
	R: AGGAGTCACGATCAGGTTGG	
P2X6	**F:** GTACAGCCGTGGCTGAAGTT	**136**
	R: CAGAAACCCCCAGCTCACTA	
P2X7	**F:** CGGTGTGCTTTCTTCGGCTA	**135**
	R: ACAGGCTCACTCTGTTTCGG	

Table 4. Primer sequences used for PCR analysis of the expression of P2Y receptors

Gene	Primer Sequence (F: Forward / R: Reverse)	Size product (bp)
P2Y1	**F:** GATGAATTTGAGGGCACGGC	**147**
	R: AAGAATGGGGTCCACACAGC	
P2Y2	**F:** GGAGATGACGGGGACCTAAAG	**142**
	R: GGGACAGAGTCACGTAATGGG	
P2Y4	**F:** GTCATCTTCTCGGCTCCGTT	**131**
	R: ATTGTGCGGGTGATGTGGAA	
P2Y6	**F:** GGGATAGGGGACAGGATCTCT	**150**
	R: CTCCCTCTCAGCCTCAAGCTA	
P2Y12	**F:** GTTCCCTTCCACTTTTGCACG	**113**
	R: AGGGTGCTCTCCTTCACGTA	
P2Y13	**F:** TGCACTTTCTCATCCGTGTT	**107**
	R: ACGGTACGACGATCTTGAGG	
P2Y14	**F:** GCAATTCTCACCCTTTCCAAGT	**98**
	R: TACTTTTCTGCGTGCTGTAGAC	

3.8. Western blot analysis

Whole ganglia of SCGs were harvested and homogenized in RIPA Lysis and Extraction buffer (Thermo Fisher Scientific) supplemented with Halt Protease Inhibitor Cocktail (Fisher Scientific) with a brief sonication. Then, the tissue solution was incubated for 20 min in ice. The lysates were centrifuged at 13,000 rpm for 20 min at 4°C to remove insoluble materials, and the supernatant with protein content was collected for further experiments. Protein levels were quantified using the Bradford assay kit (Coomassie Protein Assay Reagent, Thermo Fisher Scientific). 60 - 80 μg of the sample was electrophoresed on an SDS-polyacrylamide gel (8-10%) and transferred onto a nitrocellulose (NC) membrane (Bio-Rad Laboratories, Germany). The membrane was blocked with 0.1% Tris-buffered saline/Tween-20 (TBST) containing 5% skim milk (Santa Cruz Biotechnology) for 1h at RT and then incubated overnight at 4°C with primary antibodies against STIM1 (1:3000), Orai1 (1:1000), toll-like receptor 4 (TLR4) (1:1000), GFAP (1:1000), and GAPDH (1:10000). After washing with 0.1% TBST, the membranes were incubated with the secondary (1:2000) goat anti-mouse or anti-rabbit IgG (H+L) secondary antibody, horseradish peroxidase (HRP)-conjugated (Thermo Fisher Scientific) for 90 min at RT. After intense washing, immunoreactive bands were visualized on the NC membrane using an ECL detection reagent (Amersham, Little Chalfont, UK, no. RPN2235/2232) and Chemi Doc XRS+ imaging system (Bio-Rad Laboratories). The optical densities of the immunoreactive bands were quantified using the program Image Lab 5.2.1 (Bio-Rad Laboratories) and normalized to the loading control.

3.9. Calcium imaging with Fura-2/AM

The partially dissociated cells on glass coverslips were loaded with 2.5 μM of Fura-2-acetoxymethyl ester (Fura-2/AM) (Thermo Fisher Scientific) for 45 min at 37°C in the culture medium, and subsequently washed with normal physiological salt solution (NPSS). The coverslips were then transferred to a perfusion chamber (Warner Instrument, Hamden, CT, USA) on a TE2000 fluorescence microscope (Nikon, Kanagawa, Japan) equipped with a ratio fluorescence system (RatioMaster; Photon Technology International Inc., Lawrenceville, NJ, USA). Cells were constantly perfused at 1 ml/min with an NPSS containing: NaCl 135 mM, KCl 4.5 mM, $MgCl_2$ 1 mM, $CaCl_2$ 2 mM, HEPES 10 mM, and glucose 10 mM (pH 7.4, 289 - 295 mOsm). Cells loaded with Fura-2/AM were alternatively excited at 340 and 380 nm, and the emitted light (510 nm) was captured after filtration using a CCD imaging instrument composed of Lambda DG-4 (Sutter instrument Inc., CA, USA) and CoolSNAP CCD (Cascade, Roper Scientific Inc., Tucson, AZ, USA). Felix software for RatioMaster and Metafluor (V 6.1, Universal Imaging Gorp., West Chester, PA, USA) for CoolSNAP CCD were used for data acquisition and analysis (Fig. 7). The area under the curve (AUC) of the traces of Ca^{2+} changes during SOCE (AUC SOCE) was calculated for further comparative analysis.

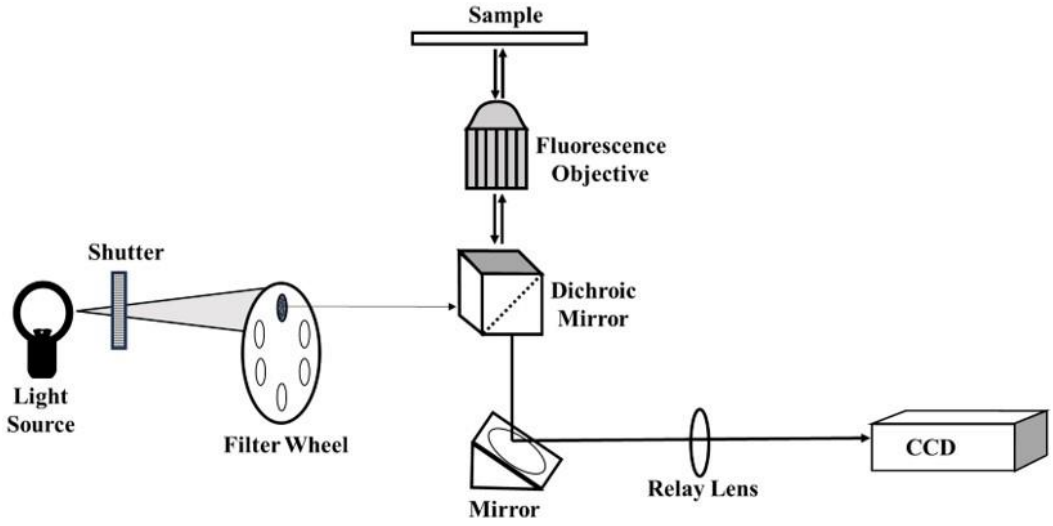

Figure 7. Charge-coupled device imaging instruments for measurement of intracellular Ca^{2+} concentration and membrane potential change.

3.10. Quantitative bioluminescence assay of somatic ATP release

The extracellular ATP concentrations *in vitro* was measured using Luciferin-luciferase based ATP bioluminescence assay, following the manufacturer's manual (ATP Bioluminescence Assay Kit CLS II, Roche, Mannheim, Germany). To prevent the extracellular ATP degradation, test samples were consistently kept on ice except during the ATP measurement process. The ATP content released from the cell populations (1×10^4) cells *per* culture well was assessed in a flat bottom black 96-well plate (Corning Costar, Sigma-Aldrich). According to the kit protocol, the calibration curve was optimized and prepared with ATP standards from 0 to 1.65 μM ATP. For each culture sample, 5 μL of supernatant and 45 μL of Tris/ EDTA buffer were pipetted in triplicates. Subsequently, 50 μL of luciferase was added by an automatic dispenser, followed by an immediate measurement of ATP luminescence. Bioluminescence readings of both the ATP standard calibration curve and samples were obtained using the FlexStation 3 Multi-Mode Microplate Reader (Molecular device, San Jose, CA, USA) at room temperature. The readings were performed in a kinetic method with one-minute cycles, totaling 5 cycles. The stabilized values of relative luminescence units (a.u.) from the final cycle were used to determine extracellular ATP concentration.

3.11. Real-time *in vitro* assay of vesicular ATP release using FM1-43 and quinacrine stain

FM 1-43 and quinacrine are fluorescent dyes which directly bind to vesicular structures.

They are commonly used in the study of vesicle cycling in neuroscience, providing valuable insights into the synaptic vesicle pools and the trafficking of neurotransmitter release [203, 204]. FM 1-43 exhibits binding to a broad range of vesicles, while quinacrine is more specific, binding to ATP and vesicles that contain ATP. Upon external stimulation, the quantification of fluorescent puncta and the observation of vesicle movement enable the assessment of neurotransmitter release and membrane dynamics.

As previously described [204-206], FM1-43 and quinacrine staining of ATP-containing vesicles were conducted with minor modifications. For live-cell imaging of vesicular ATP release, dissociated SCG neurons were incubated with either 5 μM of FM 1-43 or 10 μM quinacrine in culture media for 30 minutes, at 37℃. The cultures were then washed twice with NPSS for 10 minutes, and the neurons were immediately observed using a live cell imaging with Zeiss LSM800 confocal laser scanning microscope at high magnification (10x objective, NA 0.45; 20x objective, NA 0.8) controlled by ZEN2.3 software (Zeiss, Oberkochen, Germany). The real-time fluorescent images of SCG neurons with stained ATP vesicles was observed immediately before and after the perfusion of 80 mM KCl for 10 min at room temperature. The extracellular release of vesicular ATP from a neuron was quantified as the number of visibly stained puncta decreased upon high K^+ stimulation.

3.12. Preparation of the rat models of LPS-induced acute systemic inflammation

The LPS solution was prepared under sterile conditions with care and reconstituted in 0.9%

NaCl to a concentration of 2 mg/ml. The weights of the animals were recorded and the intraperitoneal injection of LPS (2 mg/kg) was performed carefully in the left lower quadrant of the abdomen, avoiding a needle injury to the internal organs. The control group received an injection of 0.9% NaCl in the same amount. Post-injection monitoring was conducted every 6 hours to assess the daily activities of the animals. Successful LPS models were confirmed by the appearance of the spiky furs with irritability, and discomforts, indicative of progressing endotoxemia.

3.13. Data analysis and statistics

Statistical analyses were performed using Prism 10.0 (GraphPad Software, Boston, MA, USA). Comparisons were made using Student's t-test and one-way ANOVA with Tukey's post-hoc test. Statistical significance was set at $p < 0.05$ indicated as: * $p < 0.05$, ** $p < 0.01$, *** $p < 0.001$. Data are presented as the mean ± SEM.

IV. RESULTS

PART I

Characterization of the Ca^{2+} signaling mechanisms underlying SOCE and ROCE in sympathetic neurons and SGCs

4.1. Identification of the neurons and SGCs of rat sympathetic ganglia

The H&E staining of a whole ganglia section revealed the morphologically unique location of SGCs around a large neuronal cell body (Fig. 8A). The previous studies have shown that the inwardly rectifying potassium channels Kir4.1 is an astrocyte and sensory SGCs-specific marker [207, 208]. Recently, single-cell transcriptome analysis has revealed that the mRNAs encoding Kir4.1 are expressed in the SGCs of mouse SCG [45]. Consistent with these findings, we observed that the Kir4.1-positive SGCs closely envelop the large principal neurons in the rat sympathetic ganglia (Fig. 8B). For the *in vitro* simultaneous imaging of Ca^{2+} signaling in both neurons and SGCs, we used the method of partial enzymatic digestion with a BSA-gradient centrifugation process [201] for acquiring a pool of pure neuron-SGC units from sympathetic ganglia. We observed that a single SCG neuron was associated with one or more Kir4.1 expressing SGCs (Fig. 9).

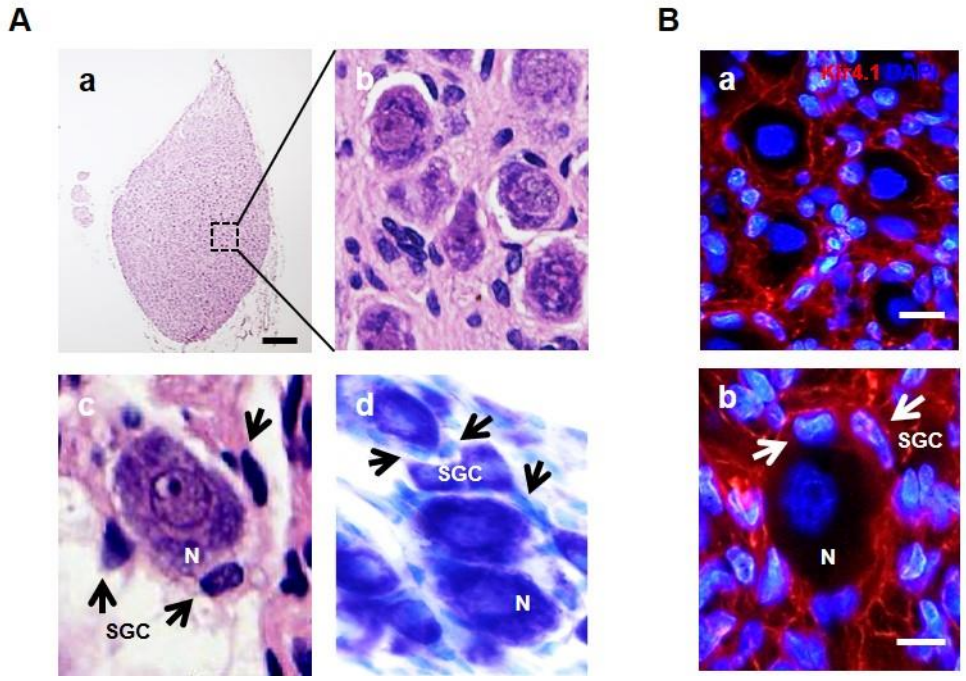

Figure 8. Immunohistochemical and immunofluorescent images of rat SCG. (Aa) H&E image of a whole SCG extracted from 6-week old male *Rattus norvegicus*. Scale bar = 200 μm. (A, b-c) Enlarged portion of ganglionic units. Histological morphology of large neuronal soma (N) and the surrounding small SGCs are seen (black arrows). (A, d) Nissl staining of the rodent SCG. Thionin dye is positive in the nissl bodies of large sympathetic neurons surrounded by small cells of SGCs. (B, a-b) Kir4.1 is one of the specific markers of SGCs. Kir4.1-positive SGCs are clearly noted (red, white arrows). Nuclear counter-stain was indicated with DAPI (blue). Large nuclei belong to sympathetic neurons while small nuclei indicate glial cells. Scale bar = 10 μm.

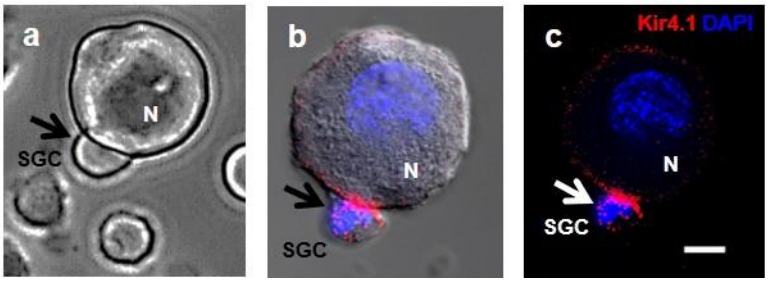

Figure 9. Identification of sympathetic neuron-SGC units. (a) Phase contrast image of a partially digested neuron (N) and SGC (black arrow) as a unit. (b) Differential interference contrast image of sympathetic neuron and SGC from superior cervical ganglion. (c) Kir4.1 is a glial specific marker and the immunofluorescent image of neuron-SGC unit clearly identifies the anatomic location of SGC attached to the sympathetic neuron. DAPI is used as a nuclear counter-stain. Scale bars = 10 μm.

4.2. Identification of the components of SOCE machinery in the neurons and SGCs of rat sympathetic ganglia

Quantitative real-time PCR analysis showed that the transcripts encoding all known SOCE components (Orai1, Orai2, Orai3, STIM1, and STIM2) were expressed in rat SCG (Fig. 10). Confocal images of immunofluorescence staining illustrated the presence of Orai1 and STIM1 in neurons and SGCs (Fig. 11A). When the ER Ca^{2+} store was depleted by 30 μM cyclopiazonic acid (CPA), an ER Ca^{2+} ATPase inhibitor, in the absence of extracellular Ca^{2+}, the Orai1- and STIM1-immunoreactivities were significantly increased on the plasma membranes of neurons and SGCs (Fig. 11A, *right panel*). The Orai1 channels were likely activated by the translocation and association of STIM1 [202]. We quantified the Orai1-immunoreactive puncta in neurons and SGCs. Compared with the control (vehicle [VEH]), CPA significantly increased the number of Orai1 puncta in SGCs (Fig. 11B) and neurons (Fig. 11C) ($p < 0.001$). On average, the number of Orai puncta before and after CPA treatment was 24 ± 1 (n = 50) and 49 ± 1 (n = 64), respectively in SGCs, and 107 ± 4 (n = 50) and 180 ± 7 (n = 64), respectively in neurons. These findings suggest that the SOCE machinery primarily comprises Orai1 and STIM1 in neurons and SGCs of the rat SCG.

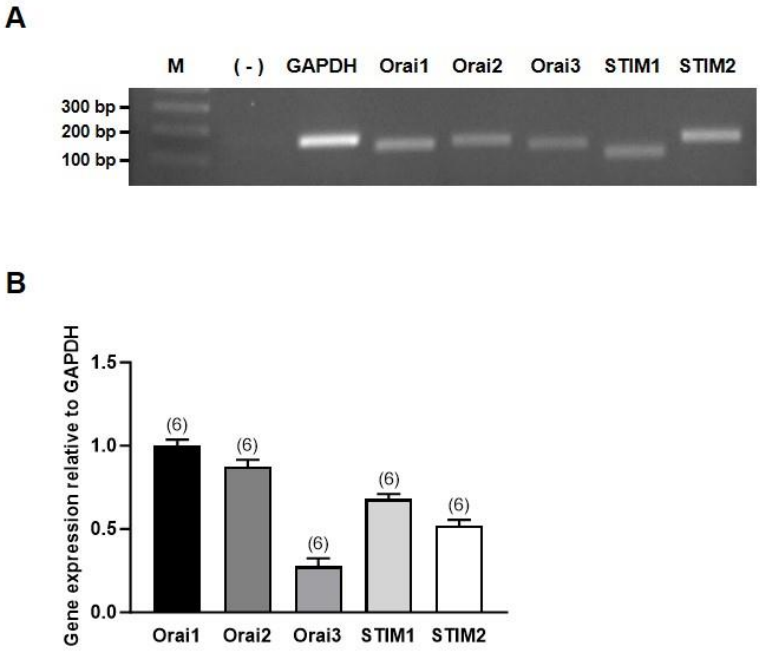

Figure 10. Expression of the transcripts encoding Orai and STIM isoforms in SCG. (A) The SOCE machinery components, Orai and STIM, in a superior cervical ganglion by RT-PCR analysis. Negative control (-) means a no reverse transcriptase control to confirm the absence of genomic DNA contamination. (B) Relative mRNA expressions of SOCE components Orai and STIM. Orai1 and STIM1 are major SOCE components in sympathetic ganglia. The number of experiments is indicated in parentheses.

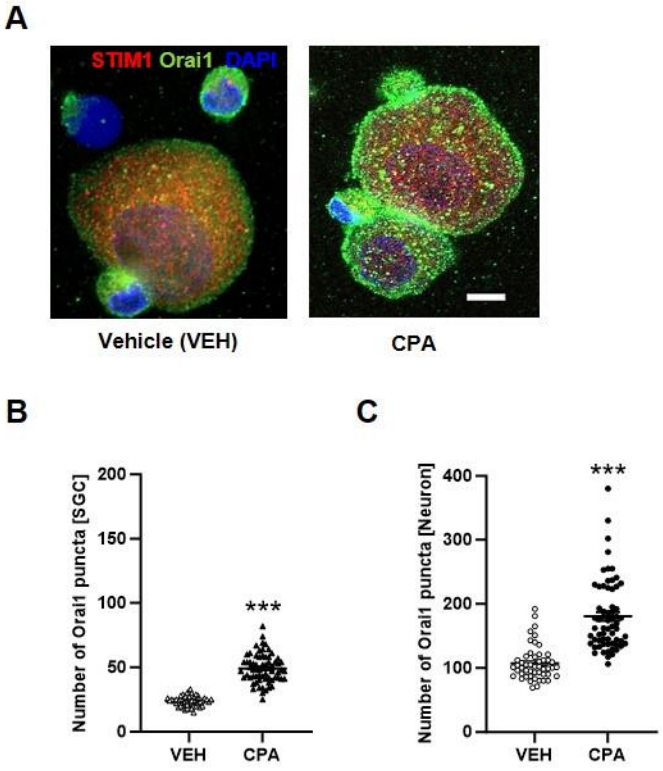

Figure 11. CPA-induced SOCE activation in neuron-SGC units. (A) Representative immunofluorescent images of the distribution of Orai1 (green) and STIM1 (red) in a sympathetic neuron-SGC unit. DAPI stained the nuclei of the neuron and SGC. Confocal images of the cells were taken before and after 10-minute treatment of 30 μM CPA. ER Ca^{2+} depletion with CPA induces a mobilization of STIM1-Orai1 aggregates as an assembly of prominent puncta formation in the cell surfaces of a neuron-SGC unit. Scale bars = 10 μm. (B) Summary of the number of Orai1 puncta in neuron-SGC units. Vehicle DMSO-

treated (VEH) and CPA-treated (CPA) groups were compared. (n = 54 - 60 cells from 5 wells per group), Data are presented as means ± SEM, Unpaired t-test (mean ± SEM), *** $p < 0.001$.

4.3. Measurement of SOCE in the neurons and SGCs of sympathetic ganglia

To ascertain whether SOCE proteins functional in sympathetic neurons and SGCs, we performed intracellular Ca^{2+} imaging experiments using Fura-2/AM. CPA-induced depletion of the ER calcium store transiently increased the cytosolic Ca^{2+} level in the absence of extracellular Ca^{2+}. Subsequent perfusion of the buffer with 2 mM Ca^{2+} increased cytosolic Ca^{2+} in neurons and SGCs (Fig. 12A), suggesting that the store refilled Ca^{2+} influx via the activated SOCE channels (Fig. 12B). Interestingly, the magnitude of SOCE as measured in AUC SOCE (see Fig. 12B caption) was significantly larger in SGCs (135 ± 4, n = 32) than neurons (35 ± 3, n = 29) ($p < 0.001$) (Fig. 12C). It should be noted that the oscillating Ca^{2+} signals are likely a key feature of SOCE. We examined whether GSK7975A (1 μM), an Orai1/3 inhibitor, and Pyr6 (3 μM), an Orai1/TRPC3 inhibitor, suppressed CPA-induced SOCE. A previous study indicates that Pyr6 typically exhibits approximately 40-fold higher potency in inhibiting Orai1-mediated Ca^{2+} entry compared to TRPC3-mediated Ca^{2+} entry [209]. Accordingly, Pyr6 at 3 μM can selectively block orai1-mediated SOCE. After pre-treatment of these inhibitors for 1h, SOCE was significantly suppressed in neurons and SGCs compared to the control (VEH) (Fig. 13). On average, GSK7975A decreased the AUC SOCE by 88% in SGCs (138 ± 5 for control vs. 17 ± 2 for inhibitor, *** $p < 0.001$) (Fig. 13A-B) and 52% in neurons (38 ± 1 for control vs. 18 ± 1 for inhibitor, *** $p < 0.001$) (Fig. 13C-D). Pyr6 decreased the AUC SOCE by 97% in the SGCs (138 ± 5 for control vs. 4 ± 1 for inhibitor, *** $p < 0.001$) (Fig. 13B) and 74% in neurons (38 ± 1

for control vs. 10 ± 1 for inhibitor, *** $p < 0.001$) and (Fig. 13D). These findings suggest that the SOCE machinery is functional in the neurons and SGCs of the rat sympathetic ganglia.

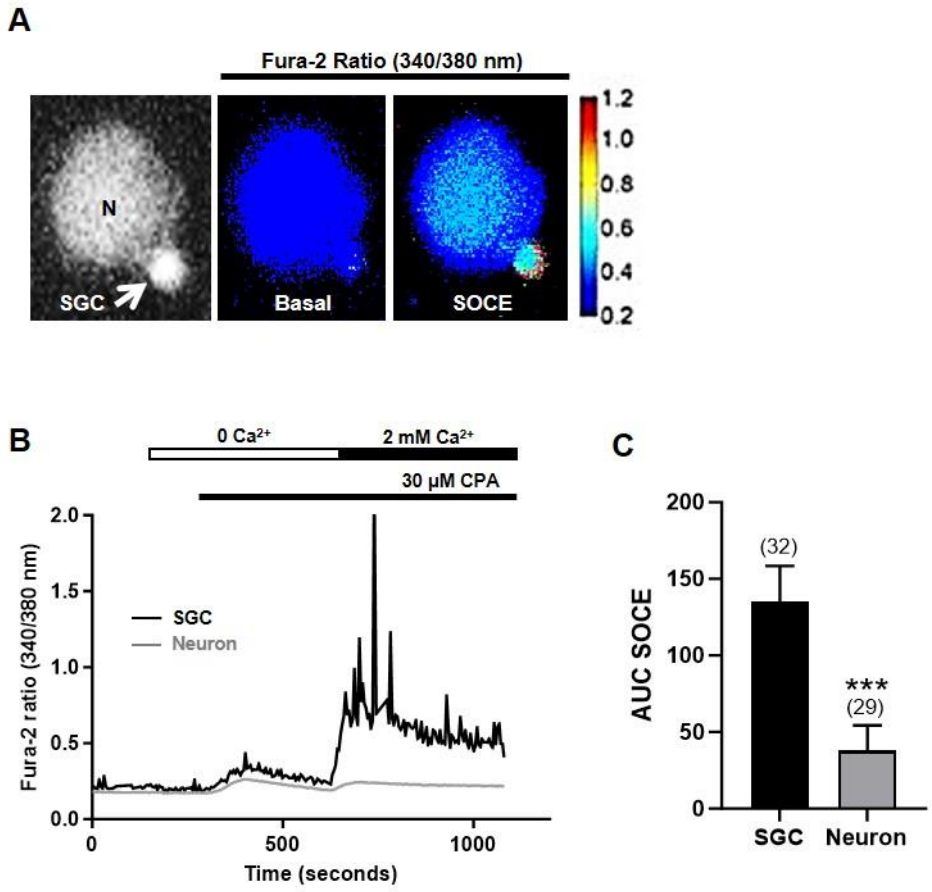

Figure 12. Measurement of SOCE in the neurons and SGCs of sympathetic ganglia. (A) The digital images showing a neuron-SGC unit (left), a 340 nm/380 nm ratio at the resting basal state (middle), and SOCE induction (right). (B) Representative traces of CPA (30 μM)-induced depletion of Ca^{2+} store in the absence of external Ca^{2+}, and a secondary Ca2+ influx (SOCE) via the activated CRAC by CPA in the presence of external Ca^{2+} (2

mM) in a neuron-SGC unit. The area under the curve (AUC) of the traces of Ca^{2+} influx during SOCE (i.e. AUC SOCE) in SGCs and neurons was measured. (C) Summary of AUC SOCE in SGCs and neurons. Unpaired Student's t-test, *** $p < 0.001$.

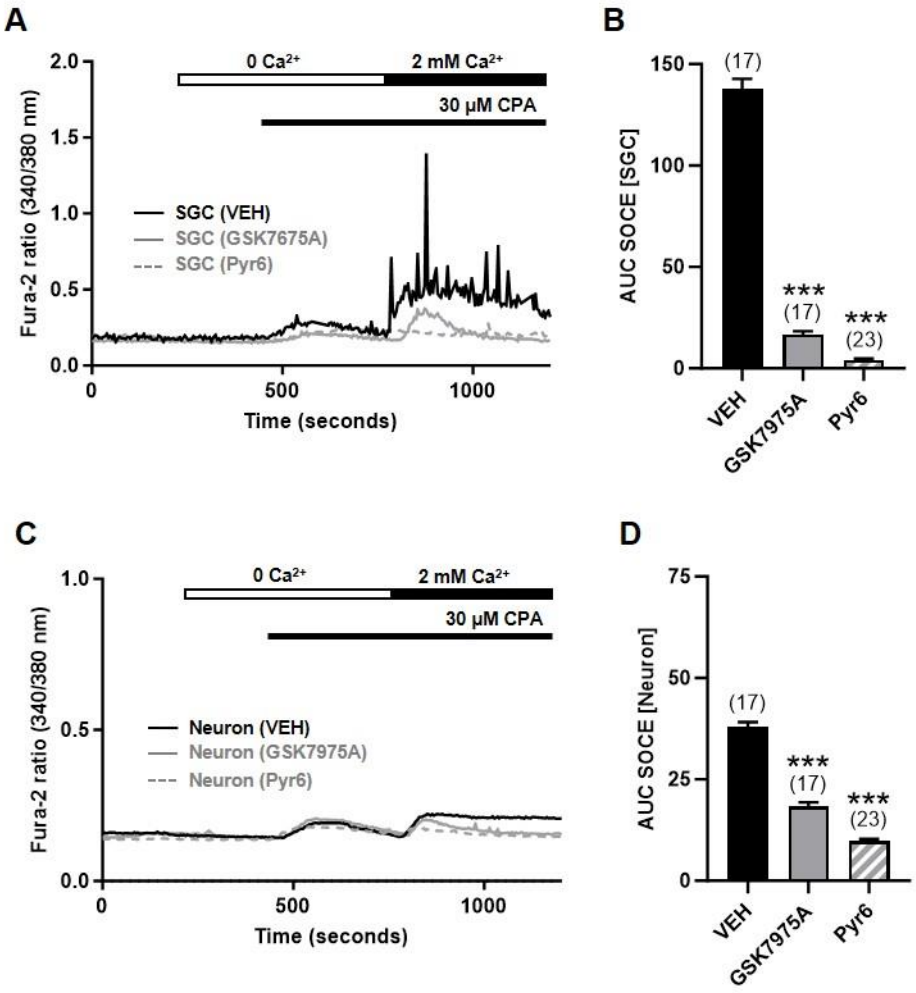

Figure 13. Pharmacological blockade of SOCE in neuron-SGC units. (A, C) Representative traces showing pharmacological inhibition of SOCE with GSK7975A (1 μM for 1h, Orai1 inhibitor) and Pyr6 (3 μM for 1h, SOCE inhibitor) in a neuron-SGC unit. (B, D) Summary of AUC SOCE in control (VEH) and inhibitor-treated SGCs and neurons.

Data are presented as means ± SEM. The number of the tested cells is indicated in parenthesis. One-way ANOVA with post-hoc Tukey's multiple comparison test, *** $p < 0.001$.

4.4. LPS-induced increase in GFAP expression: Potential involvement of TLR4

Next, we examined whether glial Ca^{2+} signaling is susceptible to pathological challenges. Acute systemic inflammation was induced in rats using LPS (2 mg/kg, i.p.) *in vivo*. One day after LPS injection, the expression of the transcripts encoding GFAP and TLR4, an LPS-responsive toll-like receptor, was upregulated approximately 4- and 1.4 folds, respectively, compared with that in the control (VEH) in the sympathetic ganglia ($p < 0.001$) (Fig. 14A-C). Immunohistochemical and immunoblotting analyses confirmed an LPS-mediated increase in GFAP expression (Fig. 15 & Fig. 17). TLR4 protein levels increased slightly in the rat sympathetic ganglia (Fig. 14C & 17C). Next, we performed immunostaining of TLR4 in the cultured neurons and SGCs. As illustrated in Fig. 16, TLR4 immunoactivity was prominently detected in neurons, while being negligible in individual SGCs under control (VEH) healthy conditions. Furthermore, 24 h following exposure to LPS (1 μg/mL) *in vitro*, TLR4 immunoactivity significantly increased in neurons. These findings suggest that LPS-induced reactive gliosis, i.e. the activation of SGCs, increases GFAP proteins in the SGCs via TLR4 activation in the rat sympathetic ganglia.

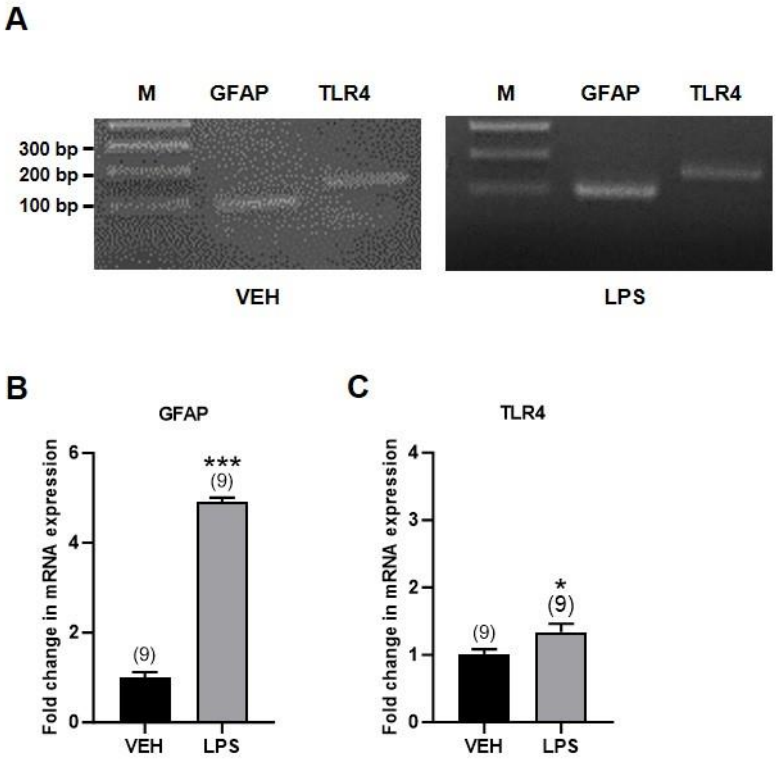

Figure 14. Expressions of transcripts encoding GFAP and TLR4 in SCG after LPS treatment. (A) After 24 h of intraperitoneal LPS (2 mg/ml) treatment *in vivo*, SCGs of vehicle and LPS groups were harvested. Then, the genomic expression levels of gliosis marker GFAP and LPS receptor TLR4 were compared by RT-PCR analysis. (B-C) Relative mRNA expressions of GFAP and TLR4 in the sympathetic ganglia before and after the LPS treatment were compared. The number of experiments is indicated in parenthesis. Data are presented as means ± SEM. The number of experiments is indicated in parenthesis. * $p < 0.05$, *** $p < 0.001$.

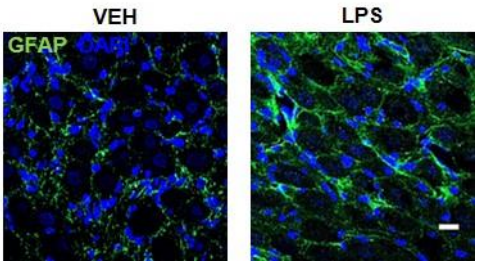

Figure 15. Glial activation after LPS treatment in SCG. Confocal images of the changes in GFAP expression in the SGCs of sympathetic ganglia 24 h after intraperitoneal LPS (2 mg/kg) injection *in vivo*. Scale bars = 20 μm.

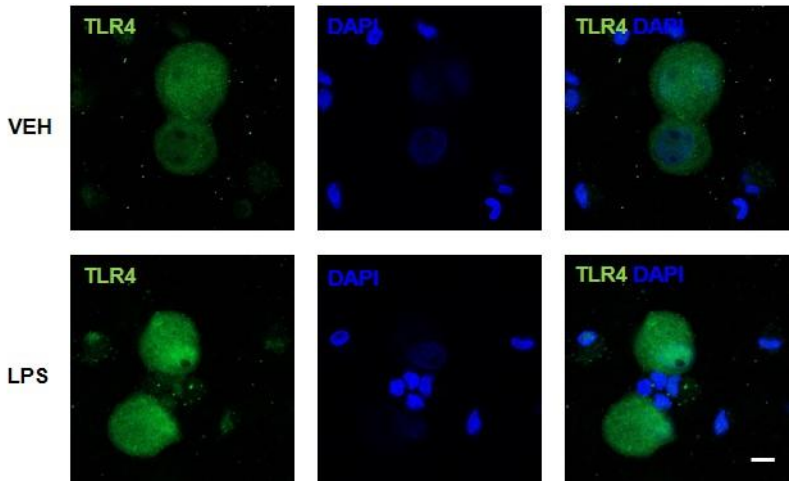

Figure 16. Identification of TLR4 in SCG. Confocal images of the localization and changes in TLR4 immunoreactivity in the control (VEH) and LPS (1 μg/mL, 24 h, *in vitro*) groups of cultured neuron-SGC units. TLR4 is mainly seen in the neurons. Scale bars = 10 μm.

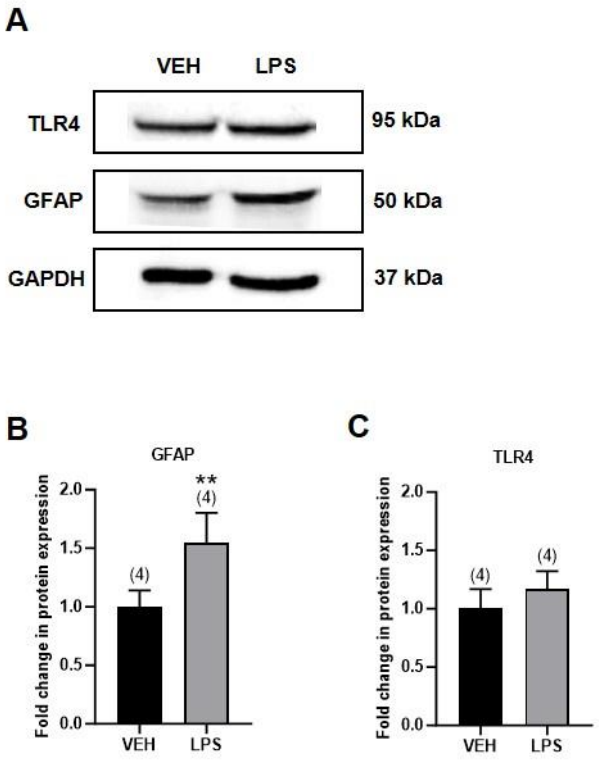

Figure 17. Changes in the levels of GFAP and TLR4 proteins after LPS treatment. (A) Immunoblots of SCG collected from the rats 24 h after injection of either vehicle or LPS, (B-C) Summary of the LPS-induced changes in expression of GFAP and TLR4 proteins in SCG. Data are presented as means ± SEM. The number of experiments is indicated in parenthesis. Unpaired Student's t-test, ** $p < 0.01$.

4.5. LPS decreased SOCE by downregulation of Orai1 and STIM1 expression in rat sympathetic ganglia

Importantly, the quantitative real-time PCR and immunoblotting analyses revealed that LPS significantly downregulated Orai1 and STIM1 expression in the rat sympathetic ganglia (Fig. 18A-E). We compared the SOCE in control and *in vitro* LPS (1 μg/ml for 24 h)-treated neurons and SGCs. LPS significantly decreased the magnitude of SOCE in SGCs and neurons (Fig. 19A-D). On average, LPS decreased the AUC SOCE by 41% in SGCs (153 ± 13 for VEH vs. 90 ± 15 for LPS, $p < 0.01$) (Fig. 19A-B) and 30% in neurons (Fig. 19C-D) (43 ± 4 for VEH vs. 30 ± 4 for LPS, $p < 0.05$).

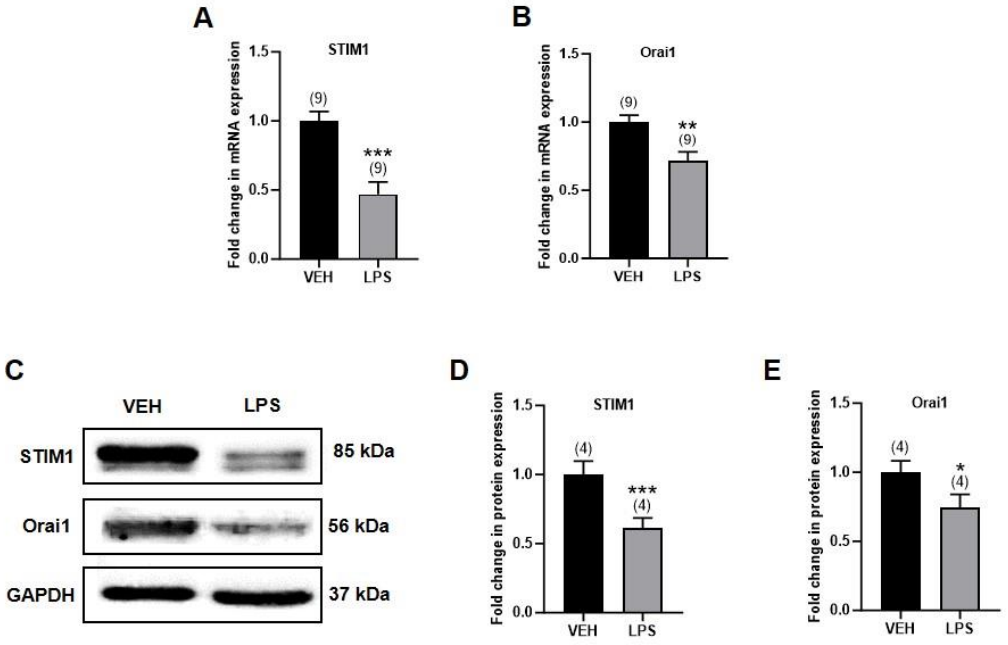

Figure 18. LPS-induced downregulation of STIM1 and Orai1 expressions in SCG. (A-B) Summary of comparing the relative expression of the transcripts encoding STIM1 and Orai1 in the control (VEH) and LPS-treated groups. (C) Immunoblots of Orai1 and STIM1 proteins in rat SCG 24 h after either vehicle or LPS injection *in vivo*. (D-E) Summary of the relative expression of Orai1 and STIM1 proteins. Unpaired Student's t-test, * $p < 0.05$. ** $p < 0.01$, *** $p < 0.001$.

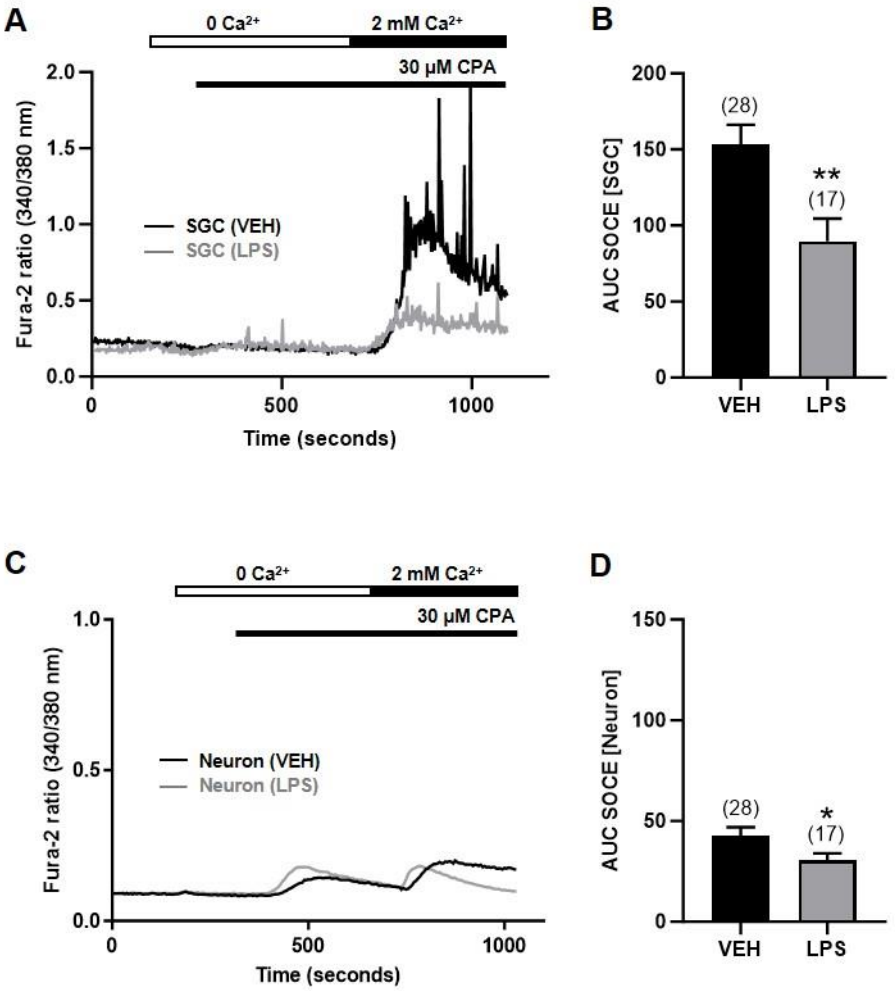

Figure 19. LPS-induced downregulation of SOCE in SCG. (A, C) Representative traces of SOCE in SGCs (A) and neurons (C) after the treatment with either vehicle or LPS (1 μg/ml, 24h *in vitro*). (B, D) Summary of the LPS-induced changes in AUG SOCE in SGCs and neurons (n = 17 - 28 cells). Data are presented as means ± SEM. The number of experiments is indicated in parenthesis. Unpaired Student's t-test, * $p < 0.05$. ** $p < 0.01$.

4.6. LPS increased the excitability of sympathetic neurons

I examined whether LPS modulates Ca^{2+} influx through voltage-gated Ca^{2+} channels (VGCCs), which represent the primary Ca^{2+} signaling pathway in neurons. Bath perfusion of high K^+ (80 mM) significantly increased cytosolic Ca^{2+} levels in neurons (Fig. 20A). In contrast, the individual SGCs in culture did not respond to high K^+ (refer to Fig. 25 in Part II results) due to the absence of VGCCs. In other experiments, I observed that high K^+-induced Ca^{2+} signaling mediates somatic ATP release from SCG neurons (refer to Fig. 27 in part II result). Consequently, somatic ATP release caused cytosolic Ca^{2+} increase in SGCs attached to neurons following high K^+ application (Fig. 20C). Twenty-four hours after exposure to LPS (1 μg/ml), high K^+-induced cytosolic Ca^{2+} was significantly augmented in both neurons and SGCs attached to the attendant neurons. In summary, LPS increased the initial slope of cytosolic Ca^{2+} rise by 1.5- and 4.6-folds, respectively, in neurons and SGCs (Fig. 20B, D). These findings suggest that LPS activates VGCC-mediated Ca^{2+} signaling, leading to an increase in somatic ATP release and, consequently, ATP-mediated Ca^{2+} signaling in SGCs of sympathetic ganglia.

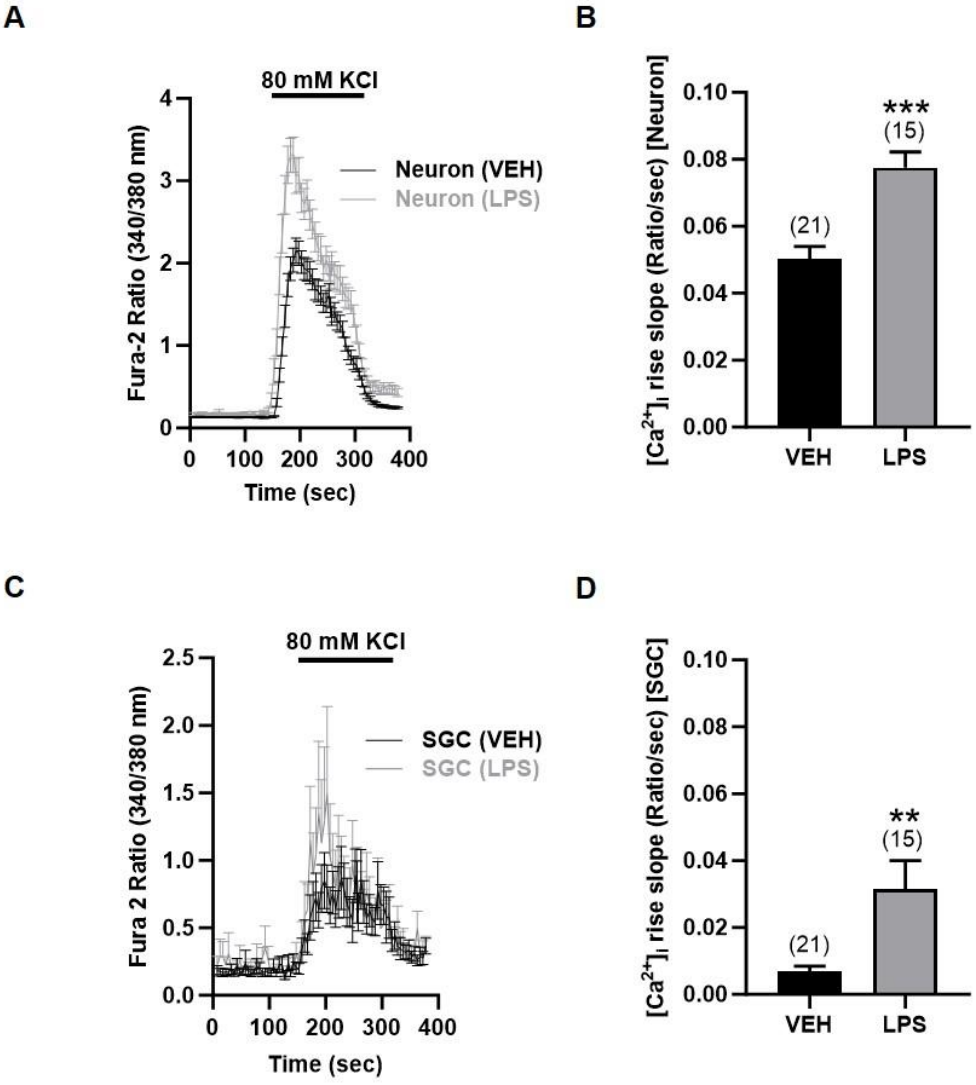

Figure 20. The effects of LPS on Ca^{2+} influx via VGCCs in SCG neurons. (A, C) High K^+ (80 mM)-induced increase in cytosolic Ca^{2+} in neurons and SGCs attached to the attendant neurons in culture. The relative concentration of cytosolic Ca^{2+} is expressed as a

340 nm/380 nm ratio. Twenty-four hours after LPS exposure (1 μg/mL), high K^+-induced increase in cytosolic Ca^{2+} was significantly augmented in neurons and SGCs attached to the attendant neurons in culture. (B, D) Summary of the effects of LPS on high K^+-induced cytosolic Ca^{2+} increase in neurons and SGCs. Comparisons were made for the rising slope of cytosolic Ca^{2+} levels over time. Data are presented as means ± SEM. The number of the tested cells from three independent experiments is indicated in parenthesis. Unpaired Student's t-test, ** $p < 0.01$, *** $p < 0.001$.

4.7. Expression of TRPC channels are expressed in the rat sympathetic ganglia

As previously indicated, TRPC1 and TRPC3 are widely recognized as components of SOCE machinery in various cellular systems [130, 150]. It has been reported that TRPC1 directly interacts with STIM and Orai channels [131-134], and STIM1 forms heteromers with other TRPC1 channels to indirectly regulate TRPC3 and 6 [135]. Our data shows that TRPC1/3/6 are predominantly present in rodent SCGs (Fig. 21). To explore the functional aspects of TRPC channels, I utilized carbachol to activate M3 muscarinic GPCRs. DAG, a byproduct of muscarinic signaling cascade, plays crucial role in subsequently activating TRPC3 and 6 is the byproduct of this calcium activation and DAG is an important mediator to activate TRPC 3 and TRPC6. Interestingly, the response to carbachol was relatively higher in neuronal Ca^{2+} signaling compared to SGCs (Fig. 22A, *red trace*). I then examined whether Pyr3 (10 μM), a selective TRPC3 inhibitor, and SAR7334 (10 μM), a potent TRPC6 inhibitor, could suppress carbachol-induced Ca^{2+} influx. Both Pyr3 and SAR7334 effectively suppressed the Ca^{2+} influx through TRPC 3 and TRPC6 in both neurons and SGCs compared to the control (VEH) (Fig. 22B, D). On average, Pyr3 decreased the peak amplitude of Ca^{2+} influx by 37% in neurons (0.92 ± 0.02 for control vs. 0.48 ± 0.07 for Pyr3, * $p < 0.05$) and 25% in SGCs (0.23 ± 0.05 for control vs. 0.18 ± 0.04 for Pyr3, n.s.) (Fig. 22B, C). Similarly, SAR7334 reduced Ca^{2+} influx by 77% in neurons (1.12 ± 0.02 for control vs. 0.43 ± 0.01 for SAR7334, *** $p < 0.001$) and 26% in SGCs (0.20 ± 0.05 for control vs. 0.13 ± 0.01 for SAR7334, * $p < 0.05$) and (Fig. 22D, E). These findings suggest

that the TRPC3 and TRPC6 are primarily functional in the neurons of the rat sympathetic ganglia. Next, the association of TRPCs with the function of SOCE was of interest in SCGs. The non-selective TRPC blocker, lanthanum chloride ($La^{3+,}$ 50 μM) was introduced to observe its effect on the SOCE activities induced by CPA. Importantly, Ca^{2+} imaging studies showed that La^{3+} significantly suppressed the SOCE activities in the rat sympathetic ganglia (Fig. 23A, C). I compared the SOCE in control and La^{3+} treated groups of neurons and SGCs. La^{3+} significantly decreased the magnitude of SOCE in SGCs and neurons (Fig. 23). On average, La^{3+} decreased the AUC SOCE by 83% in SGCs (127 ± 13 for VEH vs. 24 ± 3 for La^{3+}, *** $p < 0.001$) (Fig. 23A, B) and 30% in neurons (58 ± 4 for VEH vs. 13 ± 5 for La^{3+}, *** $p < 0.001$) (Fig. 24A, B). Similarly, Pyr3 also shows a trend to decrease SOCE activities induced by CPA by 77% in neurons (59 ± 18 for VEH vs. 33 ± 10 for La^{3+}, n.s.) (Fig. 24A, B) and 26% in SGCs (76.2 ±21 for VEH vs. 30 ± 9 for La^{3+}, n.s.) (Fig. 24C, D). Taken together, these results suggest that TRPC 1/3/6 may functionally participate in the Ca^{2+} signaling pathways regulating SOCE.

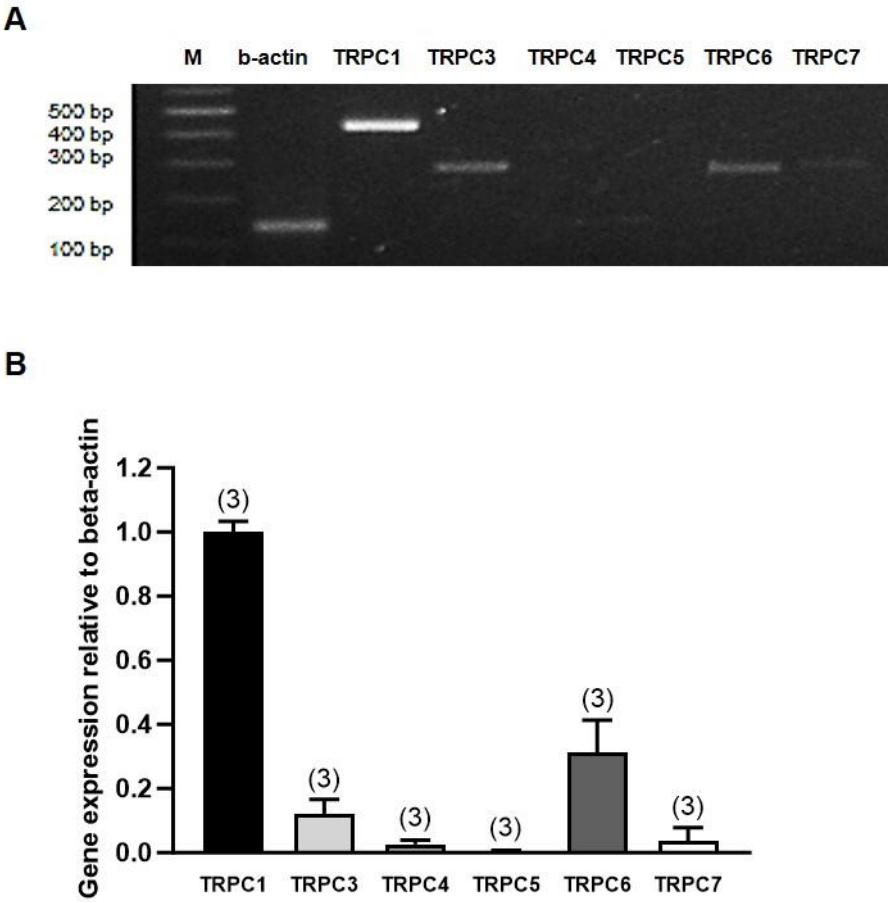

Figure 21. Expressions of the transcripts encoding TRPC isoforms in SCG. (A) The ROCE machinery components, TRPC (1-7) isoforms, in a superior cervical ganglion by RT-PCR analysis. (B) Relative mRNA expressions of ROCE components TRPC in a normal SCG. TRPC1, TRPC3, and TRPC6 are the major ROCE components in sympathetic ganglia.

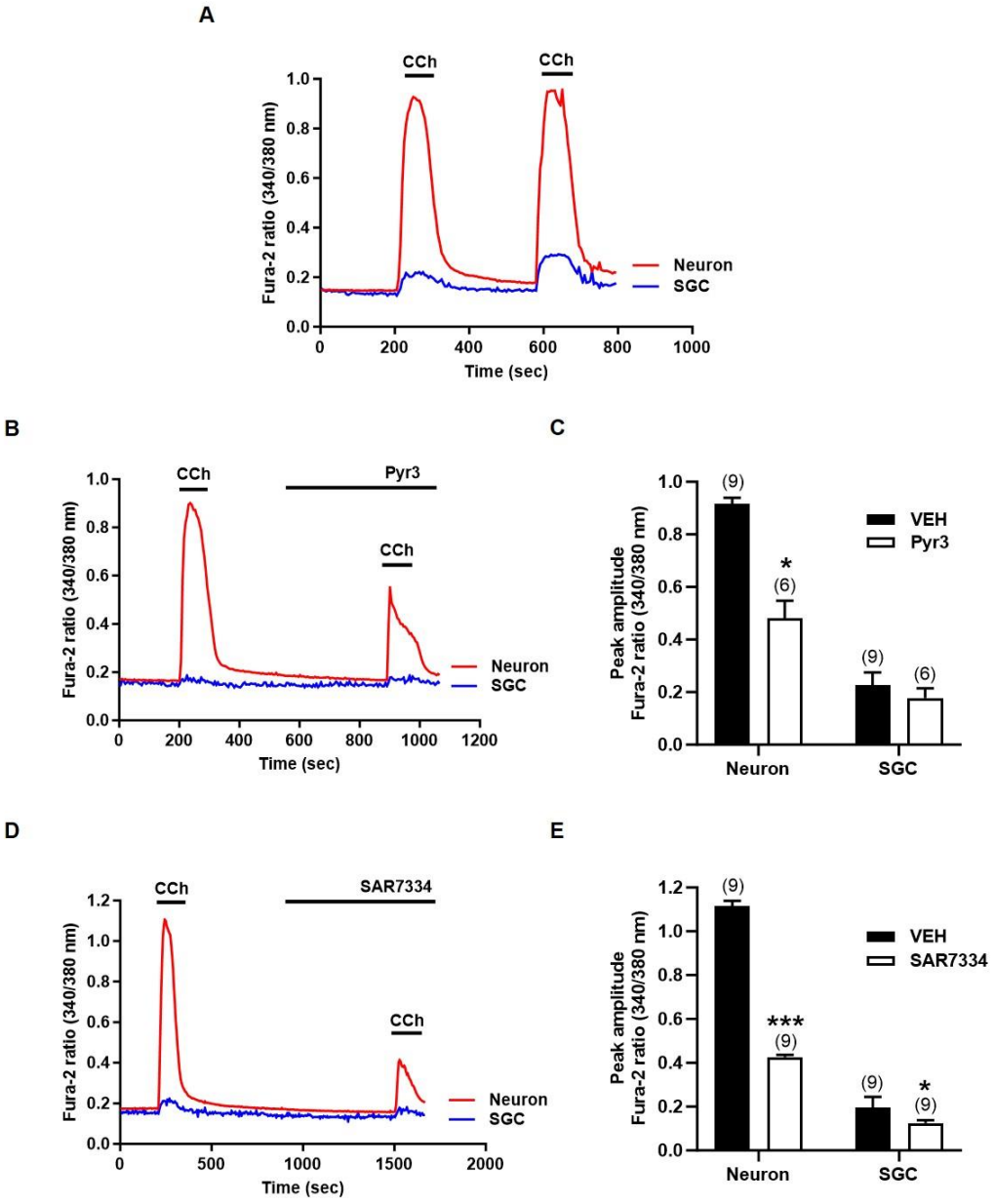

Figure 22. TRPC3 and TRPC6 are functionally present in SCG. (A) Representative

traces of serial stimulation of neuron-SGC units with M3 GPCR agonist, carbachol (CCh, 100 μM). (B, D) Representative traces of treating the neuron-SGC units with TRPC inhibitors. (C, E) Summary of the effects of pharmacological inhibitors of TRPC3 (Pyr3, 10 μM) and TRPC6 (SAR7334, 10 μM) (n = 6 - 9 cells). TRPC channels seem to be predominantly expressed in the sympathetic neurons. Data are presented as means ± SEM. The number of experiments is indicated in parenthesis. Unpaired Student's t-test, *** $p<0.001$, * $p < 0.05$.

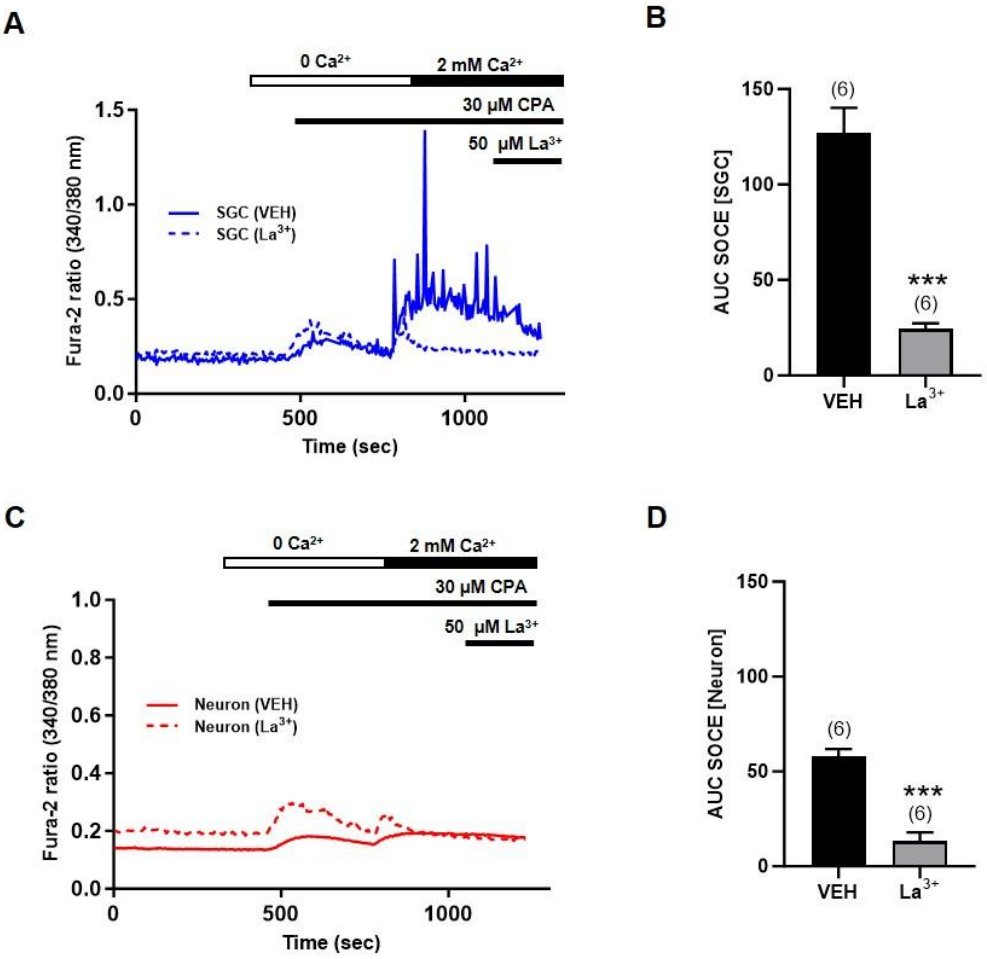

Figure 23. La^{3+}-induced downregulation of SOCE in SCG. (A, C) Representative traces of SOCE in SGCs (A) and neurons (C) after the treatment with either vehicle or La^{3+} (100 μM). (B, D) Summary of the La^{3+}-induced changes in AUG SOCE in SGCs and neurons (n = 6 cells). Data are presented as means ± SEM. The number of experiments is indicated in parenthesis. Unpaired Student's t-test, *** $p < 0.001$.

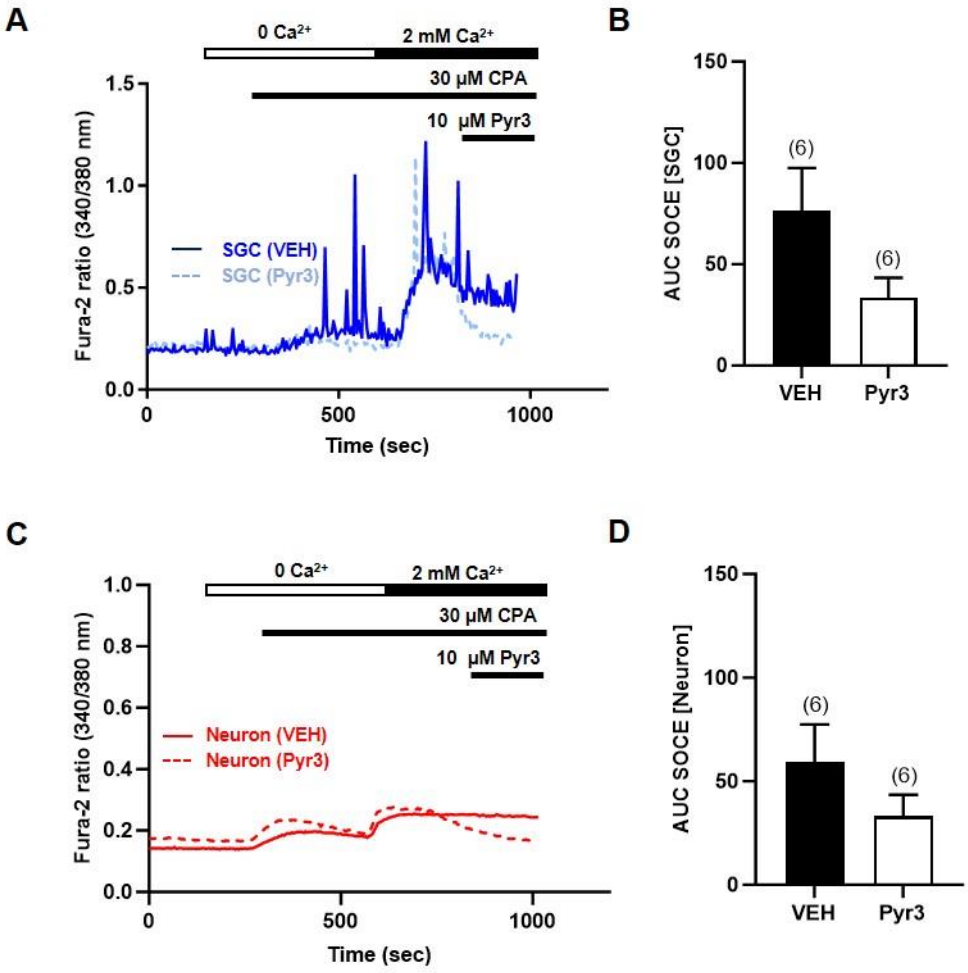

Figure 24. Pyr3-induced downregulation of SOCE in SCG. (A, C) Representative traces of SOCE in SGCs (A) and neurons (C) after the treatment with either vehicle or Pyr3 (10 μM). (B, D) Summary of the Pyr3-induced changes in AUC SOCE in SGCs and neurons (n = 6 cells). Data are presented as means ± SEM. The number of experiments is indicated in parenthesis. Unpaired Student's t-test, n.s.

PART II

The examination of somatic ATP release in sympathetic ganglia and the purinergic signaling mechanisms involved in communication between neurons and SGCs

4.8. Sympathetic neuronal depolarization activates the Ca^{2+} signaling in SGCs

Neuro-glial communication via Ca^{2+} signaling can be approached in many ways; however, the simplest method to initially provoke neuronal excitation is by applying electrical or chemical stimulation. To test my hypothesis that a neuro-glial communication occurs via Ca^{2+} signaling, I developed a short-term culture system of sympathetic neuron-SGC units obtained from partially dissociated SCGs. Changes in intracellular Ca^{2+} levels were measured to study how surrounding SGCs respond to the attached neurons when exposed to high concentrations of extracellular K^+. It is important to note that the non-excitable glial cells, when dissociated singly, did not exhibit a response to high K^+ stimulation (Fig. 25A). The narrow space between the sympathetic neuron and the ensheathing SGC is known to be approximately 20 nm [33], indicating that soluble signaling substances can be released into the extra-synaptic regions from either neurons or SGCs, and concentrated within the local microenvironment between the two cells upon external stimuli. Our evidence suggests

that Ca^{2+} response of non-excitable SGCs is mediated by potential extra-synaptic molecules released by the surrounding neurons. Increasing concentrations of extracellular K^+ concentrations rapidly depolarized the sympathetic neurons via the activation of VGCCs. Chemical depolarization of a SCG neurons evoked a rise in the intracellular Ca^{2+} levels, followed by a smaller Ca^{2+} response in the attached SGCs. At higher concentration of external K^+, the rise of slope and the amount of Ca^{2+} influx of neurons and SGCs significantly increased (*** $P < 0.001$) (Fig. 25B). In contrast, singly dissociated glial cells showed no Ca^{2+} response to high K^+. Next, the neuronal activity of VGCCs was blocked by its broad-acting inhibitor, cadmium chloride (Cd^{2+}, 100 μM). The Ca^{2+} influx by neuronal depolarization was significantly suppressed in both sympathetic neurons and SGCs. On average, Cd^{2+} decreased the AUC SOCE by 87% in neurons (581 ± 29 for control vs. 78 ± 6 for Cd^{2+}, *** $p < 0.001$) (Fig. 26A, B) and 55% in SGCs (72 ± 11 for control vs. 32 ± 5 for Cd^{2+}, *** $p < 0.001$) (Fig. 26A, B). Neuronal excitation-dependent ATP release has been reported with co-transmitters such as NE [157]. Building upon this, it is plausible to postulate that ATP can be released from the soma of neurons in sympathetic neuron-SGC units. To investigate this, with a modification in the method by Guthrie et al. [210], chemical depolarization with the pretreatment of apyrase (10 U/ml) was introduced to the neuron-SGC units. Apyrase is an ectonucleotidases that breaks down ATP in to ADP and AMP. Interestingly, apyrase almost completely suppressed the Ca^{2+} response in SGCs upon high K+ stimulation while it showed no effect on the SCG neurons (Fig. 26C, D). There may be many other bioactive molecules that can be released from the SCG neurons,

however, apyrase data showed that ATP is one of the signaling molecule that may play a role in the neuro-glial communication. Investigating further on the mechanisms and implications of somatic ATP release is necessary to understand the neuron-SGC interaction.

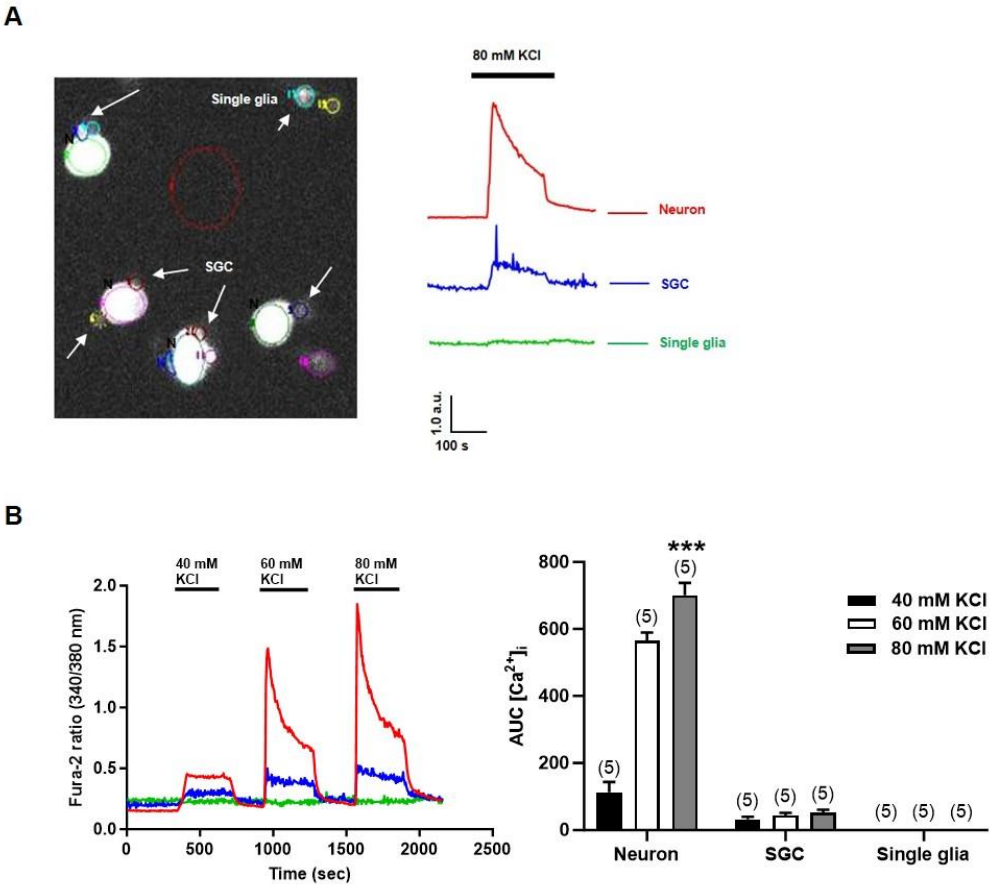

Figure 25. Sympathetic neuron-SGC communication upon neuronal excitation. (A) Only SGCs attached to the neurons responded to high K^+ stimulation. Representative traces of Ca^{2+} response of a neuron (red), SGC (blue), and singly dissociated glial cell (green) after high K^+ stimulation. (B) Chemical stimulation initially evoked Ca^{2+} increase in SCG neurons, then was followed by an increase in the cytosolic Ca^{2+} in the SGCs with a short

delay. Compared to the neurons, the Ca^{2+} signal in the SGCs upon high K^+ stimulation was much smaller. Singly dissociated glial cells did not respond to the chemical depolarization by 80 mM KCl. Summary of the High K^+-induced changes in AUC SOCE in the SGCs and neurons (n = 5 cells). Data are presented as means ± SEM. The number of experiments is indicated in parenthesis. One-way ANOVA with post-hoc Tukey's multiple comparison, *** $p < 0.001$.

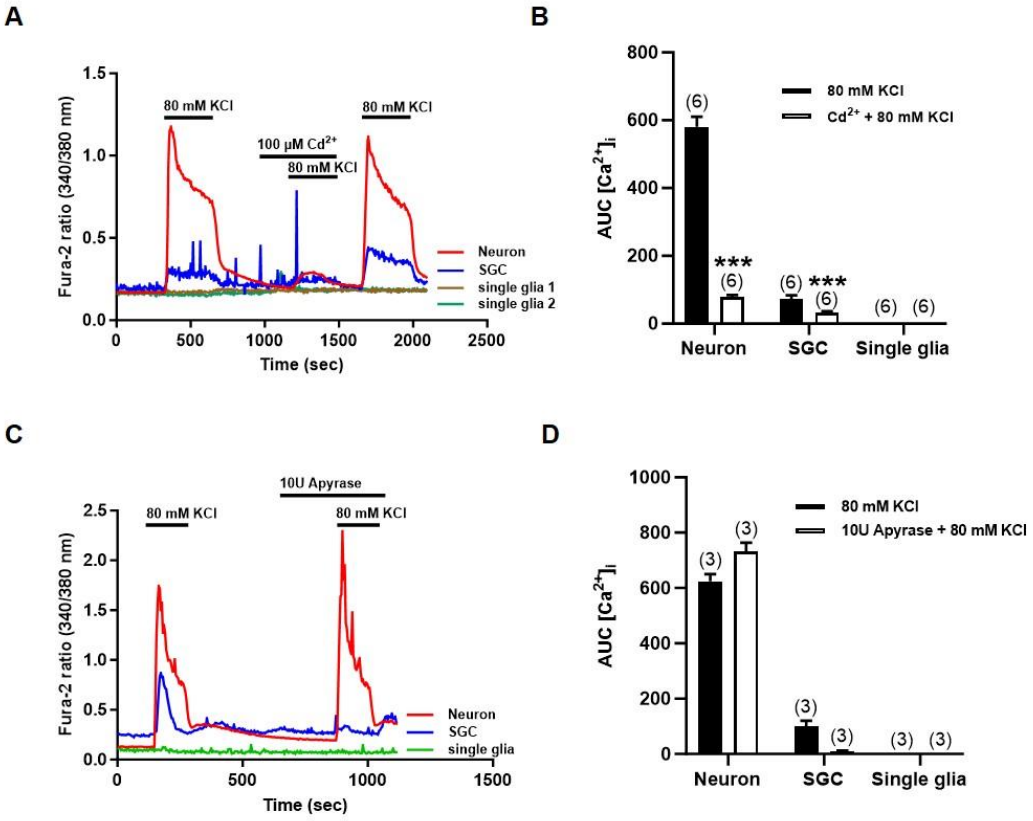

Figure 26. Inhibition of high K^+ responses in the SGCs by Cd^{2+} and apyrase. (A, C) Only SGCs attached to the excited neurons responded to high K^+ stimulation. Representative traces of blocking the Ca^{2+} response of a neuron (red) and SGC (blue) with the pretreatment of VGCC inhibitor, Cd^{2+}(100 μM), or apyrase (10 U/ml) after high K^+ stimulation. (B, D) Summary of the High K^+-induced changes in AUC in the SGCs and neurons upon the blockade of neuronal depolarization or the degradation of ATP released from the sympathetic neurons (n = 3 - 6 cells). Either suppression of neuronal

depolarization or hydrolyzing the releasable substance, ATP, blocked the Ca^{2+} increase in the surrounding SGCs. Singly dissociated glial cells did not respond to the chemical depolarization by 80 mM KCl. Data are presented as means ± SEM. The number of experiments is indicated in parenthesis. Unpaired Student's t-test, *** $p < 0.001$.

4.9. Somatic ATP release from the sympathetic neurons

Next, I aimed to verify whether the sympathetic neurons could release ATP. The identification of sub-cellular ATP-containing vesicles within the neurons were identified by labelling cultured neurons with either FM 1-43 to test the vesicular release or quinacrine dyes to stain ATP-containing vesicles. FM 1-43 or quinacrine-labelling of neuronal cells was visualized using fluorescent microscope (Fig. 27A, B). Numerous fluorescent puncta were distributed ubiquitously in the cytoplasm. High K^+ stimulation depolarized the neurons, resulting in a real-time decrease in the number of FM 1-43- or quinacrine- stained puncta during the 10-minute exposure to high K^+. The control culture without high K^+ stimulation during the same incubation time showed no difference in the number of puncta discarding the photobleaching factors. On average, the number of FM 1-43 puncta before and after 80 mM KCl stimulation was 403 ± 127 (n = 21) and 236 ± 69 (n = 18), respectively (** $p < 0.01$). Similarly, the number of quinacrine-stained puncta before and after 80 mM KCl stimulation was 1089 ± 115 (n = 43) and 713 ± 90 (n = 37), respectively (** $p < 0.01$).

The ATP accumulated in the extracellular space upon high K^+ stimulation was quantified by luminometry, showing 1.7-fold increase over the basal ATP was observed upon high K^+ application. While the basal ATP concentration was 199.8 ± 18.9 pmol per culture well, the high K^+-induced extracellular ATP concentration were 342.8 ± 23.6 pmol per culture well (** $p < 0.01$). The working range of ATP bioluminescence assay kit is between 1×10^{-5} and 1×10^{-12} M ATP. A standard curve was generated based on a series of known ATP concentrations ($R^2 = 0.9997$) and ATP concentration was calculated from the linear

equation. Furthermore, the high K^+-induced somatic ATP release was completely blocked by 100 μM Cd^{2+} and 30 μM BAPTA. Together with apyrase data, these findings suggested that somatic ATP release is neuronal Ca^{2+}-dependent activity where VGCC-mediated Ca^{2+} signaling lead to an increase in somatic ATP release, consequently, ATP-mediated Ca^{2+} signaling in SGCs of sympathetic ganglia.

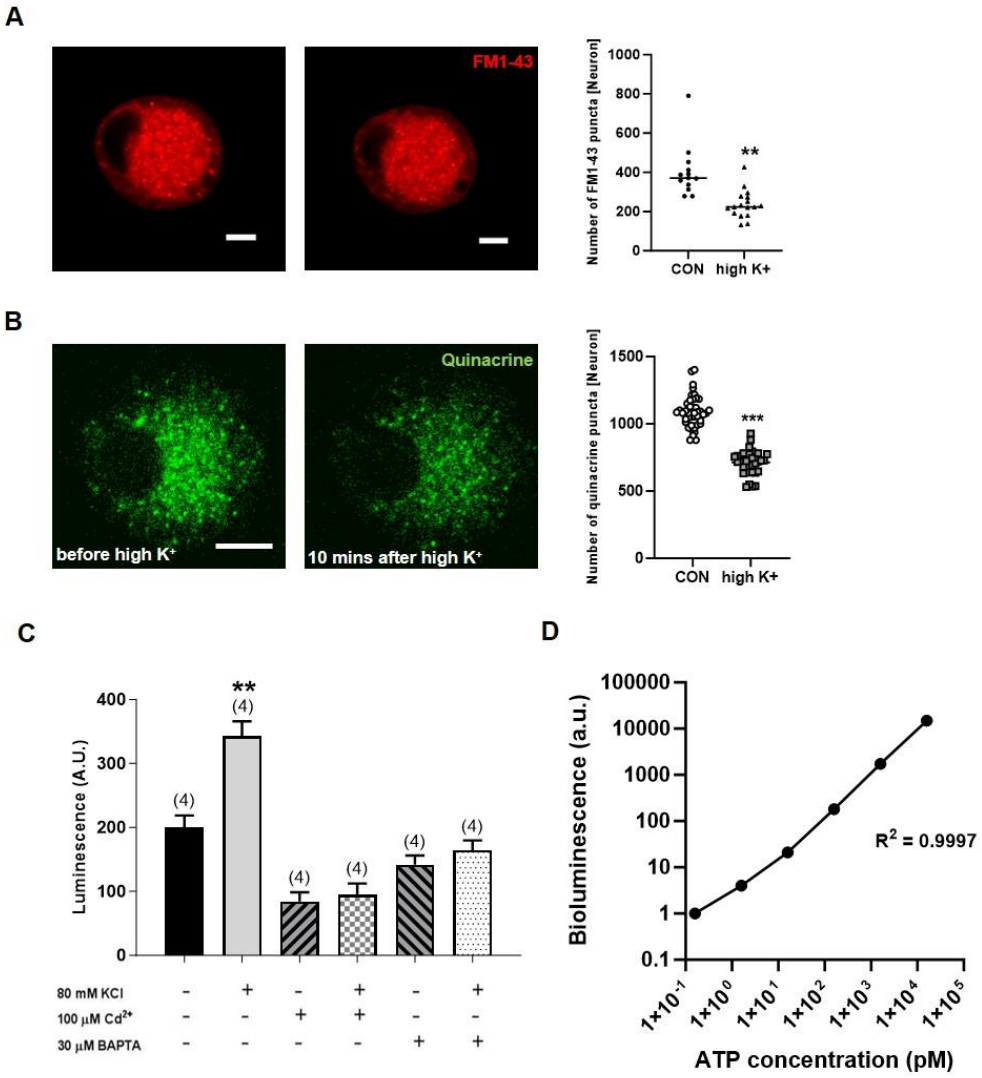

Fig. 27. Effect of high K^+ on somatic vesicles and extracellular ATP levels in sympathetic neuronal culture. (A, B) Neuronal cells were pre-incubated either with vesicle staining dye, FM 1-43 (5 μM), or ATP-staining dye, quinacrine (10 μM) for 30

minutes and prior to the application of 80 mM KCl for 10 minutes. Live cell images were recorded immediately after the loading of high K^+ solution in the external perfusion bath every 10 seconds for 10 minutes. FM 1-43 or quinacrine-positive puncta were counted and analyzed. Scale bars = 10 μm. (C, D) Neuronal cells were cultured and incubated with 80 mM KCl with or without calcium chelator BAPTA (30 μM) and VGCC antagonist (Cd^{2+}, 100 μM) for 20 minutes. Then, the medium was collected to determine the levels of extracellular ATP in kinetic mode. Upon high K^+ application, the extracellular concentration of ATP is increased in the neuron-only cultures. 4 independent experiments performed in duplicates. Data are presented as means ± SEM. The number of experiments is indicated in parenthesis. One-way ANOVA with post-hoc Tukey's multiple comparison test, ** $p < 0.01$.

4.10. Pharmacological identification of purinergic receptors in the SGCs

Ca^{2+} signaling can be mediated by various extracellular release of biomolecules such as ATP as part of neuro-glial communication [167]. Data in the previous section confirmed that ATP is one of the key players to modulate Ca^{2+} signaling within the sympathetic neuron-SGC units. The RT-PCR analyses of SCG revealed the presence of various purinergic receptors encompassing both P2X and P2Y subtypes (Fig. 28A). My primary focus was the purinergic receptor subtypes responsible for receiving somatic ATP released from excited neurons. According to the PCR data, P2X4, P2X7, and P2Y1 emerged as the abundant forms of P2 receptors. Consequently, I verified the distribution of these receptors through immunostaining studies (Fig. 28B). All three subtypes of P2 receptors were present in the SCGs with P2X4 and P2X7 predominantly present in SGCs while P2Y1 appeared to be present in both neurons and SGCs, albeit more predominantly in the neurons.

Functional studies utilizing Ca^{2+} imaging techniques were undertaken, demonstrating that ATP induced Ca^{2+} influx in both sympathetic neurons and SGCs (Fig. 29A). Notably, pan-purinergic inhibitors, i.e. suramin (30 μM) and PPADS (30 μM), effectively blocked the ATP responses in both neurons and SGCs (Fig. 29A). The inhibitors decreased the peak amplitudes of the Ca^{2+} response recorded in the ATP-stimulated neurons (0.41 ± 0.08 for control vs 0.21 ± 0.01 for suramin, *** $p < 0.001$; 0.52 ± 0.07 for control vs 0.22 ± 0.01 for PPADS, *** $p < 0.001$, $n = 6 - 8$ cells) and SGCs (0.46 ± 0.1 for control vs 0.15 ± 0.02 for suramin, *** $p < 0.001$; 0.83 ± 0.21 for control vs 0.35 ± 0.01 for PPADS, *** $p < 0.001$, $n = 6 - 8$ cells). Treatment of cultures with suramin or PPADS abolished the Ca^{2+}

signaling in neurons and SGCs (Fig. 29C, E).

To achieve greater specificity in receptor activation, I selected BzATP, an ATP analogue known for its specificity in activating P2X7. Some reviews suggest that BzATP may partially activate P2X4 and P2Y1 [211, 212]. Accordingly, I examined whether A4380879 (30 μM), a selective P2X7 inhibitor, and MRS2179 (30 μM), a selective P2Y1 inhibitor, could suppress BzATP-induced Ca^{2+} influx. Intriguingly, A438079 selectively blocked BzATP-induced Ca^{2+} influx in SGCs, but not in neurons, while MRS2179 blocked BzATP-induced Ca^{2+} increase neurons but not in SGCs. Pre-treatment with these inhibitors in bath perfusion led to suppressed Ca^{2+} influx in both neurons and SGCs compared to the control (Fig. 30A, C). On average, A438079 exhibited a pattern of suppressing peak amplitude by 69% in SGCs (0.26 ± 0.08 for control vs. 0.08 ± 0.05 for A438079, * $p < 0.05$, $n = 8$ cells) while no observable interval changes in Ca^{2+} influx was noted in neurons (Fig. 30A, B). Conversely, MRS2179 decreased peak amplitude of Ca^{2+} influx by approximately 55% in neurons (0.29 ± 0.05 for control vs. 0.13 ± 0.04 for MRS2179, * $p < 0.05$, $n = 9$ cells), while no interval changes were noted in SGCs (Fig. 30C, D).

Selective agonist for P2X4 receptors are not available so far. However, allosteric modulation by trace metals are useful tools to pharmacologically segregate P2X4 and P2X7 receptors (Fig. 5A, table adopted from Coddou et al. [190]), These P2X receptors are rich in histidine residues in the N-terminus of the receptor, specifically in the non-ligand binding site. This site can bind to trace metals such as zinc, cadmium, and copper to allosterically modulate the opening of the ion channels. For instance, zinc can potentiate the ATP

response of P2X4 receptors but inhibits P2X7 receptors. Cadmium also potentiates the ATP response of P2X4 receptors but inhibits P2X7 receptors. Zinc also potentiates also P2X2/3, which are also present in SCGs (Fig. 28A). Ivermectin (IVM, 5 μM) is another positive allosteric modulator to activate P2X4. However, the effect of IVM was not significant in a cultured system of sympathetic neuron-SGC units (Fig. 31A). On the other hand, it is interesting to note that sympathetic neurons were potentiated by zinc (Zn^{2+}, 5 μM) all the time, indicating the presence of P2X2/3 in these neurons (Fig. 31B) [152]. Immunofluorescent studies in Fig.28B, showed that P2X4 were present mainly in the SGCs. Thus, the enhanced Ca^{2+} response in neurons may not be due to neuronal P2X4. The ATP-induced Ca^{2+} response of SGCs to zinc was rather more complex (Fig. 31C). The combination cocktail of zinc and IVM was attempted to fully potentiate P2X4 receptors but only 36.4% of SGCs were potentiated while the rest of SGCs showed no different response to the agonist stimulation. Similar results were observed with cadmium (Cd^{2+}, 30 μM) (Fig. 32A, B). Cd^{2+} did not affect the neuronal calcium signaling. Only 30% of the SGCs were potentiated by Cd^{2+} while 20% of the ATP-induced response of SGCs were inhibited compared to the control. The rest half of the SGCs showed equivocal responses to the control agonist. According to recent literatures [213-215], both P2X4 and P2X7 receptors can be present in heteromers within the same cell type (Fig. B, C, adopted from Craigie et al. [216]). Perhaps, these two P2X subtypes are heterogeneously expressed in the SGCs while P2Y1 is predominantly present in sympathetic neurons. The expression levels of each purinergic receptors under different physiological conditions may vary. This

will also affect the Ca^{2+} response of SGCs to the somatic ATP released from the neurons. In sum, these findings suggest that the purinergic receptors are functional in the neurons and SGCs of the rat sympathetic ganglia.

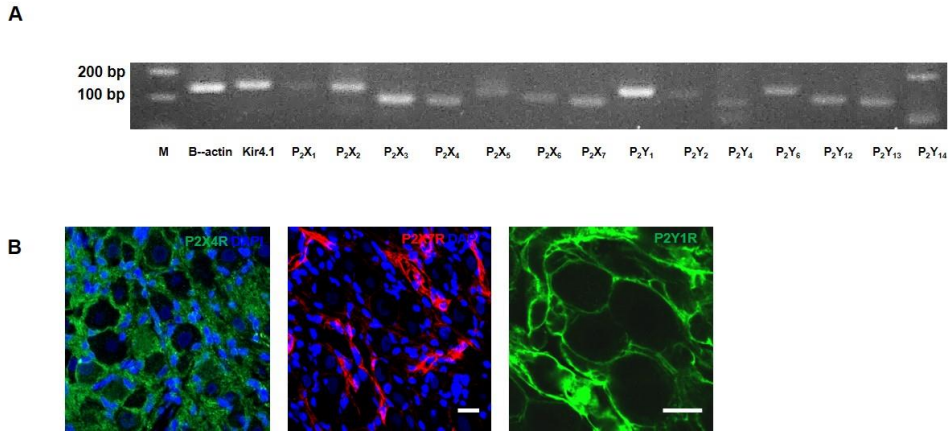

Figure 28. Identification of purinergic receptor isoforms in sympathetic neuron-SGC units. (A) The genomic expression levels of purinergic receptors (P2X and P2Y) were profiled in the SCGs. (B) P2X4 receptor is present abundantly in the SGCs. P2X7 receptor is also present in the SCGs. The expression level of P2X7 seems to be lower than P2X4. P2Y1 receptor appears to be present in both neurons and SGCs, but predominantly present in sympathetic neurons. Nuclear counter-stain was indicated with DAPI (blue). Large nuclei belong to sympathetic neurons while small nuclei indicate glial cells. Scale bar = 10 μm.

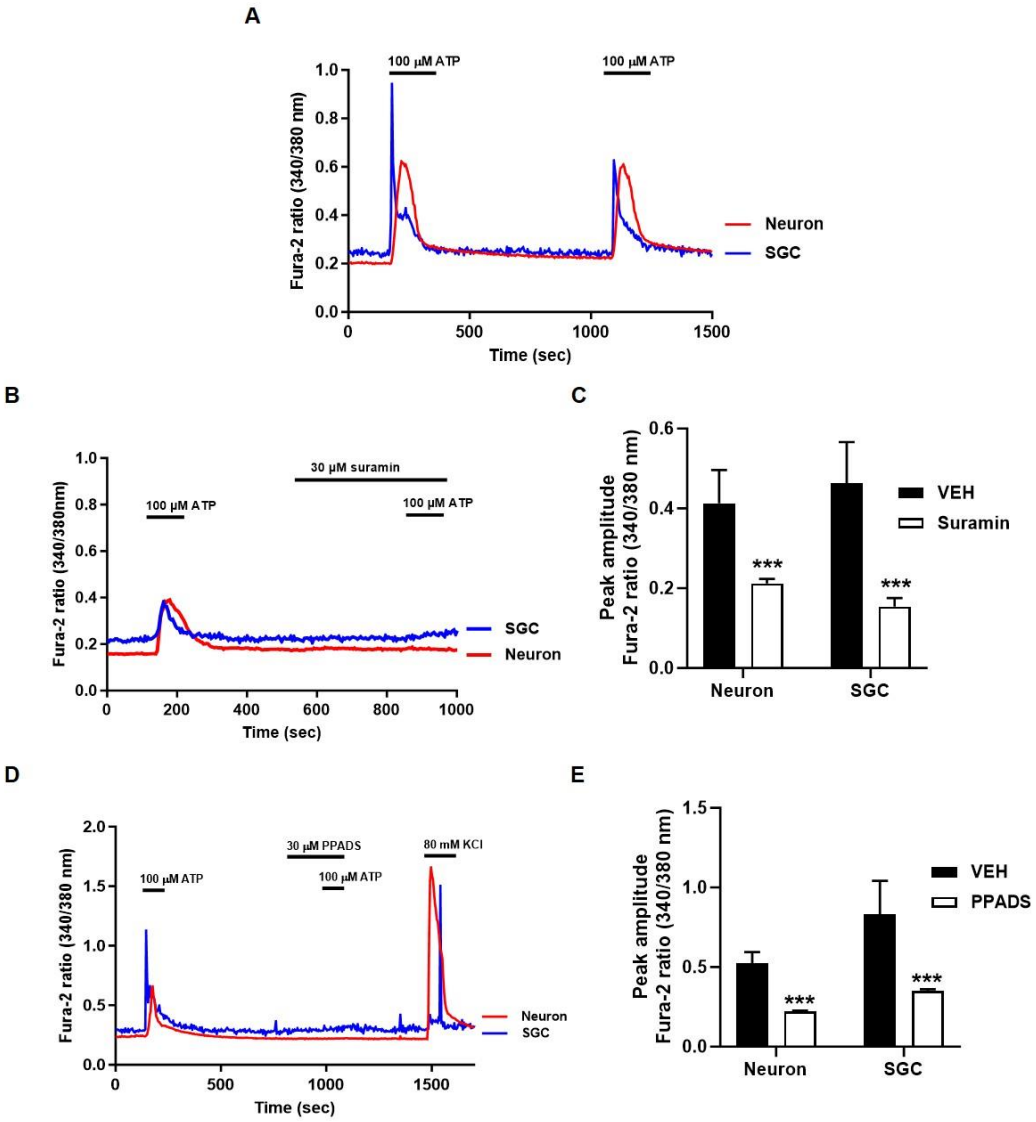

Figure 29. ATP-induced Ca^{2+} signaling in sympathetic neuron-SGC units. (A) Representative traces of serial stimulation of neuron-SGC units with pan-purinergic agonist,

ATP (100 μM). (B, D) Representative traces of the Ca^{2+} responses in neuron-SGC units with pan-purinergic inhibitors, Suramin (B) and PPADS (D). (C, E) Summary of the effects of pharmacological inhibitors of P2X (suramin, 30 μM) (C) and P2Y (PPADS, 30 μM) (E) (n = 6 - 8 cells). Data are presented as means ± SEM. The number of experiments is indicated in parenthesis. Unpaired Student's t-test, *** $p < 0.001$.

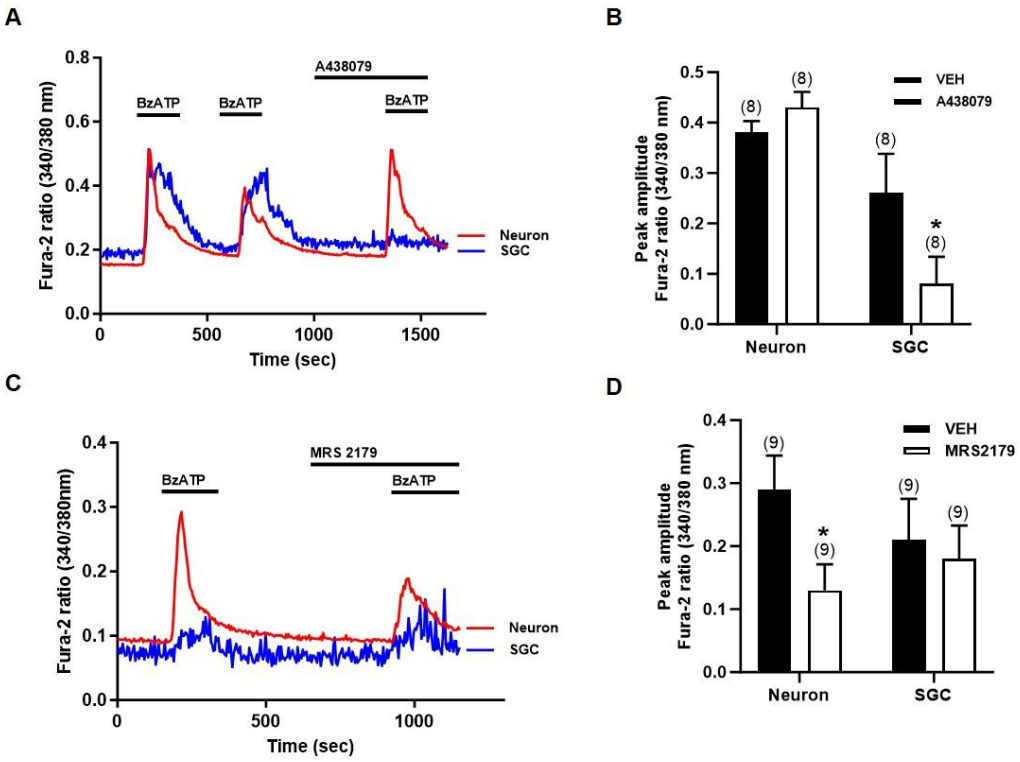

Figure 30. BzATP-induced Ca^{2+} signaling in sympathetic neuron-SGC units. (A, C) Representative traces of Ca^{2+} influx induced by 50 μM BzATP and the inhibitors of P2X7 (A438079, 30 μM) and P2Y1 receptors (MRS2179, 30 μM). BzATP is known to be a competitive agonist of P2X7. However, it can also act as partial agonists of P2Y1. BzATP can activate both sympathetic neurons and SGCs. With different antagonists, the BzATP-induced Ca^{2+} responses differed in neurons and SGCs. The P2X7 inhibitor, A438079, inhibited BzATP responses of SGCs while the neuronal response was insignificant before

and after the antagonist treatment. MRS 2179 inhibited BzATP response of the neurons while it did not affect that of SGCs. (B, D) Summary of the pharmacological inhibitions of BzATP response in the SGCs by A438079 (B) and that in the neurons by MRS2179 (D). P2X7 is present in the SGCs and P2Y1 may be present mainly in the sympathetic neurons. (n = 8 - 9 cells). Data are presented as means ± SEM. The number of experiments is indicated in parenthesis. Unpaired Student's t-test, * $p < 0.05$.

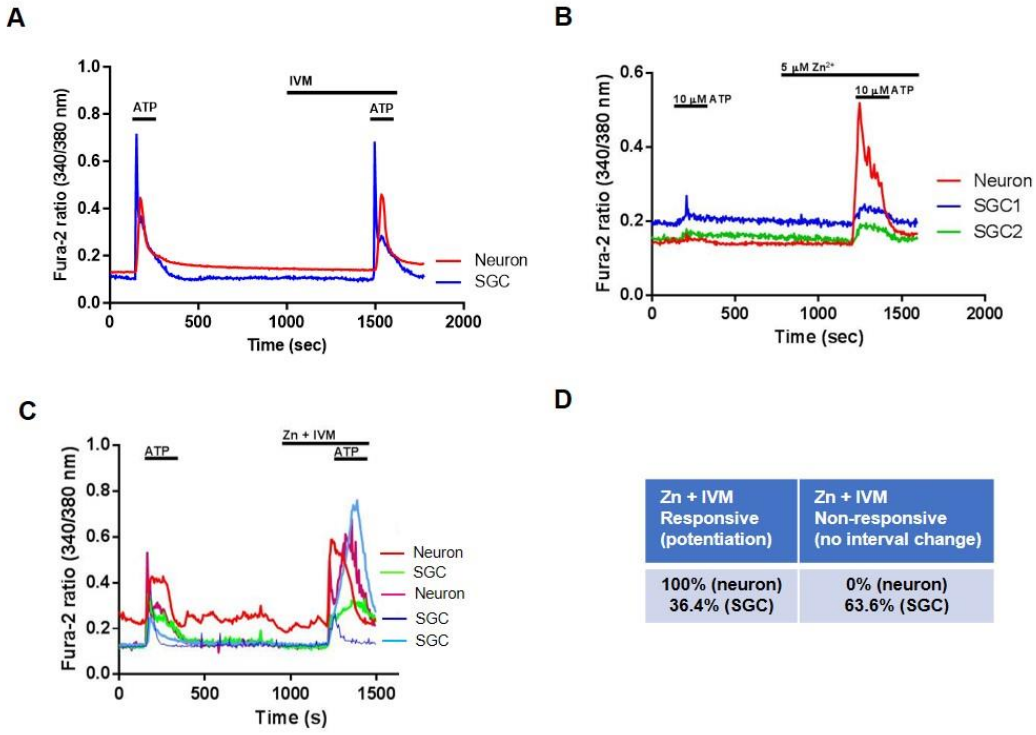

Zn + IVM Responsive (potentiation)	Zn + IVM Non-responsive (no interval change)
100% (neuron) 36.4% (SGC)	0% (neuron) 63.6% (SGC)

Fig. 31. P2X4 allosteric modulators. (A, B, C) Representative traces obtained in neuron-SGC units to functionally identify the endogenous P2X4 receptors. 100 μM of ATP induced Ca^{2+} influx in both neurons and SGCs, while the positive allosteric modulators of P2X4, ivermectin (IVM, 5 μM) and Zn^{2+} (5 μM), were applied to pharmacologically differentiate the distribution of P2X4 receptors in sympathetic neurons and SGCs. (D) Summary of responses induced by IVM and Zn^{2+} cocktails in neurons and SGCs.

A

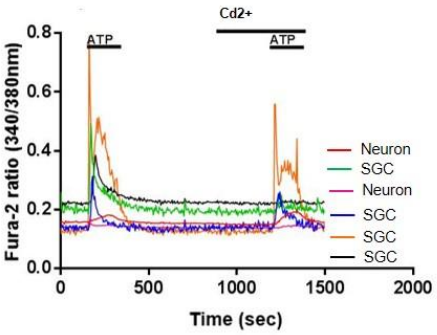

B

Cd^{2+} Responsive (inhibition)	Cd^{2+} Non-responsive (no interval change)	Cd^{2+} Responsive (potentiation)
0% (neuron) 20% (SGC)	100% (neuron) 50% (SGC)	0% (neuron) 30% (SGC)

Fig. 32. Negative allosteric modulators of P2X7. (A) Representative traces obtained in neuron-SGC units to functionally identify the endogenous P2X7 receptors. 100 μM of ATP induced Ca^{2+} influx in both neurons and SGCs, while the negative allosteric modulators of P2X7, Cd^{2+} (30 μM), was applied to pharmacologically differentiate the distribution of P2X7 receptors in sympathetic neurons and SGCs. Cd^{2+} allosterically inhibits P2X7 but potentiates P2X4 receptors (D) Summary of responses induced by Cd^{2+} in neurons and SGCs.

V. DISCUSSION

PART I

Characterization of the Ca^{2+} signaling mechanisms underlying SOCE and ROCE in sympathetic neurons and SGCs

While many groups have reported on the roles of sympathetic neurons in the autonomic nervous system [217-219], the functions of SGCs remain largely unelucidated since E. Pannese's initial report on their presence [36, 64]. Extensive researches focused on the role of SGCs in sensory ganglia, demonstrating their crucial involvement in modulating neuronal excitability and synaptic transmissions in animal models of neuropathic pain [164, 220, 221].

In this study, an *in vitro* system was developed for culturing sympathetic neuron-SGC units for further functional studies (Fig. 9). Partial digestion of SCGs was successful, yielding viable cells suitable for studying various physiological phenomena related to Ca^{2+} signaling in the sympathetic nervous system. This culture platform proves valuable in mimicking *in vivo* functions of sympathetic ganglia and can be adapted, modified, and applied for future studies on autonomic ganglia.

The sympathetic neurons (i.e. excitable cells) and SGCs (i.e. non-excitable cells) in the

peripheral nervous system, akin to the CNS, share physiological functions, enabling communication to regulate local neural homeostasis [222]. Non-excitable cells like glial cells lack the VGCCs that respond to membrane depolarization [223], Instead, they utilize alternative Ca^{2+} influx routes, such as SOCE to perform various cellular functions [120, 224, 225]. While neurons express SOCE components, the roles of SOCE in Ca^{2+} influx for excitable cells are not remarkable [226, 227]. Likewise, glial cells also express VGCCs, but these play a negligible role in glial cell Ca^{2+} signaling [228]. Over the past few decades, SOCE functions have been demonstrated in various cell types in the central and peripheral nervous systems, including cortical and hippocampal neurons, astrocytes, microglia, and Müller glia [83-88]. However, to our knowledge, the role of the SOCE functions in sympathetic neurons and satellite glial cells has not been reported. This thesis is the first time to reveal the SOCE functions in sympathetic SGCs and neurons, representing a significant contribution to the field.

The subsequent Ca^{2+} influx through Orai channels triggers cascades of intracellular signals that modulates cell proliferation, migration, exocytosis, and cell death. SOCE is also reported to be associated with the pathophysiology of neurodegenerative diseases [229, 230]. At the whole animal levels, SOCE in sympathetic neurons participates in the vasodilatory dysregulations, attempting to adjust vascular tones under stressful conditions such as cold [202]. Suppressed STIM1 activities with low SOCE activities in astrocytes have been shown to result a reduced response to adrenergic stimulation during sleep homeostasis [231]. These findings highlight the equal importance of neurons and SGCs in

the regulation of sympathetic physiology.

In the present study, I focused to identify alteration of SOCE in sympathetic neuron-SGC units during neuroinflammation. I demonstrated that the SOCE proteins, Orai1 and STIM1, are expressed and functional in rat sympathetic ganglia, particularly with high oscillating SOCE activities in the SGCs. I also discovered that the STIM1 and Orai1 protein expressions are notably decreased and functional SOCE was significantly suppressed under LPS exposure in both neurons and SGCs (Fig. 20). Sympathetic neurons and the SGCs attached to neurons showed a Ca^{2+} response to high extracellular K^+-induced depolarization, while singly dissociated glial cells was unresponsive to high K^+. Interestingly, LPS exposure increases Ca^{2+} response of neurons to high extracellular K^+ (Fig. 16). Moreover, the SGCs attached to these hyperexcitable neurons consequently showed more augmented and kinetically faster calcium transients to reflect the heightened neuronal excitability. In summary, these findings revealed that the SOCE is robustly functional in both neurons and SGCs of the sympathetic ganglia, while SOCE-mediated neuro-glial feedback loop could be drastically altered under inflammatory conditions.

In most electrically non-excitable cells, the depletion of ER Ca^{2+} store triggers secondary Ca^{2+} influx, known as SOCE, involving plasmalemmal channels [232]. Many studies have identified SOCE as the primary pathway for glial Ca^{2+} signaling in all types of glia within the central nervous system [233, 234]. However, until recently, little was known about the glial Ca^{2+} signaling mechanism in the peripheral nervous system including autonomic and sensory ganglia. Our investigation is the first time to reveal that sympathetic ganglia

possess a functional SOCE machinery for glial Ca^{2+} signaling. The key findings of our study are as follows. First, the SOCE machinery in the sympathetic ganglia primarily comprises Orai1 and STIM1. Second, the depletion of the ER Ca^{2+} induced by CPA activates the SOCE machinery, allowing the secondary Ca^{2+} influx through plasmalemmal Orai channels. Thus, SOCE may play a more significant role in SGCs than in neurons. Third, LPS-induced inflammation down-regulates the expression of Orai1 and STIM1, consequently limiting SOCE.

The CRAC is one of the plasmalemmal channels responsible for mediating SOCE and comprises Orai (the plasmalemmal channel) and STIM (the ER Ca^{2+} sensor). Three Orai isoforms (Orai1-3), and two of STIM (STIM1 and STIM2) isoforms have been identified in vertebrates[235]. STIM1 and Orai1 are the central components of the SOCE machinery in numerous cell types, including astrocyte [98-100, 236, 237]. Quantitative real-time PCR findings align with these discoveries, demonstrating the high expression of Orai1 and STIM1 in the sympathetic ganglia (Fig. 6). Notably, I visually observed, for the first time, the transient organization of STIM1-Orai1 puncta induced by ER-Ca^{2+} depletion in the sympathetic ganglia (Fig. 11). Additionally, the pharmacological inhibition of Orai1 significantly reduced the magnitude of SOCE. Our findings indicate that Orai1 and STIM1 are crucial in facilitating SOCE in sympathetic SGCs and neurons.

Cytoplasmic Ca^{2+} is an intracellular signal responsible for controlling many cellular processes. Ca^{2+} signaling in electrically excitable neurons mostly relies on the rapid and massive influx of Ca^{2+} via VGCCs, which are highly expressed on the plasma membranes.

In contrast, non-electrically excitable SGCs do not express functional VGCCs and utilize ER Ca^{2+} store as the main source of cytoplasmic Ca^{2+} signaling [80, 209, 234]. Consequently, the SOCE machinery appears to be highly developed in SGCs in compared to neurons of the sympathetic ganglia.

Typically, in the glial cells, ER Ca^{2+} serve as the primary source of cytoplasmic Ca^{2+} signaling and predominantly mobilized via IP_3 receptor activation downstream of G-protein coupled receptor activation [238]. Various sources release diverse bioactive substances that potentially activate G-protein coupled receptors, including nerve terminals, neuronal cell bodies, glial cells. Recent studies have shown that acetylcholine (ACh) increases intracellular Ca^{2+} by engaging muscarinic receptors [239]. We observed that neuronal depolarization induces somatic ATP release through activation of VGCCs, which contributes to increased intracellular Ca^{2+}, partly through the activation of metabotropic purinergic receptor activation, specifically P2Y1 (Fig. 28). Overall, ACh and ATP released from both preganglionic nerve terminals and postganglionic neuronal cell bodies are the principal mediators facilitating communication between neurons and SGCs. Hence, investigating whether the SOCE machinery (Orai1 and STIM1) is indispensable for muscarinic and purinergic receptors-mediated Ca^{2+} signaling could be an intriguing avenue for exploration.

A prominent feature of the SOCE in sympathetic SGCs is the presence of Ca^{2+} oscillations. Previous studies have suggested that the SOCE-related Ca^{2+} oscillations may originate from an intricate interplay between STIM1, transient receptor potential cation channels (TRPCs),

and plasmalemmal and ER Ca^{2+} pumps [81, 120]. Recently, we identified TRPC1, TRPC3, and TRPC6 in the sympathetic ganglia (Fig. 21-24). We explored an alternative SOCE pathway that involves the interaction between STIM1 and TRPC channels in sympathetic neurons and SGCs.

SGCs are believed to influence various neural functions within the sympathetic ganglia [44]. Growing evidence has suggested that nerve injury and inflammation can modulate the functions of sensory SGCs, which are notably linked with pain sensation through TLR4 activation and GFAP [33]. Recent studies have remarkably demonstrated that LPS-induced upregulation of SOCE increases proinflammatory cytokine production in spinal astrocytes, and initiates inflammatory signaling pathways in a mouse hippocampal cell line [89, 240]. We attempted to make an *in vivo* animal model with acute inflammation induced by LPS, bacterial endotoxin, to investigate the tole of SOCE in acute systemic inflammation. We found that LPS diminished SOCE by downregulating Orai1 and STIM1 expression in the sympathetic ganglia. LPS-induced downregulation of SOCE has been consistently reported in different glial cell types, including hippocampal astrocytes and microglia [84, 87, 241]. We are currently uncertain about the source of the discrepancy in LPS-induced regulation of SOCE. Future research on the signaling mechanisms underlying the LPS-induced downregulation of SOCE machinery in rat sympathetic ganglia is awaited.

The upregulation of GFAP is a widely used hallmark of glial activation and reactive gliosis [242]. Hanani group [243] demonstrated that LPS upregulates GFAP expression through TLR4 activation in mouse trigeminal ganglia. They also suggested that the absence of

TLR4 in mouse SCG prevents reactive gliosis in response to LPS exposure. In contrast, we observed that TLR4 is expressed in rat sympathetic ganglia, and mediates the activation of SGCs in response to LPS exposure. A previous study has shown that sciatic nerve injury causes GFAP upregulation in the sensory ganglia of rats, but not in mice [244]. There appear to be differences in how species respond to certain pathological conditions.

TLR4 mediates the production of proinflammatory cytokines such as tumor necrosis factor-alpha and interleukin 1 beta in neurons, astrocytes, and microglia [245, 246]. Unexpectedly, our immunocytochemical staining of the neuron-SGC units demonstrated that SCG neurons, but not SGCs, highly expressed TLR4, suggesting that neurons are the major cellular sources of pro-inflammatory cytokines in the rat SCG. In general, the release of proinflammatory cytokines is regulated by calcium-dependent signaling mechanisms that activate several transcription factor pathways, including nuclear factor kappa B, NFAT, and cAMP response element-binding protein [247-249]. In SCG neurons, it is unlikely that SOCE mediates the release of proinflammatory cytokines due to the LPS-induced downregulation of Orai1 and STIM1. In contrast, LPS increased Ca^{2+} influx through VGCCs (Fig. 16), suggesting an alternative mechanism for the Ca^{2+}-dependent release of proinflammatory cytokines induced in SCG neurons. VGCCs in sympathetic neurons comprise N, L, and R types [250]. Evidence supports that STIM1 can trigger the internalization of L-type Cav1.2 channels from the plasma membrane through physical binding in multiple cell types, including neurons and vascular smooth muscle [77, 251]. A recent study showed that loss of STIM1 potentiates Ca^{2+} entry through Cav1.2, resulting in

cell death [252]. Consequently, we speculate that the LPS-induced increase in Ca^{2+} entry through VGCCs is associated with the potentiation of Cav1.2 due to reduced STM1 expression in rat SCG neurons.

SGCs in the peripheral ganglia have immune properties and expressing mitogen-activated protein kinases and cytokines [50, 253]. Consequently, we consider that, in addition to neurons, SGCs can release proinflammatory cytokines through alternative pathways, even though their expression of TLR4, if any, is weak. As mentioned previously, SOCE is the primary Ca^{2+} signaling mechanism in sympathetic SGCs. An alternative Ca^{2+} signaling pathway might involve Ca^{2+} influx across the plasma membrane via ion channels such as P2X receptors. Among the known P2X receptor isoforms, P2X7 mediates LPS-induced inflammation [254]. On the other hand, interleukin 1 beta upregulates P2X7 expression in human astrocytes [255]. I observed that P2X7 was weakly expressed together with P2Y in healthy sympathetic SGCs. Overall, it might be worth examining whether LPS-induced activation of somatic ATP and cytokine release occurs through STIM1 downregulation-mediated activation of Cav1.2, and increase SGC Ca^{2+} signaling by activating the upregulated P2X7 in the sympathetic ganglia.

Moreover, concerning the modulation of neuronal excitability, Park *et al*. also demonstrated that STIM physically binds to the VGCCs to control the excitability of the neurons [77]. This implies that some portions of STIM is pre-occupied with VGCC and not available as functional SOCE machinery, resulting in low SOCE activities in neurons under normal physiology. However, linking this finding to my study, LPS reduces the actual

expression levels of STIM1 and Orai1 proteins, and suppresses the SOCE activities. VGCCs bound to STIM proteins may be freed upon LPS exposure, and, potentially boosting the net neuronal Ca^{2+} influx when chemically depolarized by high KCl. Simultaneously, I observed that the SGCs attached to the depolarized neurons showed a faster response, suggesting a paracrine effect. This further indicates that Ca^{2+} signaling in sympathetic SGCs may serve as an *in situ* sensor reflecting the excitable status of sympathetic neurons.

In an alternative scenario, SOCE activities in the SGCs may play a role in releasing of inhibitory gliotransmitters (e.g. adenosine, gamma-aminobutyric acid (GABA)) toward adjacent sympathetic neurons. Toth *et al*. extensively studied the modulation of hippocampal neuronal excitability by the gliotransmitter GABA released from astrocytes [88]. Additionally, Zhu *et al.* and Park *et al.* provided comparable data on the modulation of sympathetic neuronal N-type channels by A1-adenosine receptors [256, 257]. These reports suggested that adenosine can inhibit the activities of sympathetic VGCCs. Based on Zhang *et al.*[167] and my own observations, sympathetic neurons can extrasynaptically release ATP when depolarized and excited. I hypothesized that neuronal depolarization leads to the somatic release of certain substances (e.g. ATP), which may activate SOCE and other Ca^{2+} pathways in SGCs via metabotropic GPCRs. Consequently, an increase in intracellular Ca^{2+} in sympathetic SGCs could trigger the release of potential gliotransmitters such as adenosine, GABA and ATP, exerting tonic inhibition on the VGCCs of excited sympathetic neurons. This is likely facilitated by the close proximity of

a sympathetic neuron-SGC units, ensuring the highly concentrated transmitters act simultaneously in the local nano-environmental milieu (Fig. 1 & Fig. 8). In summary, SOCE of sympathetic SGCs might act as a hub for finely tuning the balance of excitation and inhibition of sympathetic neuronal activity. The summary of calcium signaling in the sympathetic neurons and SGCs is described in a schematic diagram in Fig. 33.

This study represents the inaugural investigation into SOCE activities in sympathetic ganglia. The bidirectional feedback observed between sympathetic neurons and SGCs via SOCE activations in SCG underscores its functional significance in regulating sympathetic control over craniofacial regions. Defining the functions of SOCE in sympathetic ganglia constitutes a substantial area of research, offering ample opportunities for future studies to develop the nuanced contributions of SOCE to both sympathetic neuronal and glial physiology.

PART II

The examination of somatic ATP release in sympathetic ganglia and the purinergic signaling mechanisms involved in communication between neurons and SGCs

Accumulating evidences suggest that Ca^{2+} signaling of glial cells with other cell types is crucial in modulating synaptic transmissions [165, 258, 259]. Despite a few studies on the Ca^{2+} signaling between neuron and glia [166, 167], little is known about the mechanisms of functional Ca^{2+} signaling in the PNS. Similar to astrocytes, SGCs are the major type glial cells in the PNS playing a role in the regulation of neural transmission [69]. Due to its unique anatomical feature of tightly wrapping around the neuronal soma, the intercellular space between the neuron and SGCs is narrow concentrating releasable substances. Thus, it is likely that SGCs are susceptible to the substances released from the neurons attached to them. SGCs have been reported to express a wide range of purinergic receptors in response to ATP via intracellular Ca^{2+} signaling mechanism [55, 58, 260]. Similar to astrocytes, the ATP-induced response of SGCs may play a role in modulating neuronal excitability and finely tuning the micro-neural environment in different peripheral ganglia. In this study, I demonstrated that SGCs and neurons from rat sympathetic ganglia undergo complementary purinergic communications via Ca^{2+} signaling. Upon chemical

depolarization of neurons with high extracellular K^+, neuronal excitation subsequently increases glial cytosolic Ca^{2+}. This finding is significant for SGCs attached to the neurons, as singly dissociated glial cells do not exhibit any Ca^{2+} influx upon high K^+ stimulation. Thus, glial Ca^{2+} signal pathways can be divided into two types: (1) released molecules from the surrounding neurons to activate the glial purinergic receptors [166, 167], and (2) gap junction-mediated pathways [165, 259]. My studies demonstrated that the somatic ATP release pathways via Ca^{2+} signals between neurons and SGCs was significantly hindered by Cd^{2+}, the non-selective VGCC blocker, indicating that glial Ca^{2+} signaling was dependent on neuronal excitation. Apyrase, ectonucleotidase, was applied to verify somatic ATP release from the neurons. Upon high K^+ stimulation after pre-treatment with apyrase, neurons were depolarized with a substantial Ca^{2+} influx, the attached SGCs showed no Ca^{2+} influx, confirming the breakdown of ATP in the extracellular space. This confirmed that ATP released from the sympathetic neurons mediates adjacent glial Ca^{2+} signaling in an intact neuron-SGC unit. FM 1-43 and acridine-based dye, quinacrine, were used to stain ATP-containing vesicles, and the natural trajectory of vesicles in the neuronal cytosol was monitored upon high K^+ stimulation. The number of ATP-containing vesicles decreased significantly, confirming the presence of Ca^{2+}-dependent vesicular ATP release from the sympathetic neurons. An ATP bioluminescence assay was conducted to detect changes in extracellular ATP concentrations. ATP levels were quantified, and the culture system enriched with neuronal cells showed an increase in extracellular ATP levels upon chemical depolarization. Purinergic receptors were characterized, and P2X4, P2X7, and P2Y1

receptors were identified to focus on the glial response to somatic ATP release. Pan-purinergic antagonists such as suramin and PPADS were applied and ATP-induced Ca^{2+} responses of neurons and SGCs were almost completely abolished. A specific agonist, BzATP, was used to target P2X7 primarily. A438079 selectively blocked BzATP-induced Ca^{2+} responses of P2X7 receptors in SGCs, but not in neurons, while MRS2179 blocked Ca^{2+} influx induced by BzATP in SCG neurons but not in SGCs. Overall, P2Y1 receptors might be more predominantly present in sympathetic neurons.

The existence of a selective agonist for P2X4 receptors are still controversial. However, traditionally, allosteric modulation by trace metals are useful tools to pharmacologically segregate the functions of P2X4 and P2X7 receptors (Fig. 5A, table adopted from Coddou et al. [142]), These receptors are rich in histidine residues in the N-terminus of the receptor, and trace metals such as zinc, cadmium, and copper can allosterically bind to P2X receptors to modulate the opening of ion channels. For instance, zinc can potentiate the ATP response of P2X4 receptors but inhibits P2X7 receptors. Similarly, cadmium also potentiates the calcium response of P2X4 receptors but inhibits P2X7 receptors. Zinc also potentiates P2X2/3 which are also present in SCGs based on the PCR profiles. Ivermectin (IVM, 5 μM) is a synthetic positive allosteric modulator used to activate P2X4 receptor. However, its effect was not significant in a cultured system of sympathetic neuron-SGC units (Fig. 31A). Interestingly, sympathetic neurons were potentiated by zinc, indicating the presence of P2X2/3 in these neurons (Fig. 31B) [115]. Immunofluorescent studies reveled that P2X4 were mainly in SGCs, suggesting that the enhanced Ca^{2+} response in neurons may not be

due to neuronal P2X4. The ATP-induced Ca^{2+} response of SGCs to zinc was more complex showing a heterologous Ca^{2+} response of SGCs (Fig. 31C). Recent literatures [156-158] suggest that both P2X4 and P2X7 receptors can co-exist in heteromers within the same cell type (Fig5. B, C, adopted from Craigie et al. [159]). It can be speculated that P2X4 and P2X7 are heterogeneously expressed in the SGCs, presenting multiple types of Ca^{2+} responses to the trace metals. The expression levels of each purinergic receptors under different physiological conditions may vary. One possibility to explain this finding is that the data presented in this project are based on the cell culture platform of neuron-SGC units. The relevance of the data to the intact sympathetic ganglia is still questionable. It is important to note that the culture system is only maintained for the short-term, allowing acutely dissociated cells to retain sympathetic properties of the intact ganglia. However, the Ca^{2+} responses to allosteric modulators are heterologous by nature, considering the presence of multiple P2 receptors in the same cell type. Perhaps, this is more closely resemble the natural functions of intact sympathetic ganglia instead of singly dissociated cells [55]. Nevertheless, I still encounter some limitations in directly reflecting the functions of intact ganglia at the cell levels in such culture systems.

Previously, I found that cultured neuron-SGC units exposed to LPS showed a significantly high amplitude of Ca^{2+} influx in both neurons and SGCs upon high K^+ stimulation compared to controls. The mechanism of inflammation increasing neuronal and SGC Ca^{2+} signaling is yet elusive. Still, it can be explained by the literature that augmented neuro-glial communication with hyperexcitable neurons might be due to the increased sensitivity

and/or expression of purinergic receptors of SGCs to somatic ATP release in the inflammation model [261]. This further proposes that the sub-cellular Ca^{2+} signaling alterations in neurons and SGCs of the autonomic nervous system can ultimately induce changes in the innervating target organs via chemical signals.

Overall, based on the findings of Part II project, the enhanced Ca^{2+} signaling in SGCs in neuron-SGC cultures demonstrates multiple Ca^{2+} signaling in sympathetic ganglia. Increasing neuronal excitation amplifies glial Ca^{2+} signal transmission, providing feedback to adjacent neurons to contribute in neural synaptic plasticity (Fig. 33). In summary, I provide some evidence to suggest that neuron-SGC units from sympathetic ganglia can communicate via Ca^{2+} signal transmissions, involving the activation of purinergic receptors. These findings suggest that purinergic receptors are functional in the neurons and SGCs of the rat sympathetic ganglia.

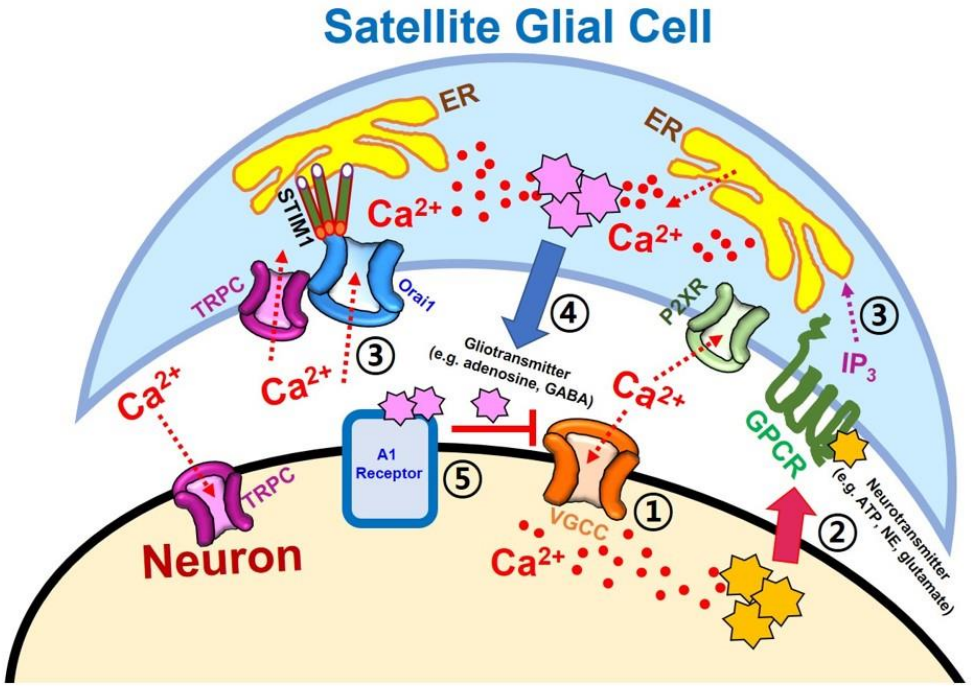

Figure 33. Summary of Ca^{2+} signaling pathways in sympathetic neuron-SGC units. This schematic diagram illustrates the communication between a sympathetic neuron-SGC unit, detailing its modulation of sympathetic tone under various physiological and pathological conditions. Following depolarization via VGCCs (①), the sympathetic neuron undergoes electrical excitation and releases neurotransmitters (②). These released neurotransmitters, such as ATP, activated glial P2X receptors or metabotropic GPCRs, triggering SOCE and TRPCs in both neurons and SGCs. This occurs by elevating intracellular Ca^{2+} through Orai1-STIM mobilization (③). Consequently, glial SOCE-

mediated gliotransmitter release (e.g. adenosine, GABA) is initiated (④). Ultimately, gliotransmitters inhibit VGCCs in sympathetic neurons (⑤). Under abnormal physiological conditions, the Ca^{2+} signaling of neurons and SGCs may be dysregulated. Leading to the release of potential gliotransmitters that modulate neuronal VGCCs. This introduces a feedback loop in sympathetic neuro-glial communication, which can be altered in pathological states.

VI. CONCLUSION

SGCs tightly wrap around the cell bodies of neurons within sympathetic ganglia, suggesting a potential signal exchange mechanism for regulating physiological homeostasis. Despite this unique anatomical arrangement, little is known about the functional roles of sympathetic neuron-SGC units. In this study, we demonstrated that both sympathetic neurons and SGCs in the rat SCG exhibited the plasmalemmal Orai1 puncta aggregates and SOCE upon the endoplasmic reticulum (ER) Ca^{2+} store depletion. Orai1 and STIM1 were identified as the major components of SOCE machinery in sympathetic ganglia. SOCE was significantly suppressed by GSK7975A (1 μM), a selective Orai1 blocker, and Pyr6 (3 μM), a SOCE blocker. Remarkably, the magnitude of SOCE was substantially larger with oscillations observed in SGCs compared to neurons. After acute LPS exposure, the SOCE of both sympathetic neurons and SGCs were remarkedly suppressed. On the other hand, the depolarization-stimulated $[Ca^{2+}]_i$ transients were significantly augmented after LPS exposure in the sympathetic neuron-SGC units.

In an effort to characterize the ROCE components in sympathetic ganglia, TRPC3 and TRPC6 were further investigated with selective TRPC inhibitors, Pyr3 and SAR7334, were employed to identify the presence of TRPCs in SCG neurons and SGCs. Additionally, TRPCs, especially TRPC3, may also be a partial component of SOCE machinery as CPA-

induced SOCE activity was reduced by lanthanum chloride and Pyr3. In contrast to sympathetic SOCE profiles, Ca^{2+} signaling through TRPCs was significantly larger in sympathetic neurons compared to the SGCs. Taken together, Ca^{2+} is mediated by Orai, STIM, and TRPC channels in sympathetic ganglia, potentially contributing to functions of sympathetic neuron-SGC units.

Neuro-glial Ca^{2+} signaling is critical for regulating the communications in neuron-SGC units. ATP is also extrasynaptically released from autonomic neurons. To date, however, the functional significance of somatic ATP release in the sympathetic ganglia remains elusive. Upon depolarization of the SCG neurons by application of high potassium (K^+), intracellular Ca^{2+} is significantly increased in the SGCs attached to the SCG neurons, but not in singly isolated glial cells. This strongly suggests that neuronal excitation causes a local release of bioactive substances that affect the attached SGCs. FM1-43-stained and quinacrine-stained vesicular puncta in the soma of SCG neuron, suggesting somatic ATP release and ATP bioluminescence assay confirmed the ATP released from cultured sympathetic neurons upon high K^+ stimulation. The purinergic receptors in neuron-SGC units were characterized by functional studies with pharmacological antagonists such as suramin, PPADS, A438079, MRS2179, and positive/negative allosteric modulators of P2X receptors. The presence of P2X4, P2X7, and P2Y1 receptors in rat SCG. Consequently, this diversity in receptor composition contributes to the provision of a wide range of Ca^{2+} responses in SGCs when exposed to external stimuli. Taken together, the somatic ATP released from the sympathetic neurons may trigger the activation of multiple candidate

purinergic receptors in the SGCs through Ca^{2+} signaling. In conclusion, our findings offer foundational insights into the major mechanism of Ca^{2+} signaling in SGCs, comparing them with the principal neurons in the sympathetic ganglia. Emerging evidence support the new hypothesis indicating that the complex network contributing to final visceral motor output involves neurons and glial cells within the autonomic ganglia. For instance, activating Gq G protein-coupled receptors in sympathetic SGCs significantly accelerates cardiovascular functions [262]. This observation suggests that maintaining glial Ca^{2+} homeostasis is critical for neural activity in the sympathetic ganglia. Several pathological conditions including chronic heart failure [65], liver cirrhosis [66], and traumatic brain injury [67], lead to autonomic imbalance characterized by sympathetic overactivity. Thus, whether dysregulation of SOCE contributes to alterations in sympathetic output during these diseased states remains to be explored.

VII. FUTURE DIRECTIONS

The accumulating evidences further underscores the crucial role of SGCs in the regulation of autonomic ganglion. This presents a initial step in identifying and characterizing the functional roles of sympathetic SGCs. The physiology of the ANS involves a coordinated balance between sympathetic and parasympathetic nervous systems. Thus, future studies should elaborate on the findings of the sympathetic SGCs to other autonomic systems, recognizing that this study contributes only a part to the broader picture.

Building upon the current study, the functional mechanisms of IP_3R- and RyR-mediated pathways of glial SOCE can be explored to gain deeper understanding of the observed Ca^{2+} oscillation phenomena in SGCs. SOCE activities of SGCs may be significantly suppressed by the application of inhibitors such 2-APB (IP_3R blocker) and U73122 (PLC blocker). Conducting genetic knock-down studies of Orai and TRPC channels using small interfering RNA (SiRNA) or short hairpin (shRNA) would be interesting to compare with the pharmacological inhibitor data. In addition to Ca^{2+} imaging data, whole-cell patch clamp studies on SGCs attached to neurons are necessary to collect electrical measurements of SOCE and ATP-induced P2X currents, providing sight into the electrophysiological profiles of the Ca^{2+}-permeable channels in SGCs. Developing gene over-expression models of P2X channels in HEK cells could be utilized for sniffer patch-clamp. Establishing co-culture of P2X over-expressed HEK cells with neuron-SGC units would enable the measurement of somatic ATP release. Finally, exploring the roles of mitochondria in Ca^{2+} homeostasis can be studied in the extension of this study scope.

VIII. REFERENCES

1. Imai, J. and H. Katagiri, *Regulation of systemic metabolism by the autonomic nervous system consisting of afferent and efferent innervation.* Int Immunol, 2022. **34**(2): p. 67-79.
2. McCorry, L.K., *Physiology of the autonomic nervous system.* Am J Pharm Educ, 2007. **71**(4): p. 78.
3. Espinosa-Medina, I., et al., *The sacral autonomic outflow is sympathetic.* Science, 2016. **354**(6314): p. 893-897.
4. Gabella, G., P. Trigg, and H. McPhail, *Quantitative cytology of ganglion neurons and satellite glial cells in the superior cervical ganglion of the sheep. Relationship with ganglion neuron size.* J Neurocytol, 1988. **17**(6): p. 753-69.
5. Ribeiro, A.A., C. Davis, and G. Gabella, *Estimate of size and total number of neurons in superior cervical ganglion of rat, capybara and horse.* Anat Embryol (Berl), 2004. **208**(5): p. 367-80.
6. Loesch, A., et al., *Stereological and allometric studies on neurons and axo-dendritic synapses in the superior cervical ganglia of rats, capybaras and horses.* Cell Tissue Res, 2010. **341**(2): p. 223-37.
7. Gibbins, I.L. and J.L. Morris, *Structure of peripheral synapses: autonomic ganglia.* Cell Tissue Res, 2006. **326**(2): p. 205-20.
8. Gibbins, I.L., *Vasomotor, pilomotor and secretomotor neurons distinguished by*

size and neuropeptide content in superior cervical ganglia of mice. J Auton Nerv Syst, 1991. **34**(2-3): p. 171-83.

9. Shaibani, A., et al., *First results in an MR imaging--compatible canine model of acute stroke.* AJNR Am J Neuroradiol, 2006. **27**(8): p. 1788-93.
10. Palmer, A.C., *Pontine infarction in a dog with unilateral involvement of the trigeminal motor nucleus and pyramidal tract.* J Small Anim Pract, 2007. **48**(1): p. 49-52.
11. Kokaia, M., et al., *Seizure development and noradrenaline release in kindling epilepsy after noradrenergic reinnervation of the subcortically deafferented hippocampus by superior cervical ganglion or fetal locus coeruleus grafts.* Exp Neurol, 1994. **130**(2): p. 351-61.
12. Bell, R.L., et al., *Traumatic and iatrogenic Horner syndrome: case reports and review of the literature.* J Trauma, 2001. **51**(2): p. 400-4.
13. Miolan, J.P. and J.P. Niel, *The mammalian sympathetic prevertebral ganglia: integrative properties and role in the nervous control of digestive tract motility.* J Auton Nerv Syst, 1996. **58**(3): p. 125-38.
14. Toscano, C.P., et al., *The developing and restructuring superior cervical ganglion of guinea pigs (Cavia porcellus var. albina).* Int J Dev Neurosci, 2009. **27**(4): p. 329-36.
15. Melo, S.R., et al., *The developing left superior cervical ganglion of Pacas (Agouti paca).* Anat Rec (Hoboken), 2009. **292**(7): p. 966-75.

16. Fioretto, E.T., et al., *Macro- and microstructure of the superior cervical ganglion in dogs, cats and horses during maturation.* Cells Tissues Organs, 2007. **186**(2): p. 129-40.

17. Reuss, S. and R.Y. Moore, *Neuropeptide Y-containing neurons in the rat superior cervical ganglion: projections to the pineal gland.* J Pineal Res, 1989. **6**(4): p. 307-16.

18. Rytel, L., et al., *Identification of neuropeptide y in superior cervical ganglion neurons that project to the oesophagus - A combined immunohistochemical labelling and retrograde tracing study in pigs.* Acta Vet Hung, 2019. **67**(1): p. 98-105.

19. Li, C. and J.P. Horn, *Physiological classification of sympathetic neurons in the rat superior cervical ganglion.* J Neurophysiol, 2006. **95**(1): p. 187-95.

20. Ernsberger, U., T. Deller, and H. Rohrer, *The diversity of neuronal phenotypes in rodent and human autonomic ganglia.* Cell Tissue Res, 2020. **382**(2): p. 201-231.

21. Jobling, P. and I.L. Gibbins, *Electrophysiological and morphological diversity of mouse sympathetic neurons.* J Neurophysiol, 1999. **82**(5): p. 2747-64.

22. Furlan, A., et al., *Visceral motor neuron diversity delineates a cellular basis for nipple- and pilo-erection muscle control.* Nat Neurosci, 2016. **19**(10): p. 1331-40.

23. Virchow, R., *On the Course of the Amyloid Degeneration.* Med Exam (Phila), 1856. **12**(138): p. 380-383.

24. Nave, K.A. and B.D. Trapp, *Axon-glial signaling and the glial support of axon*

function. Annu Rev Neurosci, 2008. **31**: p. 535-61.

25. Freeman, M.R., *Sculpting the nervous system: glial control of neuronal development.* Curr Opin Neurobiol, 2006. **16**(1): p. 119-25.
26. Allen, N.J. and D.A. Lyons, *Glia as architects of central nervous system formation and function.* Science, 2018. **362**(6411): p. 181-185.
27. Wilkins, A., et al., *Oligodendrocytes promote neuronal survival and axonal length by distinct intracellular mechanisms: a novel role for oligodendrocyte-derived glial cell line-derived neurotrophic factor.* J Neurosci, 2003. **23**(12): p. 4967-74.
28. Szalay, G., et al., *Microglia protect against brain injury and their selective elimination dysregulates neuronal network activity after stroke.* Nat Commun, 2016. **7**: p. 11499.
29. Peng, H.B., et al., *Differential effects of neurotrophins and schwann cell-derived signals on neuronal survival/growth and synaptogenesis.* J Neurosci, 2003. **23**(12): p. 5050-60.
30. Mauch, D.H., et al., *CNS synaptogenesis promoted by glia-derived cholesterol.* Science, 2001. **294**(5545): p. 1354-7.
31. Jessen, K.R. and R. Mirsky, *The repair Schwann cell and its function in regenerating nerves.* J Physiol, 2016. **594**(13): p. 3521-31.
32. Dai, X., et al., *The trophic role of oligodendrocytes in the basal forebrain.* J Neurosci, 2003. **23**(13): p. 5846-53.
33. Hanani, M. and D.C. Spray, *Emerging importance of satellite glia in nervous*

system function and dysfunction. Nat Rev Neurosci, 2020. **21**(9): p. 485-498.

34. Pomeroy, S.L. and D. Purves, *Neuron/glia relationships observed over intervals of several months in living mice.* J Cell Biol, 1988. **107**(3): p. 1167-75.

35. Pannese, E., *The satellite cells of the sensory ganglia.* Adv Anat Embryol Cell Biol, 1981. **65**: p. 1-111.

36. Pannese, E., *[Research on the morphology of the perineuronal satellite cells in the spinal and sympathetic ganglia of mammals. I. Phase-contrast findings].* Boll Soc Ital Biol Sper, 1956. **32**(1-2): p. 72-4.

37. Bunge, R.P., M.B. Bunge, and C.F. Eldridge, *Linkage between axonal ensheathment and basal lamina production by Schwann cells.* Annu Rev Neurosci, 1986. **9**: p. 305-28.

38. Pannese, E., *The structure of the perineuronal sheath of satellite glial cells (SGCs) in sensory ganglia.* Neuron Glia Biol, 2010. **6**(1): p. 3-10.

39. Ledda, M., S. De Palo, and E. Pannese, *Ratios between number of neuroglial cells and number and volume of nerve cells in the spinal ganglia of two species of reptiles and three species of mammals.* Tissue Cell, 2004. **36**(1): p. 55-62.

40. Huang, L.Y., Y. Gu, and Y. Chen, *Communication between neuronal somata and satellite glial cells in sensory ganglia.* Glia, 2013. **61**(10): p. 1571-81.

41. van Weperen, V.Y.H., et al., *Single-cell transcriptomic profiling of satellite glial cells in stellate ganglia reveals developmental and functional axial dynamics.* Glia, 2021. **69**(5): p. 1281-1291.

42. Belzer, V., N. Shraer, and M. Hanani, *Phenotypic changes in satellite glial cells in cultured trigeminal ganglia.* Neuron Glia Biol, 2010. **6**(4): p. 237-43.

43. Hanani, M., *Satellite glial cells in sympathetic and parasympathetic ganglia: in search of function.* Brain Res Rev, 2010. **64**(2): p. 304-27.

44. Enes, J., et al., *Satellite glial cells modulate cholinergic transmission between sympathetic neurons.* PLoS One, 2020. **15**(2): p. e0218643.

45. Mapps, A.A., et al., *Satellite glia modulate sympathetic neuron survival, activity, and autonomic function.* Elife, 2022. **11**.

46. Tropea, M., M.I. Johnson, and D. Higgins, *Glial cells promote dendritic development in rat sympathetic neurons in vitro.* Glia, 1988. **1**(6): p. 380-92.

47. McFarlane, S. and E. Cooper, *Extrinsic factors influence the expression of voltage-gated K currents on neonatal rat sympathetic neurons.* J Neurosci, 1993. **13**(6): p. 2591-600.

48. Zhang, H., et al., *Altered functional properties of satellite glial cells in compressed spinal ganglia.* Glia, 2009. **57**(15): p. 1588-99.

49. Woodham, P., et al., *Satellite cells surrounding axotomised rat dorsal root ganglion cells increase expression of a GFAP-like protein.* Neurosci Lett, 1989. **98**(1): p. 8-12.

50. Afroz, S., et al., *CGRP Induces Differential Regulation of Cytokines from Satellite Glial Cells in Trigeminal Ganglia and Orofacial Nociception.* Int J Mol Sci, 2019. **20**(3).

51. Kim, Y.S., et al., *Coupled Activation of Primary Sensory Neurons Contributes to Chronic Pain.* Neuron, 2016. **91**(5): p. 1085-1096.

52. Komiya, H., et al., *Connexin 43 expression in satellite glial cells contributes to ectopic tooth-pulp pain.* J Oral Sci, 2018. **60**(4): p. 493-499.

53. Vit, J.P., et al., *Satellite glial cells in the trigeminal ganglion as a determinant of orofacial neuropathic pain.* Neuron Glia Biol, 2006. **2**(4): p. 247-57.

54. Kaan, T.K., P.T. Ohara, and L. Jasmin, *Orofacial pain models and behavior assessment.* Methods Mol Biol, 2012. **851**: p. 159-70.

55. Weick, M., et al., *P2 receptors in satellite glial cells in trigeminal ganglia of mice.* Neuroscience, 2003. **120**(4): p. 969-77.

56. Magni, G., D. Riccio, and S. Ceruti, *Tackling Chronic Pain and Inflammation through the Purinergic System.* Curr Med Chem, 2018. **25**(32): p. 3830-3865.

57. Ceruti, S., et al., *Calcitonin gene-related peptide-mediated enhancement of purinergic neuron/glia communication by the algogenic factor bradykinin in mouse trigeminal ganglia from wild-type and R192Q Cav2.1 Knock-in mice: implications for basic mechanisms of migraine pain.* J Neurosci, 2011. **31**(10): p. 3638-49.

58. Ceruti, S., et al., *Purinoceptor-mediated calcium signaling in primary neuron-glia trigeminal cultures.* Cell Calcium, 2008. **43**(6): p. 576-90.

59. Nance, D.M. and V.M. Sanders, *Autonomic innervation and regulation of the immune system (1987-2007).* Brain Behav Immun, 2007. **21**(6): p. 736-45.

60. van der Poll, T., et al., *Noradrenaline inhibits lipopolysaccharide-induced tumor necrosis factor and interleukin 6 production in human whole blood.* Infect Immun, 1994. **62**(5): p. 2046-50.

61. Severn, A., et al., *Regulation of tumor necrosis factor production by adrenaline and beta-adrenergic agonists.* J Immunol, 1992. **148**(11): p. 3441-5.

62. Ignatowski, T.A., S. Gallant, and R.N. Spengler, *Temporal regulation by adrenergic receptor stimulation of macrophage (M phi)-derived tumor necrosis factor (TNF) production post-LPS challenge.* J Neuroimmunol, 1996. **65**(2): p. 107-17.

63. Kox, M., et al., *Voluntary activation of the sympathetic nervous system and attenuation of the innate immune response in humans.* Proc Natl Acad Sci U S A, 2014. **111**(20): p. 7379-84.

64. Hanani, M., A. Caspi, and V. Belzer, *Peripheral inflammation augments gap junction-mediated coupling among satellite glial cells in mouse sympathetic ganglia.* Neuron Glia Biol, 2010. **6**(1): p. 85-9.

65. Tu, H., et al., *Mitochondria-derived superoxide and voltage-gated sodium channels in baroreceptor neurons from chronic heart-failure rats.* J Neurophysiol, 2012. **107**(2): p. 591-602.

66. Lee, C.K., et al., *Decreased excitability and voltage-gated sodium currents in aortic baroreceptor neurons contribute to the impairment of arterial baroreflex in cirrhotic rats.* Am J Physiol Regul Integr Comp Physiol, 2016. **310**(11): p. R1088-

101.

67. Oh, J.W., et al., *Functional plasticity of cardiac efferent neurons contributes to traumatic brain injury-induced cardiac autonomic dysfunction.* Brain Res, 2021. **1753**: p. 147257.

68. Butt, M.T., *Sampling and Evaluating the Peripheral Nervous System.* Toxicol Pathol, 2020. **48**(1): p. 10-18.

69. Hanani, M., *Satellite glial cells in sensory ganglia: from form to function.* Brain Res Brain Res Rev, 2005. **48**(3): p. 457-76.

70. Berridge, M.J., P. Lipp, and M.D. Bootman, *The versatility and universality of calcium signalling.* Nat Rev Mol Cell Biol, 2000. **1**(1): p. 11-21.

71. Carafoli, E., et al., *The regulation of intracellular calcium.* Clin Endocrinol (Oxf), 1976. **5 Suppl**: p. 49S-59S.

72. Brini, M., et al., *Intracellular calcium homeostasis and signaling.* Met Ions Life Sci, 2013. **12**: p. 119-68.

73. Lytton, J. and S.K. Nigam, *Intracellular calcium: molecules and pools.* Curr Opin Cell Biol, 1992. **4**(2): p. 220-6.

74. Juhaszova, M., et al., *Location of calcium transporters at presynaptic terminals.* Eur J Neurosci, 2000. **12**(3): p. 839-46.

75. Boyman, L., et al., *Kinetic and equilibrium properties of regulatory calcium sensors of NCX1 protein.* J Biol Chem, 2009. **284**(10): p. 6185-93.

76. Brini, M., et al., *Neuronal calcium signaling: function and dysfunction.* Cell Mol

Life Sci, 2014. **71**(15): p. 2787-814.

77. Park, C.Y., A. Shcheglovitov, and R. Dolmetsch, *The CRAC channel activator STIM1 binds and inhibits L-type voltage-gated calcium channels.* Science, 2010. **330**(6000): p. 101-5.

78. Araque, A., *Astrocytes process synaptic information.* Neuron Glia Biol, 2008. **4**(1): p. 3-10.

79. Verkhratsky, A. and M. Nedergaard, *Physiology of Astroglia.* Physiol Rev, 2018. **98**(1): p. 239-389.

80. Perea, G. and A. Araque, *Glial calcium signaling and neuron-glia communication.* Cell Calcium, 2005. **38**(3-4): p. 375-82.

81. Prakriya, M. and R.S. Lewis, *Store-Operated Calcium Channels.* Physiol Rev, 2015. **95**(4): p. 1383-436.

82. Verkhratsky, A. and V. Parpura, *Astrogliopathology in neurological, neurodevelopmental and psychiatric disorders.* Neurobiol Dis, 2016. **85**: p. 254-261.

83. Guner, G., et al., *NEUROD2 Regulates Stim1 Expression and Store-Operated Calcium Entry in Cortical Neurons.* eNeuro, 2017. **4**(1).

84. Heo, D.K., et al., *Regulation of phagocytosis and cytokine secretion by store-operated calcium entry in primary isolated murine microglia.* Cell Signal, 2015. **27**(1): p. 177-86.

85. Korkotian, E., E. Oni-Biton, and M. Segal, *The role of the store-operated calcium*

entry channel Orai1 in cultured rat hippocampal synapse formation and plasticity. J Physiol, 2017. **595**(1): p. 125-140.

86. Molnar, T., et al., *Store-Operated Calcium Entry in Muller Glia Is Controlled by Synergistic Activation of TRPC and Orai Channels.* J Neurosci, 2016. **36**(11): p. 3184-98.

87. Pereira, O.R., Jr., et al., *Changes in mitochondrial morphology modulate LPS-induced loss of calcium homeostasis in BV-2 microglial cells.* J Bioenerg Biomembr, 2021. **53**(2): p. 109-118.

88. Toth, A.B., et al., *CRAC channels regulate astrocyte Ca(2+) signaling and gliotransmitter release to modulate hippocampal GABAergic transmission.* Sci Signal, 2019. **12**(582).

89. Birla, H., et al., *Toll-like receptor 4 activation enhances Orai1-mediated calcium signal promoting cytokine production in spinal astrocytes.* Cell Calcium, 2022. **105**: p. 102619.

90. Putney, J.W., Jr., *Biphasic modulation of potassium release in rat parotid gland by carbachol and phenylephrine.* J Pharmacol Exp Ther, 1976. **198**(2): p. 375-84.

91. Putney, J.W., Jr., *Muscarinic, alpha-adrenergic and peptide receptors regulate the same calcium influx sites in the parotid gland.* J Physiol, 1977. **268**(1): p. 139-49.

92. Abdullaev, I.F., et al., *Stim1 and Orai1 mediate CRAC currents and store-operated calcium entry important for endothelial cell proliferation.* Circ Res, 2008. **103**(11): p. 1289-99.

93. Bakowski, D., R.D. Burgoyne, and A.B. Parekh, *Activation of the store-operated calcium current ICRAC can be dissociated from regulated exocytosis in rat basophilic leukaemia (RBL-1) cells.* J Physiol, 2003. **553**(Pt 2): p. 387-93.

94. Henquin, J.C., N.I. Mourad, and M. Nenquin, *Disruption and stabilization of beta-cell actin microfilaments differently influence insulin secretion triggered by intracellular Ca2+ mobilization or store-operated Ca2+ entry.* FEBS Lett, 2012. **586**(1): p. 89-95.

95. Yang, S., J.J. Zhang, and X.Y. Huang, *Orai1 and STIM1 are critical for breast tumor cell migration and metastasis.* Cancer Cell, 2009. **15**(2): p. 124-34.

96. Thastrup, O., et al., *Thapsigargin, a novel molecular probe for studying intracellular calcium release and storage.* Agents Actions, 1989. **27**(1-2): p. 17-23.

97. Grynkiewicz, G., M. Poenie, and R.Y. Tsien, *A new generation of Ca2+ indicators with greatly improved fluorescence properties.* J Biol Chem, 1985. **260**(6): p. 3440-50.

98. Feske, S., et al., *A mutation in Orai1 causes immune deficiency by abrogating CRAC channel function.* Nature, 2006. **441**(7090): p. 179-85.

99. Liou, J., et al., *STIM is a Ca2+ sensor essential for Ca2+-store-depletion-triggered Ca2+ influx.* Curr Biol, 2005. **15**(13): p. 1235-41.

100. Roos, J., et al., *STIM1, an essential and conserved component of store-operated Ca2+ channel function.* J Cell Biol, 2005. **169**(3): p. 435-45.

101. Vig, M., et al., *CRACM1 is a plasma membrane protein essential for store-*

operated Ca2+ entry. Science, 2006. **312**(5777): p. 1220-3.

102. Zhang, S.L., et al., *STIM1 is a Ca2+ sensor that activates CRAC channels and migrates from the Ca2+ store to the plasma membrane.* Nature, 2005. **437**(7060): p. 902-5.

103. Zhang, S.L., et al., *Genome-wide RNAi screen of Ca(2+) influx identifies genes that regulate Ca(2+) release-activated Ca(2+) channel activity.* Proc Natl Acad Sci U S A, 2006. **103**(24): p. 9357-62.

104. Mercer, J.C., et al., *Large store-operated calcium selective currents due to co-expression of Orai1 or Orai2 with the intracellular calcium sensor, Stim1.* J Biol Chem, 2006. **281**(34): p. 24979-90.

105. Peinelt, C., et al., *Amplification of CRAC current by STIM1 and CRACM1 (Orai1).* Nat Cell Biol, 2006. **8**(7): p. 771-3.

106. Soboloff, J., et al., *Orai1 and STIM reconstitute store-operated calcium channel function.* J Biol Chem, 2006. **281**(30): p. 20661-20665.

107. Stathopulos, P.B., et al., *Structural and mechanistic insights into STIM1-mediated initiation of store-operated calcium entry.* Cell, 2008. **135**(1): p. 110-22.

108. Zheng, L., et al., *Biophysical characterization of the EF-hand and SAM domain containing Ca2+ sensory region of STIM1 and STIM2.* Biochem Biophys Res Commun, 2008. **369**(1): p. 240-6.

109. Park, C.Y., et al., *STIM1 clusters and activates CRAC channels via direct binding of a cytosolic domain to Orai1.* Cell, 2009. **136**(5): p. 876-90.

110. Yuan, J.P., et al., *SOAR and the polybasic STIM1 domains gate and regulate Orai channels.* Nat Cell Biol, 2009. **11**(3): p. 337-43.

111. Calloway, N., et al., *Molecular clustering of STIM1 with Orai1/CRACM1 at the plasma membrane depends dynamically on depletion of Ca2+ stores and on electrostatic interactions.* Mol Biol Cell, 2009. **20**(1): p. 389-99.

112. Muik, M., et al., *Dynamic coupling of the putative coiled-coil domain of ORAI1 with STIM1 mediates ORAI1 channel activation.* J Biol Chem, 2008. **283**(12): p. 8014-22.

113. Wu, M.M., et al., *Ca2+ store depletion causes STIM1 to accumulate in ER regions closely associated with the plasma membrane.* J Cell Biol, 2006. **174**(6): p. 803-13.

114. Luik, R.M., et al., *The elementary unit of store-operated Ca2+ entry: local activation of CRAC channels by STIM1 at ER-plasma membrane junctions.* J Cell Biol, 2006. **174**(6): p. 815-25.

115. Xu, P., et al., *Aggregation of STIM1 underneath the plasma membrane induces clustering of Orai1.* Biochem Biophys Res Commun, 2006. **350**(4): p. 969-76.

116. Feske, S., *ORAI1 and STIM1 deficiency in human and mice: roles of store-operated Ca2+ entry in the immune system and beyond.* Immunol Rev, 2009. **231**(1): p. 189-209.

117. Picard, C., et al., *STIM1 mutation associated with a syndrome of immunodeficiency and autoimmunity.* N Engl J Med, 2009. **360**(19): p. 1971-80.

118. Gwack, Y., et al., *Hair loss and defective T- and B-cell function in mice lacking ORAI1.* Mol Cell Biol, 2008. **28**(17): p. 5209-22.

119. Hulot, J.S., et al., *Critical role for stromal interaction molecule 1 in cardiac hypertrophy.* Circulation, 2011. **124**(7): p. 796-805.

120. Putney, J.W., Jr., *A model for receptor-regulated calcium entry.* Cell Calcium, 1986. **7**(1): p. 1-12.

121. Vazquez, G., et al., *The mammalian TRPC cation channels.* Biochim Biophys Acta, 2004. **1742**(1-3): p. 21-36.

122. Wang, H., et al., *TRPC channels: Structure, function, regulation and recent advances in small molecular probes.* Pharmacol Ther, 2020. **209**: p. 107497.

123. Hofmann, T., et al., *Direct activation of human TRPC6 and TRPC3 channels by diacylglycerol.* Nature, 1999. **397**(6716): p. 259-63.

124. Okada, T., et al., *Molecular and functional characterization of a novel mouse transient receptor potential protein homologue TRP7. Ca(2+)-permeable cation channel that is constitutively activated and enhanced by stimulation of G protein-coupled receptor.* J Biol Chem, 1999. **274**(39): p. 27359-70.

125. Salido, G.M., S.O. Sage, and J.A. Rosado, *TRPC channels and store-operated Ca(2+) entry.* Biochim Biophys Acta, 2009. **1793**(2): p. 223-30.

126. Zitt, C., et al., *Cloning and functional expression of a human Ca2+-permeable cation channel activated by calcium store depletion.* Neuron, 1996. **16**(6): p. 1189-96.

127. Hoth, M. and R. Penner, *Depletion of intracellular calcium stores activates a calcium current in mast cells.* Nature, 1992. **355**(6358): p. 353-6.

128. Inoue, R., et al., *The transient receptor potential protein homologue TRP6 is the essential component of vascular alpha(1)-adrenoceptor-activated Ca(2+)-permeable cation channel.* Circ Res, 2001. **88**(3): p. 325-32.

129. Zhu, X., M. Jiang, and L. Birnbaumer, *Receptor-activated Ca2+ influx via human Trp3 stably expressed in human embryonic kidney (HEK)293 cells. Evidence for a non-capacitative Ca2+ entry.* J Biol Chem, 1998. **273**(1): p. 133-42.

130. Ong, H.L., et al., *Dynamic assembly of TRPC1-STIM1-Orai1 ternary complex is involved in store-operated calcium influx. Evidence for similarities in store-operated and calcium release-activated calcium channel components.* J Biol Chem, 2007. **282**(12): p. 9105-16.

131. Liu, X., et al., *Trp1, a candidate protein for the store-operated Ca(2+) influx mechanism in salivary gland cells.* J Biol Chem, 2000. **275**(5): p. 3403-11.

132. Mori, Y., et al., *Transient receptor potential 1 regulates capacitative Ca(2+) entry and Ca(2+) release from endoplasmic reticulum in B lymphocytes.* J Exp Med, 2002. **195**(6): p. 673-81.

133. Rao, J.N., et al., *TRPC1 functions as a store-operated Ca2+ channel in intestinal epithelial cells and regulates early mucosal restitution after wounding.* Am J Physiol Gastrointest Liver Physiol, 2006. **290**(4): p. G782-92.

134. Xu, S.Z. and D.J. Beech, *TrpC1 is a membrane-spanning subunit of store-operated*

Ca(2+) channels in native vascular smooth muscle cells. Circ Res, 2001. **88**(1): p. 84-7.

135. Yuan, J.P., et al., *STIM1 heteromultimerizes TRPC channels to determine their function as store-operated channels.* Nat Cell Biol, 2007. **9**(6): p. 636-45.

136. Wu, X., et al., *TRPC channels are necessary mediators of pathologic cardiac hypertrophy.* Proc Natl Acad Sci U S A, 2010. **107**(15): p. 7000-5.

137. Eder, P., et al., *Protein-Protein Interactions in TRPC Channel Complexes*, in *TRP Ion Channel Function in Sensory Transduction and Cellular Signaling Cascades*, W.B. Liedtke and S. Heller, Editors. 2007: Boca Raton (FL).

138. Eder, P. and J.D. Molkentin, *TRPC channels as effectors of cardiac hypertrophy.* Circ Res, 2011. **108**(2): p. 265-72.

139. Eder, P., *Cardiac Remodeling and Disease: SOCE and TRPC Signaling in Cardiac Pathology.* Adv Exp Med Biol, 2017. **993**: p. 505-521.

140. Abramowitz, J. and L. Birnbaumer, *Physiology and pathophysiology of canonical transient receptor potential channels.* FASEB J, 2009. **23**(2): p. 297-328.

141. Clapham, D.E., *TRP channels as cellular sensors.* Nature, 2003. **426**(6966): p. 517-24.

142. Bush, E.W., et al., *Canonical transient receptor potential channels promote cardiomyocyte hypertrophy through activation of calcineurin signaling.* J Biol Chem, 2006. **281**(44): p. 33487-96.

143. Nakayama, H., et al., *Calcineurin-dependent cardiomyopathy is activated by TRPC*

in the adult mouse heart. FASEB J, 2006. **20**(10): p. 1660-70.

144. Gees, M., B. Colsoul, and B. Nilius, *The role of transient receptor potential cation channels in Ca2+ signaling.* Cold Spring Harb Perspect Biol, 2010. **2**(10): p. a003962.

145. Freichel, M., et al., *Functional role of TRPC proteins in native systems: implications from knockout and knock-down studies.* J Physiol, 2005. **567**(Pt 1): p. 59-66.

146. Chaudhuri, P., et al., *Elucidation of a TRPC6-TRPC5 channel cascade that restricts endothelial cell movement.* Mol Biol Cell, 2008. **19**(8): p. 3203-11.

147. Liu, Y., et al., *Sensory neuron-expressed TRPC3 mediates acute and chronic itch.* Pain, 2023. **164**(1): p. 98-110.

148. Jing, C., et al., *TRPC3 Overexpression Promotes the Progression of Inflammation-Induced Preterm Labor and Inhibits T Cell Activation.* Cell Physiol Biochem, 2018. **45**(1): p. 378-388.

149. Dong, P., et al., *TRPC3 Is Dispensable for beta-Alanine Triggered Acute Itch.* Sci Rep, 2017. **7**(1): p. 13869.

150. Liao, Y., et al., *Functional interactions among Orai1, TRPCs, and STIM1 suggest a STIM-regulated heteromeric Orai/TRPC model for SOCE/Icrac channels.* Proc Natl Acad Sci U S A, 2008. **105**(8): p. 2895-900.

151. Abbracchio, M.P., et al., *Purinergic signalling in the nervous system: an overview.* Trends Neurosci, 2009. **32**(1): p. 19-29.

152. Burnstock, G., *Physiology and pathophysiology of purinergic neurotransmission.* Physiol Rev, 2007. **87**(2): p. 659-797.

153. Burnstock, G., *Discovery of purinergic signalling, the initial resistance and current explosion of interest.* Br J Pharmacol, 2012. **167**(2): p. 238-55.

154. Boehm, S., *ATP stimulates sympathetic transmitter release via presynaptic P2X purinoceptors.* J Neurosci, 1999. **19**(2): p. 737-46.

155. Boehm, S., *P2Ys go neuronal: modulation of Ca2+ and K+ channels by recombinant receptors.* Br J Pharmacol, 2003. **138**(1): p. 1-3.

156. Vizi, E.S., et al., *Studies on the release and extracellular metabolism of endogenous ATP in rat superior cervical ganglion: support for neurotransmitter role of ATP.* Neuroscience, 1997. **79**(3): p. 893-903.

157. Burnstock, G., *Purinergic cotransmission.* Exp Physiol, 2009. **94**(1): p. 20-4.

158. Gourine, A.V., J.D. Wood, and G. Burnstock, *Purinergic signalling in autonomic control.* Trends Neurosci, 2009. **32**(5): p. 241-8.

159. Reichert, K.P., et al., *Diabetes and hypertension: Pivotal involvement of purinergic signaling.* Biomed Pharmacother, 2021. **137**: p. 111273.

160. Devor, M. and P.D. Wall, *Cross-excitation in dorsal root ganglia of nerve-injured and intact rats.* J Neurophysiol, 1990. **64**(6): p. 1733-46.

161. Reist, N.E. and S.J. Smith, *Neurally evoked calcium transients in terminal Schwann cells at the neuromuscular junction.* Proc Natl Acad Sci U S A, 1992. **89**(16): p. 7625-9.

162. Pende, M., et al., *Glutamate regulates intracellular calcium and gene expression in oligodendrocyte progenitors through the activation of DL-alpha-amino-3-hydroxy-5-methyl-4-isoxazolepropionic acid receptors.* Proc Natl Acad Sci U S A, 1994. **91**(8): p. 3215-9.

163. Mack, K.J., et al., *Transcription factor expression is induced by axonal stimulation and glutamate in the glia of the developing optic nerve.* Brain Res Mol Brain Res, 1994. **23**(1-2): p. 73-80.

164. Spray, D.C. and M. Hanani, *Gap junctions, pannexins and pain.* Neurosci Lett, 2019. **695**: p. 46-52.

165. Scemes, E., D.C. Spray, and P. Meda, *Connexins, pannexins, innexins: novel roles of "hemi-channels".* Pflugers Arch, 2009. **457**(6): p. 1207-26.

166. Zhang, W., et al., *Intercellular calcium waves in cultured enteric glia from neonatal guinea pig.* Glia, 2003. **42**(3): p. 252-62.

167. Zhang, X., et al., *Neuronal somatic ATP release triggers neuron-satellite glial cell communication in dorsal root ganglia.* Proc Natl Acad Sci U S A, 2007. **104**(23): p. 9864-9.

168. Puopolo, M., et al., *Extrasynaptic release of dopamine in a retinal neuron: activity dependence and transmitter modulation.* Neuron, 2001. **30**(1): p. 211-25.

169. Jaffe, E.H., et al., *Extrasynaptic vesicular transmitter release from the somata of substantia nigra neurons in rat midbrain slices.* J Neurosci, 1998. **18**(10): p. 3548-53.

170. Huang, L.Y. and E. Neher, *Ca(2+)-dependent exocytosis in the somata of dorsal root ganglion neurons.* Neuron, 1996. **17**(1): p. 135-45.

171. Bruns, D., et al., *Quantal release of serotonin.* Neuron, 2000. **28**(1): p. 205-20.

172. Kumral, A., et al., *Genetic basis of apnoea of prematurity and caffeine treatment response: role of adenosine receptor polymorphisms: genetic basis of apnoea of prematurity.* Acta Paediatr, 2012. **101**(7): p. e299-303.

173. Reshkin, S.J., et al., *Activation of A(3) adenosine receptor induces calcium entry and chloride secretion in A(6) cells.* J Membr Biol, 2000. **178**(2): p. 103-13.

174. Sun, D., et al., *Mediation of tubuloglomerular feedback by adenosine: evidence from mice lacking adenosine 1 receptors.* Proc Natl Acad Sci U S A, 2001. **98**(17): p. 9983-8.

175. Ledent, C., et al., *Aggressiveness, hypoalgesia and high blood pressure in mice lacking the adenosine A2a receptor.* Nature, 1997. **388**(6643): p. 674-8.

176. Del Puerto, A., F. Wandosell, and J.J. Garrido, *Neuronal and glial purinergic receptors functions in neuron development and brain disease.* Front Cell Neurosci, 2013. **7**: p. 197.

177. Gabel, C.A., *P2 purinergic receptor modulation of cytokine production.* Purinergic Signal, 2007. **3**(1-2): p. 27-38.

178. Burnstock, G., *Purinergic Mechanisms and Pain.* Adv Pharmacol, 2016. **75**: p. 91-137.

179. Burnstock, G., *P2X ion channel receptors and inflammation.* Purinergic Signal,

2016. **12**(1): p. 59-67.

180. Faroni, A., et al., *Differentiation of adipose-derived stem cells into Schwann cell phenotype induces expression of P2X receptors that control cell death.* Cell Death Dis, 2013. **4**(7): p. e743.

181. Evans, R.J., et al., *Pharmacological characterization of heterologously expressed ATP-gated cation channels (P2x purinoceptors).* Mol Pharmacol, 1995. **48**(2): p. 178-83.

182. Lewis, C., et al., *Coexpression of P2X2 and P2X3 receptor subunits can account for ATP-gated currents in sensory neurons.* Nature, 1995. **377**(6548): p. 432-5.

183. Surprenant, A., et al., *The cytolytic P2Z receptor for extracellular ATP identified as a P2X receptor (P2X7).* Science, 1996. **272**(5262): p. 735-8.

184. Li, M., S.D. Silberberg, and K.J. Swartz, *Subtype-specific control of P2X receptor channel signaling by ATP and Mg2+.* Proc Natl Acad Sci U S A, 2013. **110**(36): p. E3455-63.

185. Harkat, M., et al., *On the permeation of large organic cations through the pore of ATP-gated P2X receptors.* Proc Natl Acad Sci U S A, 2017. **114**(19): p. E3786-E3795.

186. Chen, S., et al., *Expression of purinergic receptor P2Y4 in Schwann cell following nerve regeneration.* Int J Clin Exp Med, 2015. **8**(8): p. 13203-10.

187. North, R.A. and A. Surprenant, *Pharmacology of cloned P2X receptors.* Annu Rev Pharmacol Toxicol, 2000. **40**: p. 563-80.

188. Khakh, B.S., et al., *Allosteric control of gating and kinetics at P2X(4) receptor channels.* J Neurosci, 1999. **19**(17): p. 7289-99.

189. Priel, A. and S.D. Silberberg, *Mechanism of ivermectin facilitation of human P2X4 receptor channels.* J Gen Physiol, 2004. **123**(3): p. 281-93.

190. Coddou, C., S.S. Stojilkovic, and J.P. Huidobro-Toro, *Allosteric modulation of ATP-gated P2X receptor channels.* Rev Neurosci, 2011. **22**(3): p. 335-54.

191. Rafehi, M. and C.E. Muller, *Tools and drugs for uracil nucleotide-activated P2Y receptors.* Pharmacol Ther, 2018. **190**: p. 24-80.

192. Lamarca, A., et al., *Uridine 5'-triphosphate promotes in vitro Schwannoma cell migration through matrix metalloproteinase-2 activation.* PLoS One, 2014. **9**(6): p. e98998.

193. Berti-Mattera, L.N., et al., *P2-purigenic receptors regulate phospholipase C and adenylate cyclase activities in immortalized Schwann cells.* Biochem J, 1996. **314 (Pt 2)**(Pt 2): p. 555-61.

194. Ruan, H.Z. and G. Burnstock, *Localisation of P2Y1 and P2Y4 receptors in dorsal root, nodose and trigeminal ganglia of the rat.* Histochem Cell Biol, 2003. **120**(5): p. 415-26.

195. Yi, Z., et al., *P2Y(12) receptor upregulation in satellite glial cells is involved in neuropathic pain induced by HIV glycoprotein 120 and 2',3'-dideoxycytidine.* Purinergic Signal, 2018. **14**(1): p. 47-58.

196. Lin, J., et al., *The P2Y(14) receptor in the trigeminal ganglion contributes to the*

maintenance of inflammatory pain. Neurochem Int, 2019. **131**: p. 104567.

197. Lin, J., et al., *P2Y(14) receptor is functionally expressed in satellite glial cells and mediates interleukin-1beta and chemokine CCL2 secretion.* J Cell Physiol, 2019. **234**(11): p. 21199-21210.

198. Kobayashi, K., et al., *Neurons and glial cells differentially express P2Y receptor mRNAs in the rat dorsal root ganglion and spinal cord.* J Comp Neurol, 2006. **498**(4): p. 443-54.

199. Abbracchio, M.P. and S. Ceruti, *Roles of P2 receptors in glial cells: focus on astrocytes.* Purinergic Signal, 2006. **2**(4): p. 595-604.

200. Ikeda, S.R. and S.W. Jeong, *Use of RGS-insensitive Galpha subunits to study endogenous RGS protein action on G-protein modulation of N-type calcium channels in sympathetic neurons.* Methods Enzymol, 2004. **389**: p. 170-89.

201. George, D., P. Ahrens, and S. Lambert, *Satellite glial cells represent a population of developmentally arrested Schwann cells.* Glia, 2018. **66**(7): p. 1496-1506.

202. Buijs, T.J., et al., *STIM1 and ORAI1 form a novel cold transduction mechanism in sensory and sympathetic neurons.* EMBO J, 2023. **42**(3): p. e111348.

203. Bodin, P. and G. Burnstock, *Purinergic signalling: ATP release.* Neurochem Res, 2001. **26**(8-9): p. 959-69.

204. Bodin, P. and G. Burnstock, *Evidence that release of adenosine triphosphate from endothelial cells during increased shear stress is vesicular.* J Cardiovasc Pharmacol, 2001. **38**(6): p. 900-8.

205. Verstreken, P., T. Ohyama, and H.J. Bellen, *FM 1-43 labeling of synaptic vesicle pools at the Drosophila neuromuscular junction.* Methods Mol Biol, 2008. **440**: p. 349-69.

206. Coco, S., et al., *Storage and release of ATP from astrocytes in culture.* J Biol Chem, 2003. **278**(2): p. 1354-62.

207. Butt, A.M. and A. Kalsi, *Inwardly rectifying potassium channels (Kir) in central nervous system glia: a special role for Kir4.1 in glial functions.* J Cell Mol Med, 2006. **10**(1): p. 33-44.

208. Tang, X., et al., *Inwardly rectifying potassium channel Kir4.1 is responsible for the native inward potassium conductance of satellite glial cells in sensory ganglia.* Neuroscience, 2010. **166**(2): p. 397-407.

209. Schleifer, H., et al., *Novel pyrazole compounds for pharmacological discrimination between receptor-operated and store-operated Ca(2+) entry pathways.* Br J Pharmacol, 2012. **167**(8): p. 1712-22.

210. Guthrie, P.B., et al., *ATP released from astrocytes mediates glial calcium waves.* J Neurosci, 1999. **19**(2): p. 520-8.

211. Vigne, P., et al., *Benzoyl ATP is an antagonist of rat and human P2Y1 receptors and of platelet aggregation.* Biochem Biophys Res Commun, 1999. **256**(1): p. 94-7.

212. Ballout, J., et al., *Ionotropic P2X4 and P2X7 receptors in the regulation of ion transport across rat colon.* Br J Pharmacol, 2022. **179**(21): p. 4992-5011.

213. Perez-Flores, G., et al., *The P2X7/P2X4 interaction shapes the purinergic response in murine macrophages.* Biochem Biophys Res Commun, 2015. **467**(3): p. 484-90.

214. Schneider, M., et al., *Interaction of Purinergic P2X4 and P2X7 Receptor Subunits.* Front Pharmacol, 2017. **8**: p. 860.

215. Tsuda, M., H. Tozaki-Saitoh, and K. Inoue, *Purinergic system, microglia and neuropathic pain.* Curr Opin Pharmacol, 2012. **12**(1): p. 74-9.

216. Craigie, E., et al., *The relationship between P2X4 and P2X7: a physiologically important interaction?* Front Physiol, 2013. **4**: p. 216.

217. James, S. and G. Burnstock, *Autoradiographic localization of muscarinic receptors on cultured, peptide-containing neurones from newborn rat superior cervical ganglion.* Brain Res, 1989. **498**(2): p. 205-14.

218. Ikeda, S.R., et al., *Heterologous expression of a green fluorescent protein-pertussis toxin S1 subunit fusion construct disrupts calcium channel modulation in rat superior cervical ganglion neurons.* Neurosci Lett, 1999. **271**(3): p. 163-6.

219. Cowen, T., et al., *Increase in neuropeptide Y, but not noradrenaline, in the superior cervical ganglion of rabbits chronically exposed to cold.* J Auton Nerv Syst, 1988. **24**(1-2): p. 175-8.

220. Andreeva, D., et al., *Satellite Glial Cells: Morphology, functional heterogeneity, and role in pain.* Front Cell Neurosci, 2022. **16**: p. 1019449.

221. Feldman-Goriachnik, R., E. Blum, and M. Hanani, *Exercise reduces pain behavior and pathological changes in dorsal root ganglia induced by systemic inflammation*

in mice. Neurosci Lett, 2022. **778**: p. 136616.

222. Feldman-Goriachnik, R. and M. Hanani, *How do neurons in sensory ganglia communicate with satellite glial cells?* Brain Res, 2021. **1760**: p. 147384.

223. Bading, H., D.D. Ginty, and M.E. Greenberg, *Regulation of gene expression in hippocampal neurons by distinct calcium signaling pathways.* Science, 1993. **260**(5105): p. 181-6.

224. Parekh, A.B. and J.W. Putney, Jr., *Store-operated calcium channels.* Physiol Rev, 2005. **85**(2): p. 757-810.

225. Berridge, M.J., *Capacitative calcium entry.* Biochem J, 1995. **312 (Pt 1)**(Pt 1): p. 1-11.

226. Lyfenko, A.D. and R.T. Dirksen, *Differential dependence of store-operated and excitation-coupled Ca2+ entry in skeletal muscle on STIM1 and Orai1.* J Physiol, 2008. **586**(20): p. 4815-24.

227. Shanks, J., et al., *Overexpression of Sarcoendoplasmic Reticulum Calcium ATPase 2a Promotes Cardiac Sympathetic Neurotransmission via Abnormal Endoplasmic Reticulum and Mitochondria Ca(2+) Regulation.* Hypertension, 2017. **69**(4): p. 625-632.

228. Kotturi, M.F., et al., *Identification and functional characterization of voltage-dependent calcium channels in T lymphocytes.* J Biol Chem, 2003. **278**(47): p. 46949-60.

229. Steinbeck, J.A., et al., *Store-operated calcium entry modulates neuronal network*

activity in a model of chronic epilepsy. Exp Neurol, 2011. **232**(2): p. 185-94.

230. Sun, S., et al., *Reduced synaptic STIM2 expression and impaired store-operated calcium entry cause destabilization of mature spines in mutant presenilin mice.* Neuron, 2014. **82**(1): p. 79-93.

231. Ingiosi, A.M., et al., *A Role for Astroglial Calcium in Mammalian Sleep and Sleep Regulation.* Curr Biol, 2020. **30**(22): p. 4373-4383 e7.

232. Verkhratsky, A., J.J. Rodriguez, and V. Parpura, *Calcium signalling in astroglia.* Mol Cell Endocrinol, 2012. **353**(1-2): p. 45-56.

233. Pivneva, T., et al., *Store-operated Ca2+ entry in astrocytes: different spatial arrangement of endoplasmic reticulum explains functional diversity in vitro and in situ.* Cell Calcium, 2008. **43**(6): p. 591-601.

234. Lo, K.J., et al., *Store depletion-induced calcium influx in rat cerebellar astrocytes.* Br J Pharmacol, 2002. **135**(6): p. 1383-92.

235. Verkhratsky, A. and V. Parpura, *Store-operated calcium entry in neuroglia.* Neurosci Bull, 2014. **30**(1): p. 125-33.

236. Prakriya, M., et al., *Orai1 is an essential pore subunit of the CRAC channel.* Nature, 2006. **443**(7108): p. 230-3.

237. Moreno, C., et al., *STIM1 and Orai1 mediate thrombin-induced Ca(2+) influx in rat cortical astrocytes.* Cell Calcium, 2012. **52**(6): p. 457-67.

238. Alberdi, E., M.V. Sanchez-Gomez, and C. Matute, *Calcium and glial cell death.* Cell Calcium, 2005. **38**(3-4): p. 417-25.

239. Feldman-Goriachnik, R., B. Wu, and M. Hanani, *Cholinergic responses of satellite glial cells in the superior cervical ganglia.* Neurosci Lett, 2018. **671**: p. 19-24.

240. Sun, Z., et al., *SOCE-mediated NFAT1-NOX2-NLRP1 inflammasome involves in lipopolysaccharide-induced neuronal damage and Abeta generation.* Mol Neurobiol, 2022. **59**(5): p. 3183-3205.

241. Ronco, V., et al., *Differential deregulation of astrocytic calcium signalling by amyloid-beta, TNFalpha, IL-1beta and LPS.* Cell Calcium, 2014. **55**(4): p. 219-29.

242. Liddelow, S.A. and B.A. Barres, *Reactive Astrocytes: Production, Function, and Therapeutic Potential.* Immunity, 2017. **46**(6): p. 957-967.

243. Feldman-Goriachnik, R. and M. Hanani, *The effects of sympathetic nerve damage on satellite glial cells in the mouse superior cervical ganglion.* Auton Neurosci, 2019. **221**: p. 102584.

244. Mohr, K.M., et al., *Discrepancy in the Usage of GFAP as a Marker of Satellite Glial Cell Reactivity.* Biomedicines, 2021. **9**(8).

245. Campolo, M., et al., *TLR4 absence reduces neuroinflammation and inflammasome activation in Parkinson's diseases in vivo model.* Brain Behav Immun, 2019. **76**: p. 236-247.

246. Bruno, K., et al., *Targeting toll-like receptor-4 (TLR4)-an emerging therapeutic target for persistent pain states.* Pain, 2018. **159**(10): p. 1908-1915.

247. Vuong, B., et al., *NF-kappaB transcriptional activation by TNFalpha requires phospholipase C, extracellular signal-regulated kinase 2 and poly(ADP-ribose)*

polymerase-1. J Neuroinflammation, 2015. **12**: p. 229.

248. Pulver, R.A., et al., *Store-operated Ca2+ entry activates the CREB transcription factor in vascular smooth muscle.* Circ Res, 2004. **94**(10): p. 1351-8.

249. Crabtree, G.R. and E.N. Olson, *NFAT signaling: choreographing the social lives of cells.* Cell, 2002. **109 Suppl**: p. S67-79.

250. Won, Y.J., et al., *Expression profiles of high voltage-activated calcium channels in sympathetic and parasympathetic pelvic ganglion neurons innervating the urogenital system.* J Pharmacol Exp Ther, 2006. **317**(3): p. 1064-71.

251. Wang, Y., et al., *The calcium store sensor, STIM1, reciprocally controls Orai and CaV1.2 channels.* Science, 2010. **330**(6000): p. 105-9.

252. Pascual-Caro, C., et al., *STIM1 deficiency is linked to Alzheimer's disease and triggers cell death in SH-SY5Y cells by upregulation of L-type voltage-operated Ca(2+) entry.* J Mol Med (Berl), 2018. **96**(10): p. 1061-1079.

253. Vause, C.V. and P.L. Durham, *Calcitonin gene-related peptide differentially regulates gene and protein expression in trigeminal glia cells: findings from array analysis.* Neurosci Lett, 2010. **473**(3): p. 163-7.

254. Ren, W.J. and P. Illes, *Involvement of P2X7 receptors in chronic pain disorders.* Purinergic Signal, 2022. **18**(1): p. 83-92.

255. Narcisse, L., et al., *The cytokine IL-1beta transiently enhances P2X7 receptor expression and function in human astrocytes.* Glia, 2005. **49**(2): p. 245-58.

256. Park, K.S., et al., *Modulation of N-type Ca2+ currents by A1-adenosine receptor*

activation in male rat pelvic ganglion neurons. J Pharmacol Exp Ther, 2001. **299**(2): p. 501-8.

257. Zhu, Y. and S.R. Ikeda, *Adenosine modulates voltage-gated Ca2+ channels in adult rat sympathetic neurons.* J Neurophysiol, 1993. **70**(2): p. 610-20.

258. Nedergaard, M., B. Ransom, and S.A. Goldman, *New roles for astrocytes: redefining the functional architecture of the brain.* Trends Neurosci, 2003. **26**(10): p. 523-30.

259. Scemes, E. and C. Giaume, *Astrocyte calcium waves: what they are and what they do.* Glia, 2006. **54**(7): p. 716-725.

260. Zhang, X.F., et al., *Functional expression of P2X7 receptors in non-neuronal cells of rat dorsal root ganglia.* Brain Res, 2005. **1052**(1): p. 63-70.

261. Hanani, M., et al., *Glial cell plasticity in sensory ganglia induced by nerve damage.* Neuroscience, 2002. **114**(2): p. 279-83.

262. Xie, A.X., J.J. Lee, and K.D. McCarthy, *Ganglionic GFAP (+) glial Gq-GPCR signaling enhances heart functions in vivo.* JCI Insight, 2017. **2**(2): p. e90565.

IX. ABSTRACT IN KOREAN

자율신경계에서 뉴런-위성교세포 유닛의 생리적 역할

김 소 현

연세대학교 대학원 의학과

지도교수 정 성 우

자율신경계를 구성하는 교감신경계와 부교감신경계는 내부 장기의 기능을 균형있게 조절하여 우리 몸의 항상성을 유지하는데 중심적인 역학을 한다. 이러한 단서들은 균형 잡힌 자율신경 기능을 수행하기 위해 신경절 내 개별 세포 간의 상호 작용의 중요성을 강조한다. 자율신경절은 뉴런과 이를 둘러싸고 있는 위성교세포 (SGC)로 구성된다. 이들 뉴런과 위성교세포 사이의 해부학적 독특한 구조는 상호 교신을 용이하게 하여 자율신경절의 항상성 조절에 기여하는 것으로 여겨진다. 본 연구에서는 교감신경절의 뉴런-위성교세포 단위를 배양할 수 있는 세포 배양 시스템을 개발하고 다양한 외부 자극에 반응하는 교감 신경절 뉴런과 위성교세포의 칼슘 항상성에 기반하는 기능적 메커니즘을 연구했다. 쥐의 상경신경절(SCG)을 적출하여 SGC가 부착되어 있는 뉴런-위성교세포 유닛을 분리했다. 면역조직화학 및 면역형광 실험을 통해 위성교세포를 확인 후 정

량적 RT-PCR을 사용하여 교감신경절에서 Orai1 채널, STIM1 및 TRPC 1/3/6의 발현을 확인했다. 기능적 연구는 Fura-2/AM을 이용한 칼슘 이미징 기술을 응용하여 수행했다. CPA에 의해 ER내 Ca^{2+}이 고갈될 때 뉴런과 유선교세포에서 모두 SOCE을 확인했으나 세포내 Ca^{2+} 유입은 뉴런보다 SGC에서 훨씬 더 크다는 것을 확인하였다. 또한, 뉴런과 달리 위성교세포의 SOCE는 큰 Ca^{2+} 진동을 동반했다. 뉴런-SGC 단위의 기능 변화를 확인하기 위해 동물 모델에서 LPS로 급성 염증을 유도했다. 염증 동물 모델의 상경신경절에서 GFAP와 TLR4가 많이 발현되어 있음을 확인하였고는 반대로 Orai1 및 STIM1 발현이 감소됨을 확인하였다. 따라서 SOCE는 염증에 매우 취약하며, 이는 교감 신경 활동에 영향을 미칠 수 있다. 종합하면, 위성교세포에서의 Ca^{2+}은 교감신경절의 다양한 SOCE과 TRPC 채널들에 의해 매개되며 이는 자율신경 기능조절에 기여하는 것으로 추정된다. 뉴런과 위성성교세포의 Ca^{2+} 신호전달은 교감신경 흥분성을 제어하고 자율신경 미세환경에서의 변화를 중재하는 데 중요하다. 80mM KCl을 사용하여 상경신경절 뉴런을 탈분극시키면 세포내 Ca^{2+}은 상경신경절 뉴런뿐만 아니라 뉴런 옆에 부착된 비흥분성 위성교세포에서도 유의하게 증가한다. 이는 신경 흥분성이 뉴런에 부착된 위성교세포에만 영향을 미칠 수 있는 중간 매개체의 국소 방출을 유발한다는 것을 강력히 시사하며 본 연구에서는 교감 신경 뉴런에서 방출된 소포성 ATP가 Ca^{2+} 신호 전달을 통해 뉴런에 단단히 부착된 위성교세포의 퓨린성 수용체 P2X4와 P2X7의 활성화를 유발할 수 있음을 확인했다.

핵심 단어: 자율신경, 칼슘 신호, 위성교세포, 교감신경절, ATP, SOCE, TRPC